Mathematical Modelling and Simulation of Irrigation Sprinklers

Daniel J Grose

16 October 1999

It's but little good you'll do a-watering last years' crop.
George Eliot (Mary Anne Evans) - from "Adam Bede"

Acknowledgements

Per Ricecare ad Veritas.

Abstract

A set of equations suitable for describing the dynamics of a liquid droplet - gas mixture (spray) have been developed. The equations are arrived at by considering the spray as a multiphase continuum within which the gas and droplets of different sizes constitute individual phases. By ignoring droplet-droplet interactions and considering the gas phase as an inviscid fluid a simplified form of the equations of motion has been arrived at.

The equations are considered in one dimension and used to describe the dynamics of the interior of spray produced by a large or medium scale irrigation sprinkler. When combined with data representing the distribution of droplet diameters within the spray this model can be used to predict the water application produced by a sprinkler operating in windy conditions. Such simulations have been undertaken to predict the water application from static sprinklers and the results validated by comparison with data obtained experimentally.

A simulation methodology is used to determine the uniformity of water application produced by a travelling sprinkler. By considering the results of large number of simulations produced using meteorological data spanning several years the manner in which the simulation can be used for determining optimum irrigation practice is demonstrated.

A simple model has been developed for predicting the water application from a travelling sprinkler operating in still air. The model can be used for obtaining first approximations to optimum operating conditions and provides a means for easily quantifying the performance of a given sprinkler. Further use of the model may be made for aiding in the design and control of irrigation sprinklers.

Figure 1: A Komet 101 irrigation sprinkler and trolley being used to irrigate potatoes in south-east England.

Contents

List of Figures

List of Tables

Chapter 1

Preface

1.1 Overview of Thesis

This thesis is concerned with the development of mathematical models and simulation methodologies for predicting the water application from, and performance of, medium and large scale irrigation sprinklers. As such it is an exercise in mathematical modelling and it is difficult (and probably not necessary) to identify a single definitive hypothesis. However, central to the work is the development of a model to describe the dynamics of the spray produced by an irrigation sprinkler. This model is developed from the basic assumption that :

> the dynamics of a liquid droplet spray can be described by considering the spray as a multiphase continuum within which the gas and different droplet sizes constitute individual phases.

This may, if required, be considered as the primary hypothesis of this work.

It is not the intention of this study to exhaustively simulate the process of sprinkler irrigation. Rather to provide methods for undertaking that task. However, certain simulation results have been obtained so as to demonstrate the suitability of the models and methodologies for future use in simulated studies.

1.2 Organization

The thesis is presented in the form of papers. Consequently, each chapter contains an abstract, notation, introduction, main body of the work and a discussion and/or conclusion. The only exceptions are the preface, conclusions and the reveiw in chapter 2 which does not contain an abstract or notation. This form of presentation has been adopted so that the contents will require only minor modification prior to submission for publication. Chapter 4 has already appeared in conference proceedings [43], and it is intended that chapters 5, 7 and 8 form the basis for future publications.

1.3 Notation

When required, each chapter has its own notation list. The lists are not necessarily exhaustive since many symbols are introduced as they appear. In general a symbol associated with a given entity has been used consistently throughout the work. Vectors, matrices and higher order tensors are distinguished from scalars by the use of bold type. Vector operators are represented using Nabla and unit vectors are identified by use of a "hat".

1.4 Synopsis

Chapter 2

This provides an overview of irrigation sprinkler technology and usage. Existing models used for predicting water application from sprinkler irrigators are introduced and their advantages and limitations discussed. The need for a deterministic model is identified.

Chapter 3

This reviews the dynamical theory of individual particles and droplets. The inadequacy of such theories for describing the dynamics of clouds of particles and liquid sprays is addressed. The general theory associated with a multiphase continuum is introduced and a momentum equation, constitutive relation and continuity conditions are derived which are suitable for describing the dynamics of liquid-gas sprays. The application of the theory is demonstrated for a simple duct flow problem.

Chapter 4

A one dimensional multiphase model to describe the dynamics of the core of the spray produced by an irrigation sprinkler is developed. The model accounts for the boundary layer induced by the spray and the effects of a cross-flow on its trajectory. When combined with a standard model for the dynamics of individual droplets (chapter 3) this model can be used to predict the water application from a sprinkler.

Chapter 5

Measurements have been made under controlled conditions of the distribution of droplet sizes present within the spray produced by a sprinkler. Errors induced by the measuring technique employed are examined and the suitability of a number of different probability density functions for modelling the drop size data are assessed. General features of the data are identified and the manner in which it can be used for calibrating models for sprinkler irrigators is discussed.

Chapter 6

The data of chapter 5 is used to calibrate the model developed in chapter 4. The model is used to provide simulated wetting patterns for static sectoring sprinklers. The numerical methods used for the simulation are detailed and results obtained using the simulation compared to data obtained experimentally. A procedure in which the data can be organized into a data base for use in other simulation methodologies is presented.

Chapter 7

A simulation methodology for predicting the water application from a travelling sprinkler operating in windy conditions is developed using a simulated database of static wetting patterns produced by the methods of chapter 6. The simulation is used to determine the effects of different irrigation practices on the uniformity of water application.

Chapter 8

A model is developed for predicting the uniformity of application produced by a travelling irrigation sprinkler operating in still air. The model is used to find the optimal lane spacing and sector angle for the sprinkler. These values can be as a first approximation when using the simulation developed in chapter 7 to determine optimum irrigation practice. The manner in which the model can be used in the design and control of sprinklers is introduced and further applications of the models and simulations developed in the are discussed.

Chapter 9

Conclusions.

Chapter 2

An Overview of Modelling Methods Associated with Sprinkler Irrigators

2.1 Introduction

Overhead sprinklers are extensively used in agriculture worldwide for irrigating various different crop types. Although a number of different overhead irrigation methods exist in Europe large mobile irrigation sprinklers, ("guns"), remain the most popular. In the United Kingdom over 90% of total irrigation demand is met in this manner[1]. The popularity of the method stems from its ease of use, versatility, small capital outlay and low labour costs. The demand for irrigated crops continues to grow, the increase being driven at least in part by the major supermarkets' demand for quality, consistency and continuity of supply. As a result the water volume applied by sprinkler irrigators is steadily increasing.

In any irrigation methodology, uniformity of the application of the water is of interest. This is notably due to its relation to crop uniformity, development and yield but also for environmental reasons such as minimization of nitrate leaching and water wastage. Sprinkler irrigators are widely regarded as providing poor application uniformity although in reality relatively little is known about the performance of large irrigation sprinklers when operating in windy conditions. This lack of knowledge is a consequence of the high cost of, and difficulties associated with making measurements of application uniformity, particularly when experiments are conducted at field level.

Due to the extensive use of sprinkler irrigation and its potential economic and environmental consequences there has been much interest in developing methods for predicting water application from such systems. A number of models have been proposed for this purpose which fall into one of three categories: empirical, semi-empirical and deterministic. An overview of models from each of these categories is presented here. In each case, particular attention is paid to the model's dependence on experimental data for calibration and its robustness, that being the range of operating conditions over which the model accurately predicts sprinkler application. Where possible, model predictions are compared to experimental results and in the case of the deterministic models the underlying model assumptions are considered within the context of observations made of physical processes within the water jet and spray produced by the sprinkler. Certain deficiencies associated with the models are identified and recommendations for the development of future deterministic models are made.

2.2 Model Types

An irrigation sprinkler typically consists of a rotating head containing an orifice or nozzle from which water is ejected in the form of a jet[2]. The energy required to rotate the head is provided by the flow of water via an arm that periodically interrupts the jet near to the nozzle. The sprinkler is either used statically or moved about the field on a trolley drawn by a hose reel. In both cases, the sprinkler head is located above the crop and inclined at angle to the horizontal so as to maximise the range (throw) of the water. For moving sprinklers (and occasionally static ones) the head does not fully rotate and is typically "sectored" through an angle of 220°. The sprinkler's nozzle diameter, pressure, operating height, inclination to the horizontal and sector angle all affect the application of the sprinkler. To be of use for predicting irrigation sprinkler application a deterministic model must be able to account for all

---

[1] Ministry of Agriculture Fisheries and Food (MAFF) 1995 figures.
[2] Kay [23] provides a comprehensive overview of sprinkler technology and irrigation practice.

3

of these factors as well as the effects of wind. Typically, the model would require the relevant operating parameters as input data along with meteorological data consisting of wind speed and direction. As output, the model should provide the application of water at ground level. In the case of a traveling sprinkler the model should enable the application to depend on the sprinklers motion.

2.2.1 Empirical Models

Several empirical methods for predicting the application of water from irrigation sprinklers operating in windy conditions have been developed. These models require access to a large number of measurements of sprinkler application ("wetting patterns") corresponding to a wide range of operating and meteorological conditions. Hippersons [18] model overlays wetting patterns extracted from a database and integrates them together to simulate the spatial variation in application for a traveling sprinkler. In his scheme wetting patterns are chosen from the data base so as to correspond as closely as possible to the meteorological data provided as input to the simulation. Hipperson's investigations only considered sprinklers employing a full 360° sector angle. This approach enabled all wind directions to be considered by simply rotating the wetting patterns in the database. If data for sector angles other than 360° are considered the additional problem of defining "closeness" between meteorological conditions is encountered.

The obvious drawback with empirical models is their dependency on large databases of experimental data. Acquisition of this data is generally time consuming and expensive. Lack of data restricts the range of scenarios that can be simulated and limits the robustness of the model. Furthermore, insufficient data reduces the resolution of the model. Indeed, Hipperson found lack of resolution the main shortcoming of his model.

Musa [24] extended the database used by Hipperson and introduced a means of interpolating between the measured data. This improved the simulation resolution although the database was still restricted to 360° sector angles and a limited number of operating conditions.

2.2.2 Semi-Empirical Models

A number of authors [14][5][12][24] have examined wetting patterns produced by static sprinklers and observed that the wind appears to distort the wetting pattern in several ways. In particular there is a shortening of the pattern upwind, narrowing at right angles to the wind and extension downwind. Richards and Weatherhead [44] using the data of Musa [24] demonstrated a linear relationship between wind speed and the extent of these deformations. Furthermore, they showed that simple trajectory theory, when used to describe the fate of droplets produced by the sprinkler, failed to demonstrate the narrowing of the water distribution pattern perpendicular to the wind. They argued that the motion of droplets through the air induces movement within the air itself which has the effect of extending the droplets range. The presence of a wind at right angles to the spray would then interfere with this induced air flow resulting in the observed cross wind narrowing. They also reasoned that the way in which the liquid jet produced by the sprinkler broke up into droplets and the size of droplets produced would have an affect on the sprinkler application and concluded that the combination of all of these effects was to complex to model deterministically.

From this Richards and Weatherhead [44] developed a semi-empirical model, the basic assumptions of which are:

1. The range shortening due to disruption of the induced air flow is proportional to the wind velocity perpendicular to the jet.

2. The wind drift is proportional to the wind speed

3. Evaporation of the liquid is negligible

4. The water that reaches a particular point in the wetting pattern in zero wind conditions is treated as a single entity whose position is moved by the wind

Using these assumptions, the wetting pattern is to be considered as defining a surface in three space. For no wind (quiescent) conditions the surface is defined by fitting a suitable function to single leg application depth data measured under controlled conditions. To describe the surface in the presence of wind the quiescent surface is transformed in a manner that is consistent with the modelling assumptions. The application rate described by the transformed surface is determined using the Jacobian of the transform. The transformation itself is parameterized and the parameters chosen so that the differences between predicted and measured applications are minimized for a number of different data sets. In their scheme,

Richards and Weatherhead used six parameters and three data sets (360° sector) to optimize the parameters. The method they adopted for the optimization procedure was such that they found that using more than three sets of measured data made the evaluation of the parameters prohibitively complicated. Comparison of the model output with measured values demonstrates a high degree of accuracy over a range of wind conditions and for a number of different sprinkler types.

An immediate advantage of the Richards and Weatherhead model over purely empirical models is that it can predict wetting patterns for any sector angle. This is achieved by appealing to assumption 4 above and simply removing the appropriate region from the transformed wetting pattern. Initially a shortcoming of the model was the inability to calibrate it using more than three data sets and there is some doubt as to whether the parameters obtained represented the true optimal value (i.e. there may be more than one optimal set of parameters in the search space.) Recently, more sophisticated techniques and larger data sets have been used to optimize the parameters of the model. Although more robust than purely empirical methods, once calibrated the Richards and Weatherhead model is restricted to describing the water application from a sprinkler with a fixed nozzle diameter, pressure, operating height and inclination angle.

2.2.3 Deterministic Models

Early deterministic models attempted to determine the sprinkler application by solving the equations of motion for individual droplets (section 3.3) within the spray. Initial conditions for the problem are provided by the nozzle orientation and height along with the fluid velocity at the nozzle. It is apparent however, that to correctly predict the throw of a medium or large sprinkler in this manner it is necessary to include very large droplets within the spray. Indeed, for large sprinklers droplets are required with diameters greater than the nozzle diameter and above the theoretical upper limit for droplets produced by capillary jets [28]. Even if droplets with these diameters existed in the spray they would be unstable and collapse at the speeds that are encountered near to the nozzle [42]. Furthermore, the model predicts that in quiescent conditions individual points within the wetting pattern receive droplets of only one diameter which is contrary to experimental evidence (chapter 5). A further deficiency of this simple type of deterministic model is that it does not exhibit the reduction in throw in a direction perpendicular to the wind which has been observed by a number of researchers.

Several attempts have been made to remedy the deficiencies of this simple deterministic model. Most of these approaches apply modifications to the differential equations which describe the equation of motion for individual droplets. Seginer et al [41], and later Carrion et al [19], achieved this by modifying the drag coefficient so that the range of the droplet is extended. In addition, they allowed the drag coefficient to depend upon the direction of the wind allowing for the cross wind narrowing of wetting pattern to be modelled. However, the modifications to the drag coefficient have to be determined from measurements made of sprinkler wetting patterns under a number of operating conditions.

An alternative modification to the basic deterministic model is to alter the initial conditions used to solve the equations of motion. Augier [4] adopted this approach by considering a spray consisting of a dense jet liberating droplets along its length. The trajectory of the jet was described by a parabola determined from the initial conditions at the nozzle. The jet position and velocity at points along the jet are then used to provide the initial conditions for individual droplets leaving it. The trajectory of the droplets are described using the equation of motion for an individual autonomous droplet. The number and size of the droplets leaving the jet have to be either assumed in advance or determined from measurements of the composition of the spray (chapter 5). This approach is appealing because it requires relatively few experimental results for calibration which is the primary objective of a deterministic model. Furthermore, it leads to good estimates for sprinkler throw and allows for droplets of differing sizes to arrive at the same point within the wetting pattern. Unfortunately, the model provides no mechanism for describing how the jet interacts with a cross flow and as a consequence underestimates the cross wind narrowing of the wetting pattern.

The attraction associated with the use of deterministic models to describe sprinkler performance is the reduced requirement for experimental data for calibration purposes. Furthermore, deterministic models tend to be more robust and can be used to simulate sprinklers when operating under a wider range of conditions than empirical or semi-empirical methods. Unfortunately, existing deterministic models do not predict sprinkler application with a sufficient degree of accuracy to be of practical use. Those that do have compromised most advantages expected from a deterministic model by incorporating experimental data into the physical models.

2.3   Future Developments for Deterministic Models

It is apparent upon observing the behavior of the spray produced by a sprinkler that it may be considered as an unstable jet which breaks up into droplets of different sizes at a distance relatively close to the nozzle when compared to the overall throw of the sprinkler. The distance from the nozzle at which the jet breaks up decreases with increasing liquid velocity, an observation that is consistent with existing breakup theories for jets of this type [8]. The process of the jet breakup results in a compact spray from which droplets are released as it travels through the air. Eventually a sufficient number of drops are removed from the spray and its perceived structure disappears. Measurements made of the trajectory of the core of the spray suggest that its path can be considered as parabolic at distances near the nozzle. Further down stream its progress becomes increasingly retarded due to the exchange of momentum between the liquid and the surrounding air. In the presence of a cross wind the trajectory of the spray is deflected. An important observation is that a considerable movement of air is induced by virtue of the motion of the spray through the atmosphere. This induced airflow has the effect of reducing the net drag experienced by spray and thereby increasing the throw of the sprinkler.

Thus, given the above considerations, for a deterministic model to accurately describe water application from an irrigation sprinkler it is necessary this it should be capable of describing

1. The momentum transfer between the spray and the air

2. The deflection of the spray by a cross wind

3. The trajectories of individual droplets released from the spray

4. The distribution of the droplet sizes within the spray

5. The rate at which droplets leave the spray

Having identified limitations associated with existing deterministic models it is clear that requirement 1 above is of primary importance. Ideally a general theory for the momentum balance in a liquid spray is required rather than an ad-hoc method which may only be applicable in certain special cases.

A number of methods have been developed to account for the momentum balance in liquid droplet - gas systems. Crowe *et al* [36] developed a numerical scheme (PSI-CELL method) for determining how the flow of gas is modified by the presence of liquid droplets. This method also considered heat transfer between the droplets and the gas allowing it to be used for modelling spray cooling systems. Weinacht *et al* [10][11] independently developed a similar method. In these schemes the trajectories of individual droplets are determined within a grid of non-overlapping control volumes. The momentum lost by the droplets is calculated and is accounted for as a source term in the solution of the flow of the gas. Since the momentum lost by the droplets depends on the gas flow this system has to be solved iteratively. In such a method, the way in which the solution region is constructed from control volumes is critical, particularly when there are large gradients in the flow field. It is also unclear how reliable the convergence of the method is.

An alternative approach to modelling the dynamics of liquid sprays is to consider the liquid droplet - gas system as consisting as a multiphase continuum, an approach which has been successfully applied to a number of physical phenomena involving gas particle flows. This method is attractive since the associated theory is developed from first principles and forms a coherent well established body of work. The underlying equations represent the dynamics of general multiphase system and can allow for effects such as surface tension, heat transfer, phase change and diffusion. As such the theory forms a framework for modelling multiphase flow systems and consequently when considering any particular system it is usual to make certain assumptions about its behavior and discard unnecessary terms from the governing equations. This is certainly the case for liquid droplet - gas systems.

Use of multiphase fluid dynamics to describe the spray produced by an irrigation sprinkler immediately allows the effect of a cross wind on the spray to be determined (requirement 2). Unfortunately, the theory provides no information regarding the structure of the spray. There being no appropriate structure theories in the literature, empirical methods have to be adopted to quantify the processes identified as requirements 4 and 5.

2.4   Conclusions

Due to the extensive use of large sprinklers in irrigation and its economic and environmental impact, there is a clear need for a model of this process. Such a model should have as little reliance as possible on

empirical results because of the high overheads associated with experimentation. Existing deterministic models are generally ad hoc in their derivation, and their predictions often match poorly with measurements of sprinkler application. Multiphase flow theory provides a general theory which accounts for the physical processes within the spray and allows the development of a new deterministic model. Although such a model still requires some empirical results to describe the structure of the spray, these experiments are significantly less time-consuming than those required for non-deterministic models.

Chapter 3

Transport Models for Liquid Sprays

3.1 Abstract

The equations of motion for rigid and deformable particles moving through a surrounding fluid are derived and their suitability for modelling liquid sprays reviewed. The concept of a multiphase continuum is introduced and a general formulation of the equations of motion for such a system presented. A constitutive relationship for a liquid droplet - gas multiphase mixture is developed using a force balance derived from the dynamics of individual droplets and incorporated into the equations of motion for a system where viscous dissipation is small compared to the dissipation due to drag. The result is a system of coupled first order partial differential equations. The application of the resulting equations is then demonstrated by modelling a one dimensional liquid - droplet gas flow in a duct.

Notation			
C_d	drag coefficient	r	droplet radius
ϵ	void fraction	χ	body force
ρ_l	liquid density	ρ_g	gas density
μ	viscosity	Re	Reynolds number
p	pressure	f	drag force

3.2 Introduction

Systems where large numbers of particles or liquid drops move through a surrounding fluid are common in many commercial applications such as pneumatic conveying, food processing, agricultural spraying and irrigation. Although the dynamics of an individual particle or drop in a surrounding fluid is well understood it is difficult to apply this theory directly to sprays. This is primarily due to the exchange of momentum that takes place between the drops and the surrounding fluid. Attempts have been made previously to modify the equations of motion to account for this effect by modifying, for example, the drag coefficient C_d. A more fruitful approach is to consider the spray as a multiphase continuum where not only the surrounding fluid but drops of different sizes constitute continuous phases. By considering the spray in such a way it is possible to derive equations of motion for each phase which include a constitutive equation which describes the momentum coupling between the phases.

In this work the dynamics of both rigid and deformable particles is overviewed. A constitutive relationship is then derived which is suitable for modelling the momentum coupling in a liquid drop - gas spray. An example of the use of the resulting mathematical model is provided.

3.3 The Dynamics of a Rigid Spherical Particle in a Surrounding Fluid

Let the position of a spherical particle be described by $\mathbf{r}$ and the motion of the surrounding fluid by the vector field $\mathbf{u}$. The manner in which $\mathbf{r}$ varies in time is then given by the second order system

$$m\ddot{\mathbf{r}}(t) = \mathbf{F}(\dot{\mathbf{r}}(t), \mathbf{u}(t); \gamma) + \mathbf{B} \tag{3.1}$$

where $\mathbf{B}$ is the body force, m the mass of the particle, γ a set of parameters dependent on the physical properties of the particle and surrounding fluid and $\mathbf{F}$ the force acting on the particle due to its motion through the fluid, (drag). If it is assumed that any modifications to the flow $\mathbf{u}$ due to the presence of the particle can be ignored then the dynamics of the particle are fully described by the form of $\mathbf{F}$ in conjunction with suitable initial/boundary conditions. It is conventional to define the scalar, (drag coefficient),

$$C_d = \frac{|\mathbf{F}|}{(\pi r^2)(\frac{1}{2}\rho v^2)} \tag{3.2}$$

where r is the radius of the particle, ρ the density of the surrounding fluid and $v = |\mathbf{u} - \dot{\mathbf{r}}|$. Equation (3.1) can then be rewritten

$$\ddot{\mathbf{r}} = \frac{3\rho_l C_d}{8\rho_p r}\mathbf{F}|\mathbf{F}|^{-1}v^2 + \mathbf{b} \tag{3.3}$$

where $\mathbf{b}$ is the body force per unit mass, and ρ_p the density of the particle. If it is further assumed that the force due to the motion through the fluid acts in a direction opposed to the relative velocity between particle and fluid then

$$\mathbf{F}|\mathbf{F}|^{-1} = (\mathbf{u} - \dot{\mathbf{r}})|\mathbf{u} - \dot{\mathbf{r}}|^{-1} \tag{3.4}$$

such that

$$\ddot{\mathbf{r}} = \frac{3\rho_l C_d}{8\rho_p r}(\mathbf{u} - \dot{\mathbf{r}})|\mathbf{u} - \dot{\mathbf{r}}| + \mathbf{b}. \tag{3.5}$$

The dynamics of a particle described by eqn.(3.5) are then fully specified by the properties of the particle and fluid along with the form of C_d.

Newton's experiments of 1710 gave

$$|\mathbf{F}| = 0.22\pi r^2 \rho_l v^2 \tag{3.6}$$

leading to $C_d = 0.44$. The experiments were conducted for fairly large v. By analysing the flow about a sphere at these velocities using the Navier-Stokes equation it is apparent that eqn.(3.6) accounts mainly for inertial effects. In 1850 Stokes suggested that at low relative velocities inertial effects are small enough so as to be ignored in the Navier-Stokes equation which lead him to postulate

$$|\mathbf{F}| = 6\pi\mu r v \tag{3.7}$$

giving

$$C_d = \frac{24.0}{\text{Re}} \tag{3.8}$$

where Re is the Reynolds number defined in terms of the particles diameter. The accumulation of further experimental work over a wide range of Reynolds number lead to the "standard" drag curve. The departure of Newton's and Stokes' results from the standard curve prompted the development of further expressions for C_d to account for the effects of vortices, wake and boundary layers [32]. The form of several of these expressions were chosen for ease of calculation during numerical analysis of eqn.(3.5). With recent advances in computer performance it has become viable to use less efficient but more accurate and robust representations of the standard drag curve using piecewise polynomial interpolation. Such an interpolation is provided by Morsi and Alexander [2] using

$$C_d = \frac{a}{\text{Re}^2} + \frac{b}{\text{Re}} + c. \tag{3.9}$$

The manner in which the coefficients a, b and c depend on Re is given in table 3.3. It is worth noting that care must be taken in evaluating C_d when given by eqn.(3.8) or eqn.(3.9) when $\dot{\mathbf{r}}$ is close to zero in which case the expression for drag should be combined with eqn.(3.5) and the Reynolds number canceled out.

Range	a	b	c
Re < 0.1	0	24.0	0
0.1 ≤ Re < 1.0	0.0903	22.73	3.69
1.0 ≤ Re < 10.0	-3.8889	29.1667	1.222
10.0 ≤ Re < 100.0	-116.67	46.5	0.6167
100.0 ≤ Re < 1000.0	-2778	98.33	0.3644
1000.0 ≤ Re < 5000.0	-4.75×10^4	148.62	0.357
5000.0 ≤ Re < 10000.0	57.87×10^4	-490.546	0.46
10000.0 ≤ Re < 50000.0	5.4167×10^6	-1662.5	0.5191

Table 3.1: Morsi and Alexander Coefficients for Approximating C_d.

3.4 The Dynamics of a Deformable Spherical Particle in a Surrounding Fluid

When modelling the drag forces acting on a fluid particle (droplet) moving through a surrounding immiscible fluid it may be necessary to consider the effects of particle deformation and the velocity distribution of the particle interior. Early studies attempted to form modifications to Stokes' law (3.8), such as that due to Hadamard [17] and Rybczynski [31]

$$|\mathbf{F}| = 6\pi\mu r v \frac{2\mu + 3\mu_p}{3(\mu + \mu_p)} \tag{3.10}$$

where μ_p is the viscosity of the particle interior. In the case of a water particle in air where $\mu_p \approx 64\mu$ the drag force is 90% of that as given by eqn.(3.8). However, as with Stokes law eqn.(3.10) is only valid for Re ≤ 1. Grace and Wairegi [42] provide an experimental comparison of C_d for a rigid particle using the standard drag curve to that of a water droplet in air for 0.1 ≤ Re ≤ 1000 (table 3.4). The manner in which

System	Re = 0.1	Re = 1.0	Re = 10	Re = 100	Re = 1000
C_d Standard Drag Curve	244.1	27.32	4.29	1.096	0.471
C_d Water Droplet in Air	239	27	4.23	1.08	0.51

Table 3.2: Drag Coefficients for Water Droplets in Air at Different Re. (Grace and Wairegi)

drops deform due to their motion is dependent on the properties of the drop and the surrounding fluid. Grace and Wairegi [42] characterised the deformation of bubbles and drops and in terms of the volume equivalent Reynolds number at terminal velocity and the dimensionless Eötvös number $E_o = 4\Delta\rho g r^2/\sigma$ where $\Delta\rho$ is the density difference between the phases and σ is the surface tension of the dispersed (droplet) phase. Their scheme indicates that water drops with $r > 0.7mm$ ($E_o \geq 0.3$) exhibit a significant departure from spherical at terminal (or greater) velocities. For $E_o \geq 16$ ($r \geq 3.65mm$) the drops are unstable and generally collapse before reaching terminal velocity.

In general, the internal flow and deformation of a drop moving through a surrounding fluid depends on the properties of the two fluids involved. Consequently it is difficult to arrive at an equivalent of the standard drag curve for deformable particles. As a result of this difficulty, the dynamics of liquid droplets are usually modelled using the standard drag curve. In general, for water droplets in air, this approach only results in small errors for Reynolds numbers of Re < 1000.

3.5 Multiphase Continuum Models

Eqn.(3.5) has been used in many areas for determining the trajectory of solid particles and drops. For example, Morsi and Alexander [2] have used it to determine the impact energy of particles on turbine blades. More recently it has been used in conjunction with computational fluid dynamics to predict the collection efficiency of environmental monitoring equipment. Indeed, most computational fluid dynamics packages offer a facility for injecting and tracking particles in the solution domain. However, in all of these cases, the flow of the surrounding fluid u is prescribed in advance and the particles presence does not alter this flow. However, when there are a sufficient number of particles (drops) present the flow can

be modified which in term alters the trajectories of the individual particles. Thus to successfully model the dynamics of such systems it is necessary to properly quantify the momentum exchange between the particles (or drops) and the surrounding fluid.

The use of field equations to describe the dynamics of a single pure fluid amount to one of the most significant products of applied mathematics. The field equations are arrived at by expressing the conservation of momentum and mass in terms of the field variables within an arbitrary control volume. The momentum (Navier-Stokes) equation when expressed in cartesian coordinates is

$$\rho \frac{d\mathbf{v}}{dt} = \rho \left[\frac{\partial \mathbf{v}}{\partial t} + \mathbf{v}(\nabla.\mathbf{v}) \right] = \chi + \nabla.\mathbf{T} \tag{3.11}$$

where q is the fluid velocity, ρ its density, $\mathbf{T}$ the (symmetric) stress tensor and χ the body force. Conservation of mass leads to the continuity condition

$$\frac{d\rho}{dt} + \rho \nabla.\mathbf{v} = \Gamma \tag{3.12}$$

where Γ represents a mass source/sink term. The tensor $\mathbf{T}$ forms the constitutive equation for the fluid and is generally expressed in terms of the hydrostatic pressure p and the rate of shear tensor e. For a Newtonian fluid the components T_{ij} of $\mathbf{T}$ are given by

$$T_{ij} = -p\delta_{ij} + 2\mu e_{ij} \tag{3.13}$$

where μ is dynamic viscosity and δ_{ij} the Kronecker delta defined in the usual manner. Taking the divergence of $\mathbf{T}$ and simplifying gives for an incompressible fluid

$$T_{ij,j} = -p_{,j} + \mu \nabla v_i^2 \tag{3.14}$$

such that the momentum equation (3.11) becomes

$$\rho \frac{\partial \mathbf{v}}{\partial t} + \mathbf{v}(\nabla.\mathbf{v}) = -\nabla p + \mu \nabla^2 \mathbf{v} + \chi \tag{3.15}$$

The nature of $\mathbf{T}$ is dependent on the type of fluid being modelled and the form used in deriving eqn.(3.15) corresponds to a Newtonian fluid. Eqns.(3.11) and (3.12) along with appropriate boundary conditions have been used to model fluid behavior with great success in a wide range of different circumstances.

Some fluid systems contain more than one type of fluid. When the fluids are homogeneously mixed it may be possible to treat the amalgam as a single fluid, the properties of which depend on the relative concentration of its components. This is common practice when considering the dynamics of gases such as air. Alternatively, some of the components may be immiscible in which case there is a boundary between two or more fluid types and each fluid can be thought of constituting a different phase. A general formulation of such a system usually requires the dynamics of the boundary to be considered in terms of inertia, pressure, phase change, mass flow, heat flow, surface tension and viscous forces. In these cases the regions filled by different fluids are usually solved as independent flow regimes with free boundaries and are generally difficult to analyse. However, certain special cases exist. For instance the case of pure stratified flow where only phase change, viscous resistance and heat transfer take place at the boundary. In a highly dispersed flow, such as may be encountered in fluidised beds and bubbly columns, the amalgam may be sufficiently mixed to consider forming the volume integrals associated with the derivation of the dynamics of a single phase and averaging the effects of the boundary interactions [35]. Intrinsic to such a derivation is the assumption that the suspension is saturated and as such its composition is quantified by the introduction of the volume or void fraction of each phase as basic variables. Where each phase is considered to be incompressible such a formulation in general leads to the following field equations.

$$\rho_i \frac{\partial \mathbf{v}_i}{\partial t} + \rho_i \mathbf{v}_i (\nabla.\mathbf{v}_i) = \rho_i \chi_i + \nabla.\mathbf{T}_1 \tag{3.16}$$

$$\frac{d\rho}{dt} + \rho \nabla.\mathbf{v}_i = \Gamma_i \tag{3.17}$$

$$\sum_i \epsilon_i = 0 \tag{3.18}$$

Here eqn.(3.16) and eqn.(3.17) are the momentum and continuity equations for the i_{th} phase and eqn.(3.18) is the saturation condition. Although it is possible to derive the $\mathbf{T}_i$ from first principles [35]

their form is not generally well understood and in many cases physical models for $\mathbf{T}_i$ lead to the equations of motion being ill conditioned [26]. However, a number of authors have arrived at successful formulations for several types of flow system. Applications have been found in the modelling of fluidised beds [37] [22], pneumatic conveyance [3], gas particle flows [45], bubbly columns and many other areas.

Equations (3.16), (3.17) and (3.18) may also be used to describe the dynamics of liquid droplets when moving through a gas i.e. sprays. In this case the flow is dispersed and for small diameter / high surface tension the droplets behave like solid particles and the the dynamics of the interface between the phases can be ignored. Furthermore, the momentum balance between the phases can be modelled by considering the void fraction of each phase and the force experienced by individual droplets as they pass through the gas which can be described by a modified version of eqn.(3.5). However, because the relationship between the droplets inertia and drag force varies according to its radius, each droplet size constitutes a new phase in the system. With these considerations the steady state momentum equations for each droplet phase can be written as

$$\rho_i \mathbf{v}_i (\nabla . \mathbf{v}_i) = \mathbf{f}_i + \chi_i \tag{3.19}$$

and

$$\rho_g \mathbf{v_g} (\nabla . \epsilon_g \mathbf{v}_g) + \sum_i \rho_i \epsilon_i \mathbf{v}_i (\nabla . \mathbf{v}_i) = -\nabla p + \chi_g \tag{3.20}$$

for the (incompressible) gas phase. In arriving at these equations droplet-droplet interactions have been ignored which eliminates the need to model pressure changes in the droplet phases. Furthermore, the gas phase is considered as inviscid, which proves to be a good approximation when the dissipative effects of drag are more significant than viscous dissipation. Continuity in each phase is expressed using

$$\rho_i \nabla . \epsilon_i \mathbf{v}_i = \Gamma_i \tag{3.21}$$

for the droplet phase and

$$\rho_g \nabla . \epsilon_g \mathbf{v}_g = \Gamma_g \tag{3.22}$$

for the gas. For n droplet phases in p dimensions, these equations along with the saturation condition

$$\epsilon_g + \sum_i \epsilon_i = 1 \tag{3.23}$$

result in $n(p+1) + p + 2$ equations in as many unknowns. Here, the $\mathbf{f}_i$ are given by eqn.(3.5) as

$$\mathbf{f}_i = \frac{3\rho_g C_d}{8r_i} (\mathbf{v}_g - \mathbf{v}_i) |\mathbf{v}_g - \mathbf{v}_i|. \tag{3.24}$$

where r_i is the radius of the i_{th} droplet.

In arriving at eqns.(3.19) and (3.20) a number of assumptions have been made regarding the nature of the constitutive relationship for the droplet - gas multiphase mixture. These assumptions have been made in such a manner as to encapsulate the physical properties of the mixture and to produce a system of equations which are well posed and amicable to numerical analysis. Furthermore, the formulation of the constitutive relationship has been made such as to satisfy the necessary criteria of consistency, isotropy and coordinate invariance.

3.6   One Dimensional Duct Flow

As an example of the application of multiphase equations the simple case of one dimensional duct flow is examined. In the case considered a multiphase mixture is injected into a duct such that all of the droplet phases have the same velocity. Furthermore, the droplet phase velocity is greater than the gas velocity. The velocity and void fraction of each phase at injection provide the initial conditions for the system. For $N = n + 1$ droplet phases the one dimensional form of eqns.(3.19)(3.20) (3.21)(3.22) and (3.23) can be written (having isolated the derivative terms and used eqn.(3.23) to eliminate ϵ_g) as

$$\mathbf{A(s)} \frac{\mathrm{d}}{\mathrm{d}x} \mathbf{s} = \lambda(\mathbf{s}) \tag{3.25}$$

where

$$\mathbf{s} = \begin{bmatrix} \epsilon_0 & v_0 & \cdots & \epsilon_n & v_n & v_g & p \end{bmatrix}^T \tag{3.26}$$

is the state vector for the system

$$
\mathbf{A(s)} =
\begin{bmatrix}
\rho_l v_0 & \rho_l \epsilon_0 & 0 & \cdots & & \cdots & 0 \\
0 & \rho_0 v_0 & 0 & \cdots & & & 0 \\
0 & 0 & \rho_l v_1 & \rho_l \epsilon_1 & & & \vdots \\
\vdots & \vdots & 0 & \rho_1 v_1 & & & \\
& & & & \ddots & & \\
& & & & \rho_l v_n & \rho_l \epsilon_n & \\
\vdots & \vdots & & & 0 & \rho_n v_n & \vdots \\
-\rho_g v_g & 0 & -\rho_g v_g & 0 & \cdots & -\rho_g v_g & 0 & \rho_g(1 - \sum_{i=0}^{n} \epsilon_i) & 0 \\
-\rho_g v_g^2 & \rho_l \epsilon_0 v_0 & -\rho_g v_g^2 & \rho_l \epsilon_1 v_1 & \cdots & \rho_g v_g^2 & \rho_l \epsilon_n v_n & \rho_g v_g(1 - \sum_{i=0}^{n} \epsilon_i) & 1
\end{bmatrix}
\tag{3.27}
$$

and

$$
\lambda(\mathbf{s}) = \begin{bmatrix} \Gamma_0 & f_0 + \chi_0 & \cdots & \Gamma_n & f_n + \chi_n & \Gamma_g & 0 \end{bmatrix}^T
\tag{3.28}
$$

Here quantities subscripted g relate to the gas phase. The determinant of the matrix $\mathbf{A(s)}$ is

$$
\rho_g(1 - \sum_{i=0}^{n} \epsilon_i) \prod_{j=0}^{n} \rho_l v_i
\tag{3.29}
$$

such that eqn.(3.25) has solutions so long as the $v_i \neq 0$ for all i. This is a potential limitation of the above formulation but does not affect this example or most other systems of the type being considered. Given an initial state vector $\mathbf{s}_0$ then $\mathbf{s}$ can determined by solving

$$
\mathbf{s} = \mathbf{A}^{-1}(\mathbf{s})\lambda(\mathbf{s})
\tag{3.30}
$$

using a suitable numerical scheme, in this case an adaptive fourth fifth order Runge-Kutta method [38].

A duct containing air [1] and ten water [2] droplet phases with diameters of 0.1mm to 1.0mm in 0.1mm increments has been considered. The droplet phases were injected at 20.0ms^{-1} into air flowing at 5.0ms^{-1}. Each droplet phase contained the same number of droplets (uniform droplet size distribution) and there are no sources or sinks in any of the phases. The system was solved for initial values of gas void fraction of $\epsilon_g(0) = 0.5$ and $\epsilon_g(0) = 0.9$ (50% and 90% gas by volume respectively). Figure 3.1 shows the results obtained.

It is clear that different initial gas void fractions have an effect on the evolution of the system. In particular the equilibrium velocity which the mixture convergages toward is significantly different. Changing the manner in which the droplet diameters are distributed also changes this equilibrium velocity but the difference is only small in comparison to those that result as a consequence of changing the initial gas void fraction. Changes in initial void fractions also alter the relaxation distance of the system. For smaller concentrations of gas the system tends toward its equilibrium velocity over a greater distance. A further point of interest is that in both cases the considered, the smaller droplets are decelerated to velocities smaller in magnitude than the equilibrium velocity.

Results have also been obtained for a duct with the same initial gas void fractions as above but with only one droplet phase. By varying the diameter of the droplet phase it is possible to determine a diameter which results in a similar equilibrium velocity and response distance as is given when considering a larger number of droplet phases. Several different distributions of droplet diameters have been considered in this way and in each case the diameter of the single phase is approximately the ratio of the third and second moments of the distribution. This diameter is commonly referred to the Sauter mean diameter[25].

3.7 Discussion

The use of the equations of motion of an individual droplet eqn.(3.5) is of limited use when describing the dynamics of systems where the motion induced in the surrounding fluid cannot be ignored. Modifications to eqn.(3.5) to account for the effect of this induced flow are difficult to develop and any implementation of this kind is usually system specific. A more general formulation of the dynamics of a liquid droplet - gas spray can be achieved by considering the spray as a multiphase mixture. Such a formulation has been presented for a system of liquid droplets (particles) in a surrounding gas where the dissipative effects of viscosity are small when compared to that due to drag.

---

[1] Density of air taken as 1.2 kg.m^{-3} and dynamic viscosity as 18.15 × 10^{-5} kg.m^{-1}.s^{-1}

[2] Density of water taken as 998.2 kg.m^{-3}

Clearly, the application of a one dimensional multiphase model for liquid sprays is of limited use. However, in systems that exhibit axial symmetry such as the case considered here, one dimensional models have been used with some success. Furthermore, analysis of the one dimensional equations of motion provides some insight to the nature of the phase space in which the solution trajectory $s(x)$ is contained. This in turn allows the uniqueness of the solutions to be determined and the suitability of various numerical schemes for application to the equations to be assessed [27]. Analysis of the multiphase equations suggest that they are amicable to numerical analysis in higher dimensions. Types of method suitable for this kind of analysis are a variety finite difference, finite volume and finite element schemes. In particular, multiphase systems have been solved in two dimensions using finite difference schemes [22], although the manner in which such methods are applied are highly dependent on the nature of the boundary conditions and solution domain geometry. Preliminary work undertaken by the author suggest that finite element methods may be employed to analyse multiphase systems of the type developed in section 3.5 in two and three dimensions, although the efficiency of such schemes tends to be poor when a large number of phases have to be considered.

It is difficult to assess the validity of the constitutive equation used in deriving the equations of motion the multiphase droplet - gas system. This is true of all but the most general representations for multiphase constitutive equations and this area is still a source of much research and debate within the fluid dynamics community. Consequently, the suitability of the multiphase equations of motion presented here for modelling the dynamics of a liquid sprays must be addressed prior to use by examining the physical significance of the assumptions made during their derivation. Ultimately, their suitability can only be judged via their application to modelling systems which provide experimental data for validation of the model.

Possible areas of application for the use of the mutliphase equations of motion for modelling the dynamics of liquid (or particle) sprays are in pneumatic transport and food processing, spray/evaporative cooling, combustion systems and agricultural spraying and irrigation.

3.8 Conclusions

The equations of motion for rigid and deformable particles passing through a surrounding fluid are well understood when considering individual particles. However, when considering groups of particles, (e.g. sprays), it may be necessary to modify the equations of motion to accurately account for the momentum balance between the particles and surrounding fluid. To achieve this a model has been developed whereby the mixture of particles and surrounding fluid is considered as a multiphase continuum. In the model, particles of different sizes constitute individual phases. A simple example showing how the equations of motion can be used to describe the dynamics of a liquid droplet-gas mixture has been presented.
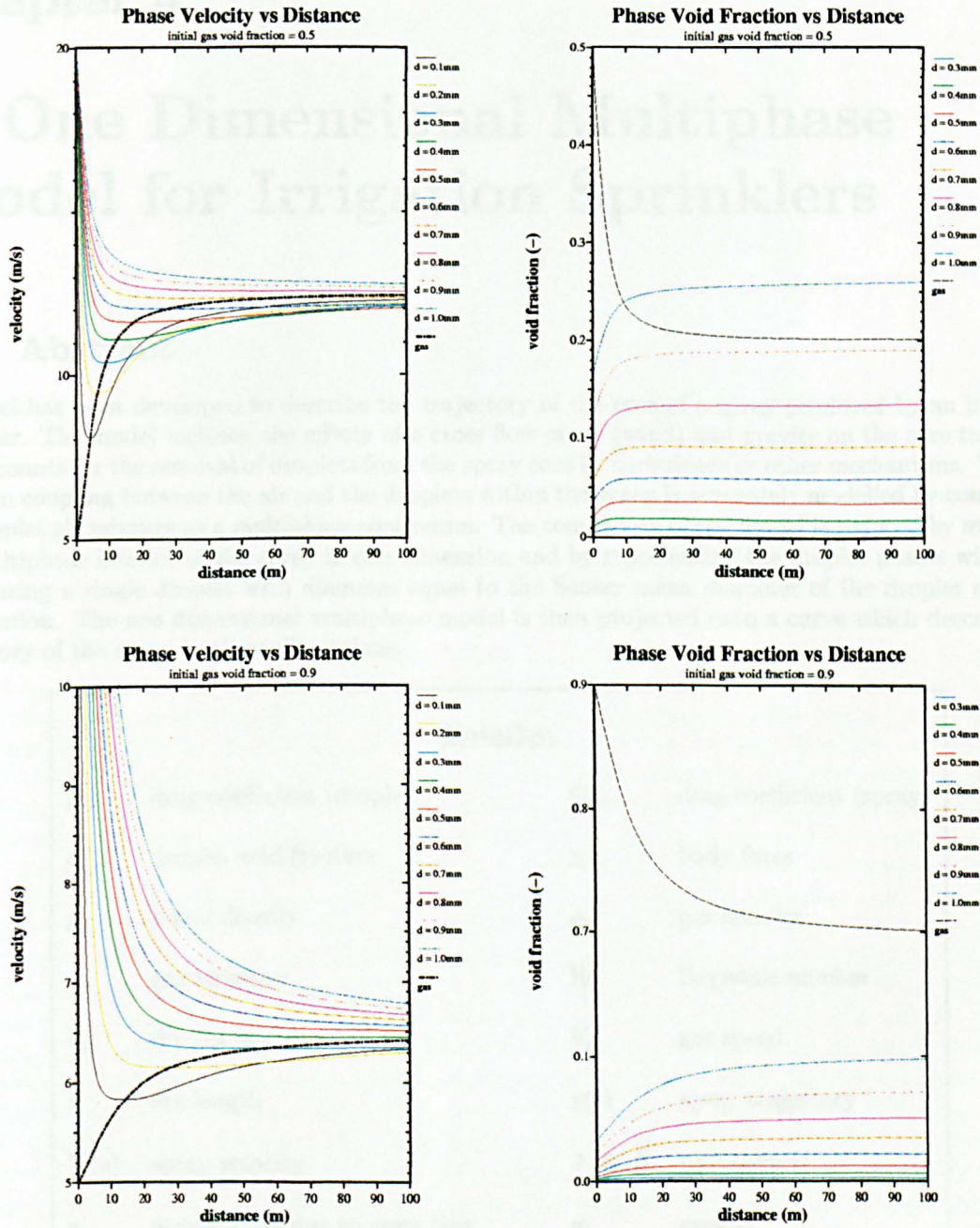
Figure 3.1: Variation of velocity and void fractions in a one dimensional duct. Initial gas void fraction of 0.5 (top) and 0.9 (bottom). Void fractions for smaller diameter drops have been removed for clarity.

Chapter 4

A One Dimensional Multiphase Model for Irrigation Sprinklers

4.1 Abstract

A model has been developed to describe the trajectory of the core of a spray produced by an irrigation sprinkler. The model includes the effects of a cross flow of air (wind) and gravity on the core trajectory and accounts for the removal of droplets from the spray core by turbulence or other mechanisms. The momentum coupling between the air and the droplets within the spray is accurately modelled by considering the droplet air mixture as a multiphase continuum. The complexity of the model is reduced by modelling the multiphase interior of the spray in one dimension and by representing the droplet phases within the spray using a single droplet with diameter equal to the Sauter mean diameter of the droplet diameter distribution. The one dimensional multiphase model is then projected onto a curve which describes the trajectory of the spray in three dimensions.

	Notation		
C_d	drag coefficient (droplets)	C_{dc}	drag coefficient (spray)
ϵ_d	droplet void fraction	χ	body force
ρ_d	liquid density	ρ_g	gas density
μ_g	gas viscosity	Re	Reynolds number
V_d	droplet speed	V_g	gas speed
s	arc length	$\mathbf{r}(s)$	spray trajectory
$\mathbf{V}(s)$	spray velocity	$\hat{\tau}\ \hat{n}\ \hat{\beta}$	unit vectors
$\mathbf{a}_c$	acceleration due to cross flow	$\mathbf{g}$	gravity
r_d	droplet radius	$\mathbf{w}$	cross flow
Γ_d	droplet sink/source	Γ_g	gas sink/source
p	pressure	$\mathbf{f}$	droplet drag force
r_j	plume radius		

4.2 Introduction

It is apparent that some systems which eject liquid at high velocity from a nozzle into a surrounding gas, such as irrigation sprinklers, produce a spray which consists of high speed jet or plume which liberates droplets along its length, figure 4.1. Previous studies regarding the structure of such plumes show that

Figure 4.1: Typical irrigation sprinkler and trolley.

for typical nozzle velocities the plume is fully broken up, (consists of individual droplets), at distances close to nozzle compared to the overall length of the plume [1]. Under these circumstances it may be possible to consider the plume as a compact spray such that the dynamics of the plume can be described using eqns.(3.19),(3.20),(3.21), (3.22) and (3.23). It is apparent however that the plume occupies only a small fraction of the volume of the overall spray, the remainder containing droplets which are dispersed to an extent whereby they can be considered as behaving autonomously. Consequently, it is inefficient to treat the whole region as a multiphase continuum, especially since, as in the case of irrigation sprinklers, the primary area of interest lies outside the plume. A more efficient approach is to model the plume as a multiphase continuum and treat individual droplets leaving it ballistically using eqn.(3.5). Furthermore, if radially averaged quantities are used to represent the plume and any interaction with a cross-flow and surrounding boundary layer are modelled separately (figure 4.2 B), eqns.(3.19),(3.20),(3.21), (3.22) and (3.23) can be solved as a one dimensional flow representing the core of the plume. This approach is particularly justifiable when the plume exhibits low curvature which is generally the case for irrigation sprinklers, (flat ejection angle). The complexity of the underlying equations can be further reduced by considering the plume as a two phase mixture consisting of a gas (air) phase and a single droplet phase with drop radius chosen to represent the bulk structure of the spray. The dynamics of this flow can then be superimposed onto a parameterized representation of the jet trajectory (figure 4.2 A). Effectively, this approach to modelling irrigation sprinklers is similar to that of Augier [4] with the jet trajectory modified to account for the presence of a cross-flow and momentum coupling between the droplet and gas phases.

4.3 Mathematical Model

4.3.1 Plume Dynamics

Let a point on the plume of droplets produced by the sprinkler be represented by the position vector $\mathbf{r}(s)$ parameterized in terms of the trajectory arc-length s (figure 4.2 A). The trajectory can then be described in terms of $\mathbf{r}(s)$ as

$$\begin{bmatrix} |\mathbf{V}(s)| & 0 \\ 0 & |\mathbf{V}(s)| \end{bmatrix} \frac{d}{ds} \begin{bmatrix} \mathbf{r}(s) \\ \mathbf{V}(s) \end{bmatrix} = \begin{bmatrix} \mathbf{V}(s) \\ \chi \end{bmatrix} \tag{4.1}$$

where $\mathbf{V}(s)$ is the plume velocity. Here χ is the force per unit mass acting on the jet and includes the effects of gravity, cross flow and boundary layer growth (figure 4.2 C). The components of force acting on
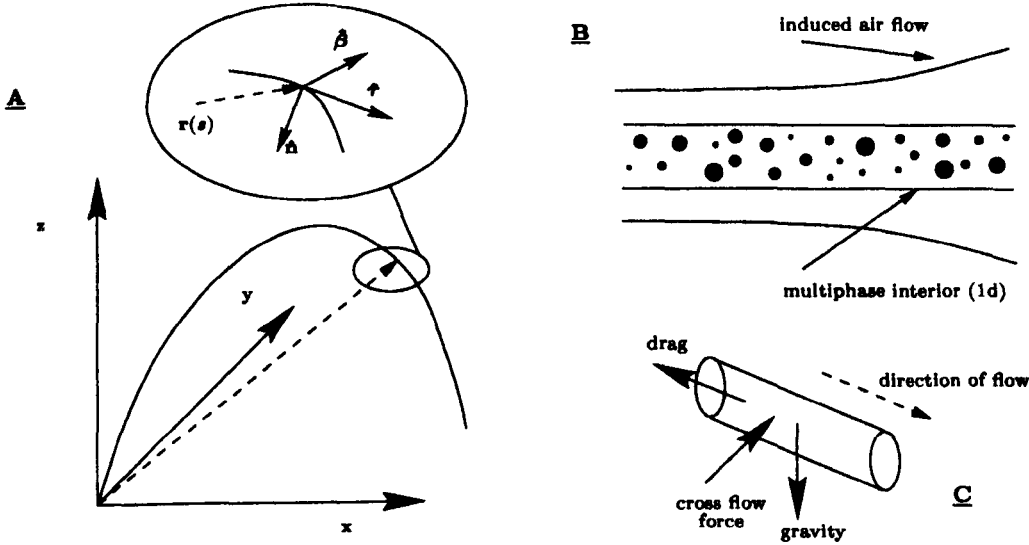
Figure 4.2: Model concept. A) Parameterised description of spray trajectory and using curvilinear coordinate system. B) Multiphase representation of spray interior and induced boundary layer. C) External forces acting on a section of the spray.

the plume are best described using a curvilinear coordinate system defined at a point along the trajectory in terms of the unit vectors $\hat{\tau}$, $\hat{n}$ and $\hat{\beta}$, (the unit tangent, normal and binormal). These can be expressed in terms r by using the Frenet Serret formula

$$\hat{\tau} = \frac{d\mathbf{r}}{ds} \tag{4.2}$$

$$\hat{n} = |\frac{d\hat{\tau}}{ds}|^{-1}\frac{d\hat{\tau}}{ds} \tag{4.3}$$

$$\hat{\beta} = \hat{\tau} \times \hat{n}. \tag{4.4}$$

Quantities expressed in this coordinate system are subscripted accordingly using τ, n or β.

If the speed of the plume interior is $V_d(s)$ then the acceleration acting along the tangent of the trajectory is simply

$$\mathbf{a} = |V_d|\frac{d}{ds}V_d\hat{\tau} \tag{4.5}$$

So long as any component of cross flow $\mathbf{w}$ acting along the tangent of the trajectory is incorporated into the multiphase equations (chapter 3) then its effect can be accounted for within eqn.(4.5). The other components of acceleration due to the cross flow are accounted for by projecting $\mathbf{w}$ onto the plane containing $\hat{n}$ and $\hat{\beta}$ and considering the plume of radius r_p to interact with the cross flow as if it were an impermeable cylinder. The resulting acceleration acting on the plume due to the cross flow is

$$\mathbf{a}_c = \frac{\rho_g C_{dc}}{2\pi\rho_l r_p}\left((\mathbf{w}.\hat{n})\hat{n} + (\mathbf{w}.\hat{\beta})\hat{\beta}\right) \tag{4.6}$$

where $C_{dc} = 1.80$ is the effective drag of the multiphase cylinder [7]. Expressing the acceleration due to gravity in the local coordinate system gives

$$\mathbf{g} = (\mathbf{g}.\hat{\tau})\hat{\tau} + (\mathbf{g}.\hat{n})\hat{n} + (\mathbf{g}.\hat{\beta})\hat{\beta} = \mathbf{g}_\tau + \mathbf{g}_n + \mathbf{g}_\beta \tag{4.7}$$

Once again, the tangential component $\mathbf{g}_\tau$ is removed and incorporated into the multiphase equations representing the plume interior. Combining eqns.(4.5),(4.6) and (4.7) to form χ gives from eqn. (4.8)

$$\begin{bmatrix} V_d(s) & 0 \\ -V_d(s)\frac{d}{ds}V_d(s) & V_d(s)| \end{bmatrix} \frac{d}{ds} \begin{bmatrix} \mathbf{r}(s) \\ \mathbf{V}(s) \end{bmatrix} = \begin{bmatrix} \mathbf{V}(s) \\ \mathbf{a}_c + \mathbf{g}_n + \mathbf{g}_\beta \end{bmatrix} \tag{4.8}$$

noting that $V_d(s)$ has been substituted for $|\mathbf{V}(s)|$, a good approximation when the curvature of the plume is small.

4.3.2 One Dimensional Plume Flow

In general when modelling a multiphase liquid droplet gas system it is necessary to consider droplets of different diameters within the spray as constituting a phase in their own right (chapter 3 section 3.5). When considering n droplet phases in one dimension this approach leads to $2n + 2$ coupled first order differential equations. To reduce the number of calculations necessary for describing the dynamics of the spray the model only considers one droplet phase and hence a single droplet diameter. This diameter is chosen so as to represent the distribution of droplet diameters within the spray. In practice it is found that choosing the Sauter mean diameter of the distribution for this purpose leads to a good representation of the bulk characteristics of the spray (chapter 3 section 3.6). The use of a single droplet diameter has the further advantage of making $V_d(s)$ in eqn.(4.8) easy to evaluate.

Writing eqns.(3.19),(3.20),(3.21),(3.22) and (3.23) in one dimension for a two phase (gas/liquid droplet) system gives

$$\rho_g \frac{d}{ds}\left[\epsilon_g(s)V_g(s)\right] = \Gamma_g(s) \tag{4.9}$$

$$\rho_d \frac{d}{ds}\left[\epsilon_d(s)V_d(s)\right] = \Gamma_d(s) \tag{4.10}$$

$$\rho_g(s)V_g(s)\frac{d}{ds}\left[\epsilon_g(s)V_g(s)\right] + \rho_d(s)\epsilon_d(s)V_d(s)\frac{d}{ds}V_d(s) + \alpha(V_g(s) - \mathbf{w}.\hat{\tau}) = -\frac{d}{ds}p + \rho_g\mathbf{g}.\hat{\tau} \tag{4.11}$$

$$\rho_d V_d(s)\frac{d}{ds}V_d(s) = f + \rho_d\mathbf{g}.\hat{\tau} \tag{4.12}$$

$$\epsilon_g(s) + \epsilon_d(s) = 1 \tag{4.13}$$

where the subscripts g and d have been used for the gas and droplet phases respectively. Here, V represents the phase velocity, ϵ the void fraction, Γ source/sink terms, p pressure and f the drag force acting on the droplet phase. The tangential components of body force have been included in the momentum equations. In eqn.(4.11), the term $\alpha(V_g(s)-\mathbf{w}.\hat{\tau})$ represents the momentum exchanged between the multiphase plume and the surrounding air (boundary layer) and includes the contribution from the tangential component of $\mathbf{w}$. It is based on the result obtained by Morton [40] that was subsequently used by Gosh and Hunt [21] when modelling the dynamics of flat fan sprays. Following Gosh and Hunt $\alpha = 0.11$.

Having expanded any derivatives of products and eliminated ϵ_g using eqn.(4.13) then eqns.(4.9), (4.10),(4.11) and (4.12) can be written in matrix form as

$$\mathbf{A}(s)\frac{d}{ds}\mathbf{x}(s) = \mathbf{b}(s) \tag{4.14}$$

where

$$\mathbf{A} = \begin{bmatrix} \rho_d V_d & \rho_d\epsilon_d & 0 & 0 \\ 0 & V_d & 0 & 0 \\ -\rho_g V_g & 0 & \rho_g(1-\epsilon_d) & 0 \\ -\rho_g V_g^2 & \rho_d\epsilon_d V_d & \rho_g V_g(1-\epsilon_d) & 1 \end{bmatrix} \tag{4.15}$$

and

$$\mathbf{x} = \begin{bmatrix} \epsilon_d & V_d & V_g & P \end{bmatrix}^T \quad \mathbf{b} = \begin{bmatrix} \Gamma_d & f + \rho_g\mathbf{g}.\hat{\tau} & \Gamma_g & \alpha(\mathbf{w}.\hat{\tau} - V_g) + \rho_g\mathbf{g}.\hat{\tau} \end{bmatrix}^T \tag{4.16}$$

The gas-liquid drag force f is taken as that as would act on an individual droplet and is given by

$$f = \frac{3\rho_g C_d}{8r_d}(V_g - V_d)^2 \tag{4.17}$$

with the Reynolds number Re defined as

$$Re = \frac{2\rho_g r_d|V_d - V_g|}{\mu_g} \tag{4.18}$$

where μ_g is the kinematic viscosity of the gas. The droplet radius r_d used to represent the spray interior is taken as the Sauter mean diameter (section 3.6 and the form of drag coefficient used is that as given by Morsi and Alexander [2]. When combined with initial conditions for ϵ_d, V_d, V_g and p eqns.(4.8) and (4.14) can be solved using an appropiate numerical technique to obtain the trajectory of the core of the multiphase plume. As noted previously, the structure of the plume is represented by a single droplet size, r_d in eqn.(4.18), calculated using the Sauter mean diameter. To allow for a wide range of Reynolds number the form of the drag coefficient C_d used is that as given by Morsi and Alexander [2].

4.4 Model Analysis and Conclusions

Together, eqns.(4.8) and (4.14) provide a means of predicting the trajectory of a multiphase plume in the presence of a cross-flow. Both these equations are of the form

$$\mathbf{B}\frac{d}{ds}\mathbf{y} = \mathbf{c} \tag{4.19}$$

and in general solutions are obtained using a numerical technique. Such solution schemes rely on $\mathbf{B}$ being non-singular everywhere along the trajectory. This is the case for eqn.(4.8) when $V_d \neq 0$. Evaluation of the determinant of A yields

$$|\mathbf{A}| = \rho_d \rho_g V_d^2 (1 - \epsilon_d) \tag{4.20}$$

It is apparent that $\mathbf{A}$ is singular for values of $V_d = 0$ and/or $\epsilon_d = 1$, the latter condition occurring at the nozzle of the sprinkler where the initial conditions for the model are imposed. In practice, the dynamics of the spray near the nozzle can be represented by a parabolic trajectory until droplets have been removed from the spray such that $\epsilon_d < 1$. The parabolic model can then be used to provide the appropriate initial conditions for multiphase model.

For the model to be of practical use it is necessary to quantify the source/sink terms Γ_g and Γ_l. The model does not provide a means of predicting the removal rate of droplets from the plume although it can be assumed that

$$\Gamma_g = \frac{\rho_d}{\rho_g}\Gamma_d \tag{4.21}$$

Consequently some means of evaluating Γ_d is required before the model can be used (see chapter 5). Drops which make up the sink term Γ_d are assumed to have an exit velocity equal to that of the plume at the ejection point. Thus the plume trajectory provides the initial conditions necessary for solving the equations of motion for individual droplets leaving it. This allows for determination of Γ_d by measurements made outside the plume.

Having specified Γ_d the model can be used to predict the dynamics of the spray produced by an irrigation sprinkler under a variety of different operating conditions and variable cross flows (winds).

Chapter 5

Droplet Size Distributions

5.1 Abstract

The distribution of droplet diameters within the spray produced by several different overhead sprinklers operating at different pressures and using different nozzle diameters has been measured. The measurements have been made at different distances from the sprinkler nozzle at ground level using two optical particle sizing instruments. Sources of errors within the data have been considered and the suitability for describing the sample data using a number of different types of continuous distribution function have been examined. The application rate of the sprinklers has also been measured to allow the distribution data to be normalized. The normalized distribution functions are then used to provide a parametric model of the data which allows the number distribution of the droplet diameters to be predicted at different distances from the nozzle. This information is necessary for the development of models to simulate water application from overhead sprinklers operating under different conditions.

	Notation		
D	droplet diameter	λ_m	m_{th} moment
v	volume fraction	X^2	chi squared figure
$\bar{D}_{pq}^{p-q}$	$= \lambda_p / \lambda_q$	$d\Lambda(D\|\mu, \sigma)$	lognormal distribution

5.2 Introduction

The one dimensional model developed in chapter 4 represents the plume interior by use of a single droplet diameter which for a given sprinkler has to be determined. Furthermore, to use the model successfully, the sink term Γ_d of the droplet phase in eqn.(4.16) has to be quantified. Both of these quantities could be determined from knowledge of the structure of the plume interior. Unfortunately, because of the scale of the system, conducting measurements within the plume interior is impractical. However, it is possible to determine the structure of the spray at ground level and having made certain assumptions about how droplets leave the plume (chapter 6) it is possible to reconstruct the plume interior from this information. This approach requires knowledge of the distribution of droplet diameters within the spray at each point on the ground for a single radial extending from the sprinkler to the extremities of the wetted region. To allow the droplet size distribution to be specified for an arbitrary point along the radial, interpolations between the measured distributions are necessary. To achieve this parameterized probability density functions are used to describe the distribution of droplet diameters and the suitability of a number of different distribution types for this purpose are examined in section 5.6.

Once the parameters of the probability density functions have been determined for each measurement point their values can be interpolated between to provide information about the spray structure for each point on the ground. The use of interpolation in this way prevents mixing the distribution types used to model the spray.

5.3 Droplet Size Measurements

Many methods for droplet sizing exist [25] and the suitability and accuracy of any one method depends on the nature of the system being investigated. For certain systems, sampling efficiency is also a consideration. In the case of measuring the droplet size distributions within the spray produced by a large sprinkler, the potential for the existence of large energetic droplets precludes the use of most intrusive collection methods such as sensitive paper, imiscible liquids or fibrous medias. Some attempts have been made to use the "flour pellet" method [20] though the validity of the results are questionable[1] and this approach is known to be highly inefficient. Non intrusive optical techniques are in general considered to be more suitable for measuring droplet size distributions produced by sprinklers. However these methods also exhibit certain limitations which must be addressed and some of these limitations are discussed in section 5.5.

To provide the droplet size measurements required as input data to the simulation, two optical techniques were used simultaneously. The use of two different techniques provides some insight to the consistency between these methods when used for this type of measurement. Both of the methods use purpose built instrumentation, the Spectro Optique Pluviometre (SPO) developed by L'Institut de Mécanique de Grenoble and the Particle Measuring Systems Optical Array Probe 260X (OAP). The measurements of droplet/particle size made by both of these instruments are based on the obscuration of light directed to fall on a detector. In the case of the OAP, the light source is a low power Helium Neon laser which is directed across a sampling region onto an array of sixty four photo-diodes. The design of the optics of this system is such that only the diameter of the droplet is measured. In the case of the SPO, an infrared source is used and the detector is a single photo resistor. The change of resistance of the photo resistance is proportional to the droplets cross sectional area from which its diameter can be calculated. Since the duration of the change in resistance can also be measured, some indication of the particles speed is possible. The largest droplet that can be measured by the SPO is 15mm diameter compared to 4.7mm diameter for the OAP. However, the resolution provided by the OAP is 75μm.

5.4 Methodology

The measurements were undertaken at the purpose built test facility in Aix en Provence maintained by CEMAGREF[2]. The facility consists of a 70m long tapered drainage channel with a turret housing the sprinkler under test located at the narrow end (figure 5.1). The turret is designed such that water only leaves it in directions whereby it can be collected in the drainage channel. Water delivered by the sprinkler can then be drained from the turret and channel and returned to the water source, in this case a small river, with minimal loss. This allows prolonged and uninterrupted measurements to be made. Catch cans are located in the drainage channel every 0.5m which allow the radial variation of the application rate from the sprinkler to be measured. Water is supplied to the sprinkler by an electric pump and a controller is used to maintain a constant head.

For the purposes of the investigation a framework was constructed to which the OAP and SPO were mounted (5.1) enabling droplets within the spray to be sampled simultaneously by both instruments. The framework could be located at any point along the drainage channel and inclined so as to maximize collection efficiency. Measurements were taken at 5m intervals along the drainage channel starting at 5m from the sprinkler nozzle. The duration of each sampling period was chosen such that in general > 3000 droplets were sampled at each location. However, as the distance from the nozzle is increased the time required for this requirement to be met prevented this number being collected at the extremities of the sprinklers throw.

Measurements were made in this manner for the sprinkler types[3], nozzle sizes and operating pressures indicated in table 5.1. The measurements were only made during periods when there was little or no wind, typically during the night. No measurements were made when measurements of instantaneous wind speeds rose above 1.0ms^{-1}. Prior to use, both instruments were calibrated using glass and steel balls of varying diameter. Individual droplets produced using a constant head tank and needle were measured to assess the effectiveness of the instruments when measuring liquid droplets.

---

[1]Personal communication with E. K. Weatherhead, Institute of Water and Environment, Cranfield University at Silsoe, Silsoe, Bedfordshire. UK.

[2]Centre National du Machinisme Agricole, du Génie Rural, des Eaux et des Fôrets.

[3]Equipment supplied by Komet.

Figure 5.1: Test facility at Aix-en-Provence (top and middle). The SPO (silver) and OAP (bronze) (bottom).

Sprinkler Model	Komet 101						Komet 202			
Nozzle Diameter (mm)	18			22			25		27.5	
Pressure (Bar)	3.5	4.5	5.5	3.5	4.5	5.5	4.5	5.5	4.5	5.5

Table 5.1: Summary of sprinkler models, nozzle diameters and operating pressures for which droplet sizes were measured

5.5 Measurement Errors

There are several sources of error within the droplet size measurements undertaken in the manner described in the previous section. Most of these are a consequence of the design of the instrumentation and the signal processing algorithms used to process the data. Some of these errors, such as those due to resolution and the maximum (minimum) measurable droplet size are quantifiable. Another quantifiable error is generated due to the use of a finite sampling area. The design of both the OAP and the SPO are such that droplets that cross the boundary of the sampling region are "edge" rejected from the sample. If the sampling area width is ω then the nominal probability $p(D)$ of sampling a droplet with diameter D from the spray is reduced to $p'(D)$ where

$$p'(D) = \begin{cases} (\omega - D)p(D) & 0 \leq D \leq \omega \\ 0 & \text{otherwise} \end{cases} \tag{5.1}$$

It is straightforward to reconstruct the sample from the edge rejected data using the relationship between $p(D)$ and $p'(D)$, however errors induced through this process can become significant when D is close to ω, particularly when the sample size is small. The effect of this kind of perturbation has been simulated for a uniform variate $x[0,1]$ and is demonstrated in figure 5.2 along with the original and reconstructed sample.

In addition to edge rejection the SPO and OAP "bulk area" rejected data that correspond to droplets that overlap in the sampling region. In the case of the OAP this is performed internally by the instruments hardware whereas the SPO relies on the its post processing software. Neither instrument has the capability of determining the size of these image coincidence errors so it is important that this rejection process is performed. If it were not droplets of artificially large diameter would be included in the data and could account for a significant percentage of the volume of the spray. The effects of bulk area rejection are harder to quantify than those due to edge rejection. Certainly, the effects are dependent on spray density and the distribution of the droplet diameters. The effects of bulk area rejection have been simulated for the case of a dense spray using the same data as used for the edge rejection simulation. The results are shown in figure 5.2. It may be possible to quantify these effects analytically, in which case it should be determined if the sample can be uniquely reconstructed from the data.

The effects of droplet deformation discussed in section 3.4 have been examined in the laboratory by allowing droplets of known diameter to fall under the influence of gravity through the sampling region of the OAP, (the OAP has a better resolution than the SPO). The droplets were produced using a constant head reservoir and hyperdermic needles of different diameters. Varying the height of the reservoir serves to increase the speed of the droplets as they pass through the sampling area. As the speed is increased the measured droplet diameters becomes increasingly distributed and the mean value increases. The distribution of measured diameters is produced due to oscillations in the droplet surface initiated when the droplet is released from the needle. The increase in the mean value corresponds to the deformation of the droplets due to their motion (3.4). The deformation of droplets of 1mm diameter was typically $150\mu m$ when traveling at $\sim 70\%$ of terminal velocity. It is difficult to account for this type of error in the measurements made of the spray. Even though the SPO can nominally determine the droplet speed the extent of the deformation is determined by the relative speed of the droplet and surrounding air and significant induced air motion is expected in the sampling region.

Further errors within the measurements occur due to the environment in which the instrumentation is used.
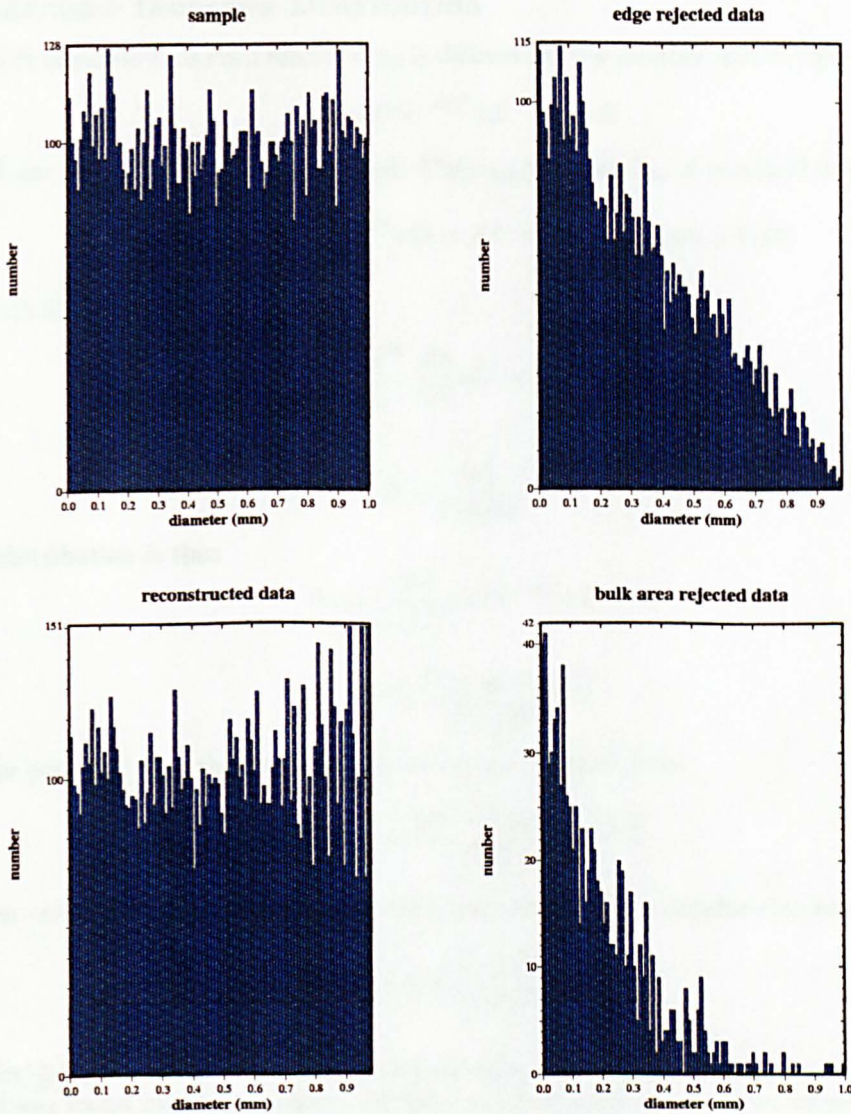
Figure 5.2: Sources of error in the droplet size data. Test sample (top left), edge rejected sample (top right), sample reconstructed from edge rejected data (bottom left) and bulk area rejection of the sample (bottom right).

In particular, droplets within the spray can strike the instrument casing producing secondary droplets. The measurements made using individual droplets to determine the effects of droplet deformation demonstrate the presence of these secondary droplets. Their diameters are typically less than 275μm and their number increases with droplet energy.

5.6   Statistical Models for Droplet Diameter Data

Several types of distribution function have been considered for describing the droplet size data. The relative suitability of each type is determined by estimating the parameters of each distribution and comparing the resulting X^2 in each case. Since any one distribution type may not produce the lowest X^2 for every data set modelled it is necessary to choose the type which results in the smallest X^2 in the greatest number of cases. Although some of the distributions considered are more successful when describing the droplet size data in terms of its volume or area distribution only number distributions are compared since this is form required for simulation purposes. However accurate representation of the volume data is important since individual distributions are normalized against the catch can data (5.7). A brief description of each distribution is provided.

5.6.1 Nukiyama-Tanasawa Distribution

The empirical Nukiyama-Tanasawa relationship is defined for the number distribution as

$$dn = \beta D^2 e^{-bD^\delta} dD \quad 0 \le D \tag{5.2}$$

where b and δ are parameters to be determined. The m_{th} moment λ_m of eqn.(5.2) is given by

$$\lambda_m = \beta \int_0^\infty D^{m+2} e^{-bD^\delta} dD = \beta \delta^{-1} b^{-(m+1)/\delta} \Gamma((m+1)/\delta) \tag{5.3}$$

such that eqn.(5.2) can be normalized using

$$\int_0^\infty \frac{dn}{dD} dD = 1 \tag{5.4}$$

giving

$$\beta = \frac{\delta b^{\frac{3}{\delta}}}{\Gamma(3/\delta)}. \tag{5.5}$$

The number distribution is then

$$dn = \frac{\delta b^{\frac{3}{\delta}}}{\Gamma(3/\delta)} D^2 e^{-bD^\delta} dD \tag{5.6}$$

and

$$\lambda_m = \frac{b^{-\frac{m}{\delta}} \Gamma((m+3)/\delta)}{\Gamma(3/\delta)} \tag{5.7}$$

It follows from eqn.(5.7) that the mean diameters can be obtained from

$$\bar{D}_{pq}^{pq} = \frac{\lambda_p}{\lambda_q} = \frac{b^{(q-p)/\delta} \Gamma((p+3)/\delta)}{\Gamma((q+3)/\delta)} \tag{5.8}$$

For a given value of δ, b can be estimated for a data set $\{D_i\}$ by transforming eqn.(5.6) to

$$\ln(\frac{1}{D^2} \frac{dn}{dD}) = \ln\left[\frac{\delta b^{\frac{3}{\delta}}}{\Gamma(3/\delta)}\right] - bD^\delta \tag{5.9}$$

This renders $\ln(\frac{1}{D} \frac{dn}{dD})$ linear in D^δ allowing standard regression techniques to be employed. Traditionally, the value of δ was found by trial and error. Mugele and Evans [16] suggest that values for δ of 1, $\frac{1}{2}$, and $\frac{1}{3}$ usually provide the best fit to the transformed data, though it is unclear why this should be the case. The value for δ which results in the smallest X^2 for a given data set can be obtained in a systematic manner by employing relatively simple recursive techniques. For the droplet size data, such a method was employed using the built in functions available in Applixware[4].

5.6.2 Rosin-Rammler Distribution

The Rosin-Rammler distribution is usually defined in terms of the volume distribution as

$$v = 1 - e^{-(D/\alpha)^\delta} \quad D \ge 0 \tag{5.10}$$

where v is the volume fraction, $(0 \le v \le 1)$. Differentiating eqn.(5.10) with respect to D, dividing by D^3 then normalizing gives the number distribution

$$dn = \frac{\delta \alpha^{3-\delta}}{\Gamma(1-3/\delta)} D^{\delta-4} e^{-(D/\alpha)^\delta} dD \tag{5.11}$$

The m_{th} moment is then given by

$$\lambda_m = \alpha^{m-3} \Gamma(1 - (n-3)/\delta) \tag{5.12}$$

From eqn.(5.12) the mean diameters can be determined as

$$\bar{D}_{pq}^{p-q} = \frac{\alpha^{p-q} \Gamma(1 - (p-3)/\delta)}{\Gamma(1 - (q-3)/\delta)} \tag{5.13}$$

---

[4]See Red Hat's home page at http://www.redhat.com.

Estimation of the parameters δ and α can be undertaken by using a transformed version of eqn.(5.10)

$$\ln(\ln(\frac{1}{1-v})) = \delta(\ln(D) - \ln(\alpha)) \quad 0 \le v < 1 \tag{5.14}$$

and employing linear regression.

It is interesting to note that the Rosin-Rammler distribution is equivalent to that of Nukiyama-Tanasawa when $\delta = 6$ in eqns.(5.6) and (5.11).

5.6.3 Lognormal Distribution

Defined by

$$dn = \frac{1}{D\sigma\sqrt{2\pi}}\exp\left[-\frac{1}{2\sigma^2(x)}(\ln(D) - \mu)^2\right]dD = d\Lambda(D|\mu,\sigma) \tag{5.15}$$

the lognormal distribution describes the variate D such that $\ln(D)$ is normally distributed with mean μ and variance σ. It has found application in a many fields and its properties and uses are well documented, (Atchison and Brown [9] provide a comprehensive overview). The m_{th} moment is given by

$$\lambda_m = e^{m\mu + \frac{1}{2}m^2\sigma^2} \tag{5.16}$$

allowing the mean diameters to be calculated using

$$\bar{D}_{pq}^{p-q} = e^{(p-q)\mu + \frac{1}{2}(p-q)^2\sigma^2} \tag{5.17}$$

The lognormal distribution has a number of interesting properties. For instance, if x_1 and x_2 are distributed lognormally then so is the product $x_1 x_2$. Another important property is that the m_{th} moment distribution of a lognormal variate is also lognormal. This means that if the number distribution of a spray is lognormal then so are its area and volume distributions. Motivation for application of the lognormal distribution to droplet size data is in general provided by the close link of the distribution with breakage models that is, if the production of droplets within a spray is considered to be a result of proportionate effect, then the resulting distribution is lognormal [9].

For estimation of μ and σ methods associated with the normal distribution can be used by considering $\ln D$ rather than D itself. For modelling the sprinkler data the method of maximum likelihood has been employed.

5.6.4 Upper Limit Lognormal Distribution

The upper limit lognormal distribution (ULLN) proposed by Mugele and Evans [16] can be used to describe the distribution of droplet size data by considering the transformed variate

$$y = \ln(\frac{D^s}{D_u^s - D^s}) \quad 0 < D < D_u \quad s = 1,2,3,\ldots \tag{5.18}$$

to be normally distributed, D_u being the diameter of the largest droplet contained within the spray. The value of s is usually chosen to be 1 2 or 3 depending on whether droplet number, area or volume is being considered. Setting $s = 1$ gives the number distribution as

$$dn = \frac{D_u}{D(D_u - D)\sigma\sqrt{2\pi}}\exp\left\{-\frac{1}{2\sigma^2}\left[\ln\frac{D}{D_u - D} - \mu\right]^2\right\}dD \quad 0 < D < D_u \tag{5.19}$$

where μ and σ are the mean and variance of the associated normal distribution. Obviously the rational behind the use of eqn.(5.19) is to provide a model that makes the probability of a droplet with diameter greater than D_u occurring within the spray zero. This is in contrast to the other distributions considered thus far which assign small but non zero probabilities for all droplets with $D > 0$ occurring.

If D_u is known then as with the lognormal distribution estimation methods associated with the normal distribution can be applied to the transformed variate. If D_u is not known *a priori* some means of estimating it needs to be applied. Mugele and Evans [16] develop a method in which eqn.(5.19) is transformed giving $\frac{D}{D_u - D}$ linear in the volume fraction v allowing linear regression to be used to obtain μ and σ. They suggest that within this scheme it is possible to determine D_u by "trial and error", picking the value of D_u which leads to the best linear description of the transformed data. An alternative method using estimates for the 10_{th}, 50_{th} and 90_{th} percentiles of the transformed data is also described. For
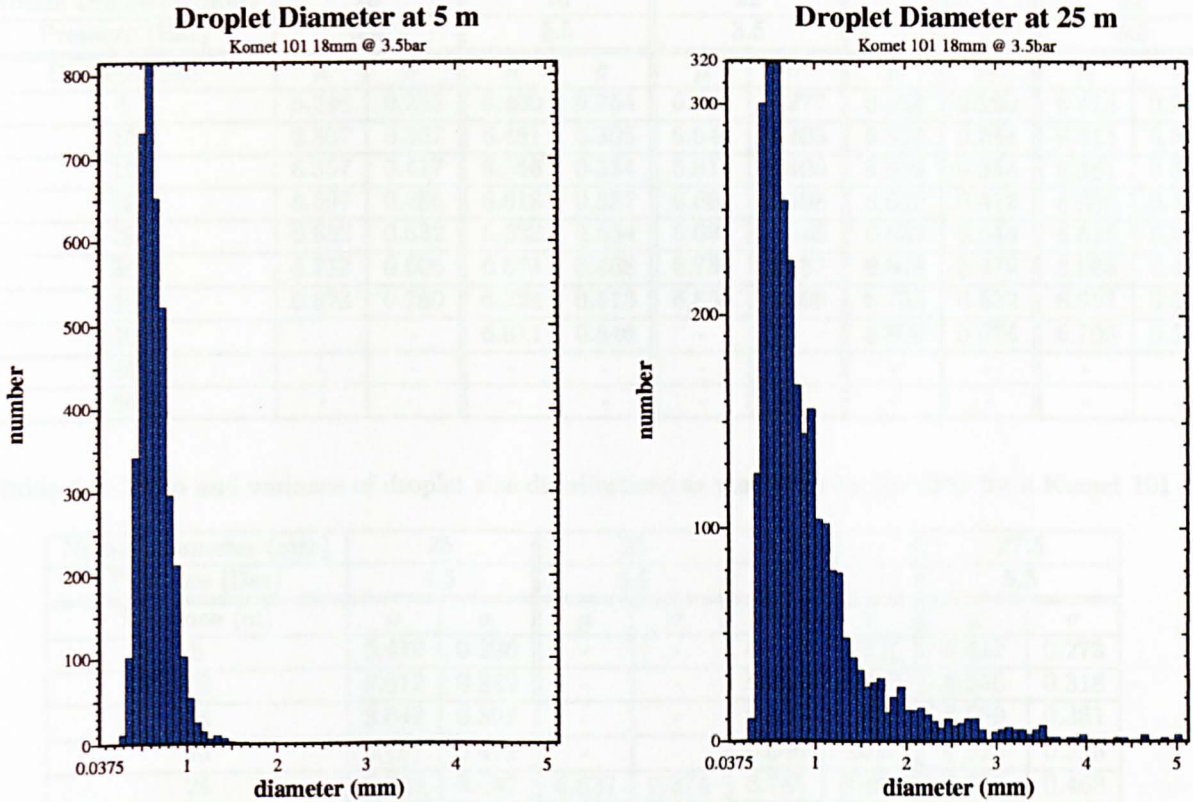
Figure 5.3: Histograms of drop diameter obtained using the SPO.

modelling of the sprinkler data the former method was used, the optimum value of D_u being determined systematically by employing a recursive method implemented using the macro features of Applixware.

Mugele and Evans [16] claim that the ULLN can be shown to be a consequence of proportionate effect when a finite initial value of droplet size is considered within certain breakage models, thereby providing motivation for its application to spray data. Unfortunately, the ULLN does not retain most of the appealing features of the lognormal distribution described in section 5.6.3.

The ULLN corresponds to a special case of the four parameter lognormal distribution introduced in Aitchison and Brown [9]. This distribution allows for both an upper and lower bound on a variate. By setting the lower bound to zero the ULLN is produced.

5.7 Results

Post processing of the the OAP and SPO data leads to the results being allocated to bins according to diameter and thus can be used to produce histograms that approximate the distribution of droplet diameters within the spray. Figure 5.3 contains two examples of such data acquired at different distances from the sprinkler nozzle. From these examples it is clear that the distribution of droplet diameters is, as expected, dependent upon distance from the nozzle.

The data used in figure 5.3 was provided by the SPO and it is clear that droplets with diameters in excess of that measurable by the SPO have been recorded. Further examination of the SPO data suggests that for measurement distances greater than 20m this is generally the case. Of course, this precludes the use of the OAP data to model the distribution of droplet diameters within the spray and consequently only the SPO data has been analysed.

The parameters for each of the distribution functions described in section 5.6 have been estimated for each droplet distribution and the corresponding X^2 value determined. In almost every case the lognormal distribution resulted in the smallest X^2 values and consequently has been chosen to model the data. Figure 5.4 shows how the different distributions compare to the data for an individual sample. The lognormal parameters (μ and σ) corresponding to each measurement made are given in tables 5.2 and 5.3. Tables containing the parameters along with the number of droplets sampled, degrees of freedom

Nozzle Diameter (mm)	18		18		22		22		22	
Pressure (Bar)	3.5		5.5		3.5		4.5		5.5	
Distance (m)	μ	σ	μ	σ	μ	σ	μ	σ	μ	σ
5	6.398	0.255	6.400	0.254	6.441	0.277	6.383	0.260	6.415	0.269
10	6.507	0.367	6.481	0.306	6.640	0.403	6.556	0.344	6.513	0.328
15	6.557	0.417	6.556	0.354	6.614	0.400	6.559	0.354	6.561	0.370
20	6.597	0.486	6.618	0.387	6.680	0.468	6.610	0.416	6.600	0.405
25	6.632	0.532	6.632	0.434	6.698	0.525	6.639	0.443	6.615	0.426
30	6.732	0.606	6.674	0.468	6.783	0.587	6.669	0.479	6.668	0.472
35	6.623	0.780	6.724	0.513	6.858	0.669	6.735	0.532	6.657	0.508
40	-	-	6.811	0.646	-	-	6.806	0.624	6.705	0.560
45	-	-	-	-	-	-	-	-	-	-
50	-	-	-	-	-	-	-	-	-	-

Table 5.2: Mean and variance of droplet size distributions as measured by the SPO for a Komet 101

Nozzle Diameter (mm)	25		25		27.5		27.5	
Pressure (Bar)	4.5		5.5		4.5		5.5	
Distance (m)	μ	σ	μ	σ	μ	σ	μ	σ
5	6.419	0.296	-	-	6.518	0.341	6.412	0.273
10	6.612	0.382	-	-	6.687	0.412	6.550	0.318
15	6.642	0.392	-	-	6.649	0.426	6.559	0.361
20	6.767	0.472	-	-	6.646	0.437	6.572	0.395
25	6.828	0.497	6.637	0.374	6.745	0.494	6.716	0.468
30	6.871	0.527	6.626	0.391	6.834	0.558	6.890	0.492
35	6.832	0.550	6.673	0.442	7.116	0.598	7.119	0.552
40	6.768	0.576	6.667	0.464	6.865	0.675	7.217	0.584
45	6.947	0.668	6.697	0.500	-	-	7.2221	0.614
50	-	-	6.764	0.543	-	-	6.993	0.705

Table 5.3: Mean and variance of droplet size distributions as measured by the SPO for a Komet 202

within the sample and the X^2 value are given in appendix A.2. The mean diameters for each sample calculated directly from the data D_i using

$$D_{pq}^{p-q} = \sum_i D_i^p / \sum_i D_i^q \qquad (5.20)$$

and from the continuous distribution used to model the data are tabulated in appendix A.3.

For a given sprinkler the droplet diameter distributions at different distances from the sprinkler nozzle can be generated using the zeroth ($m = 0$) moment distribution. The volume distributions can be generated in the same way using the third moments ($m = 3$) of the distributions. The number and volume distributions are compared for different distance from the nozzle in figure 5.6.

The primary motivation for modelling the droplet size distributions is to predict how the relative number of a given droplet size varies according to distance from the sprinkler nozzle. Before the parametric model can be used for this purpose it is necessary to normalize the number distribution at a particular point with respect to the overall composition of the spray. This need arises as a consequence of the efficiency of the the measuring techniques varying with distance. The normalization can be made with respect volume using the application rate of the sprinkler at a given point. At the i_{th} measurement point the normalization factor α_i can be determined from the measured application rate v_i using

$$\frac{4\pi\alpha_i}{3} \int_0^\infty D^3 d\Lambda(D|\sigma_i, \mu_i) = \frac{4\pi\alpha_i}{3} \lambda_{3,i} = \frac{4\pi\alpha_i}{3} e^{3\mu_i + \frac{9}{2}\sigma_i^2} = v_i. \qquad (5.21)$$

The v_i have been acquired using the automatic catch can facility at the CEMAGREF facility. Figure 5.7 demonstrates how the application rate varies with distance for different sprinkler nozzles and operating pressure. The manner in which the number of droplets varies with distance is demonstrated in figure 5.5.
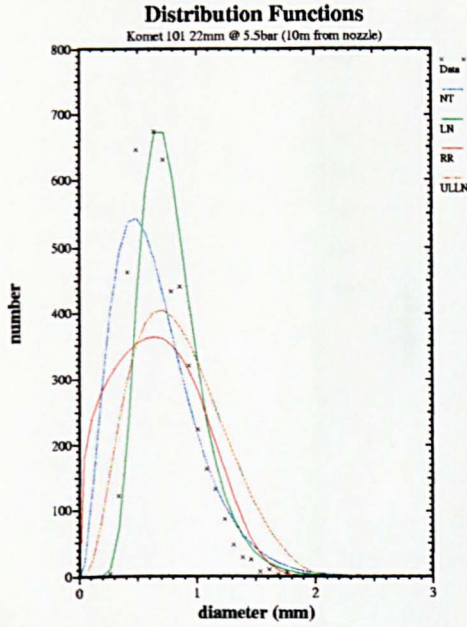
Figure 5.4: Comparison of the different distribution functions with the sprinkler data. NT = Nukiyama-Tanasawa, RR = Rosin-Rammler, LN = Lognormal, ULLN = Upper Limit Lognormal.
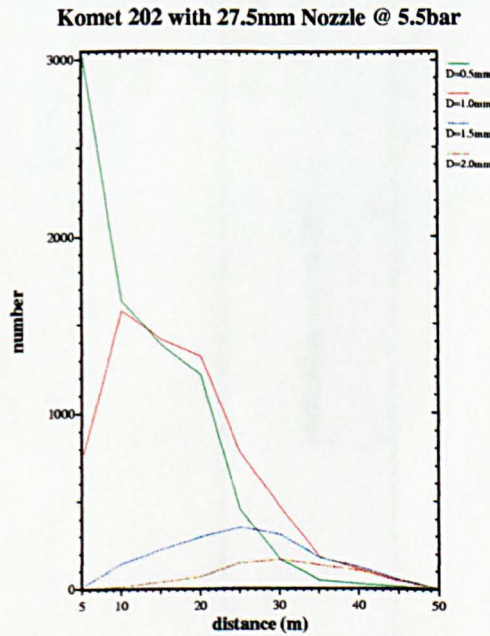
Figure 5.5: Number of droplets as a function of distance from the nozzle for different size droplets.

Number Distribution
Komet 101 22mm at 4.5Bar

Volume Distribution
Komet 101 22mm at 4.5Bar
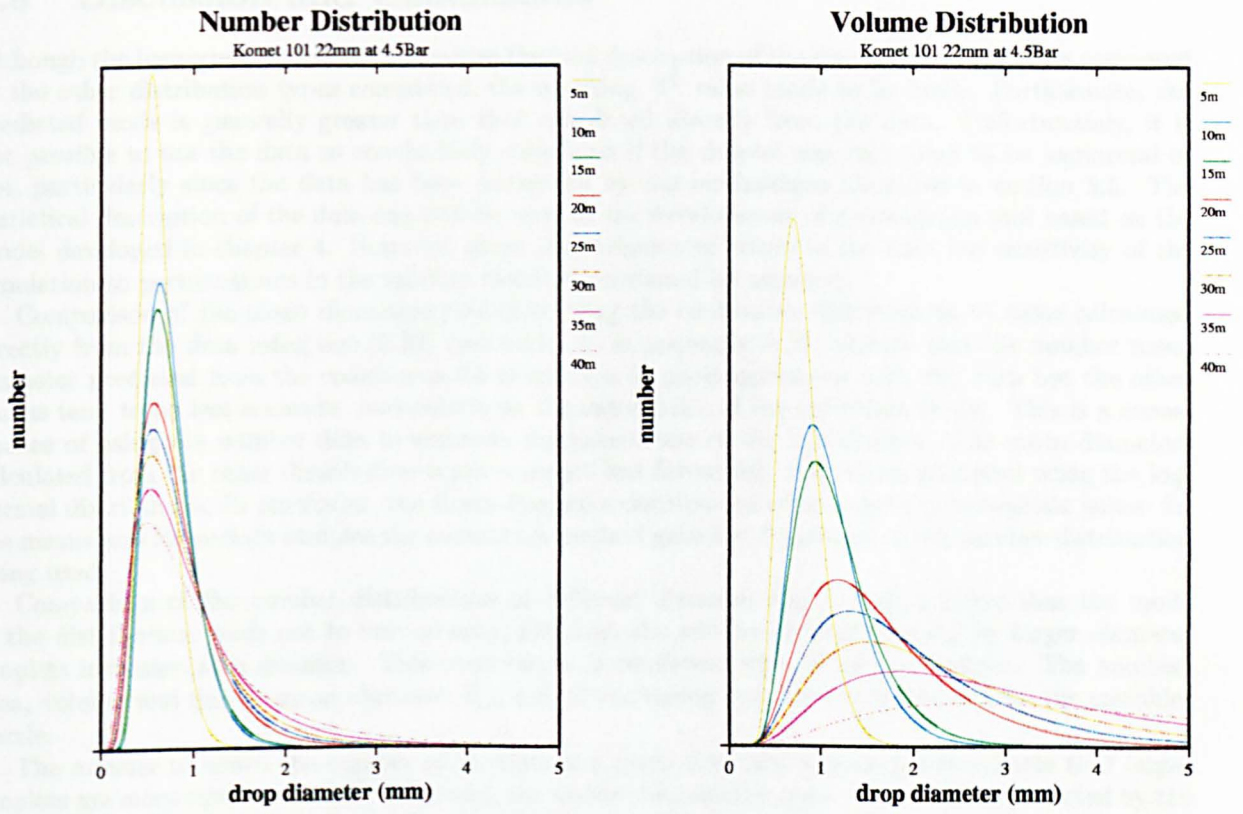
Figure 5.6: Number and volume distributions (normalized) for varying distances from the nozzle.

Komet 101 with 22mm Nozzle

Komet 202 with 25mm Nozzle
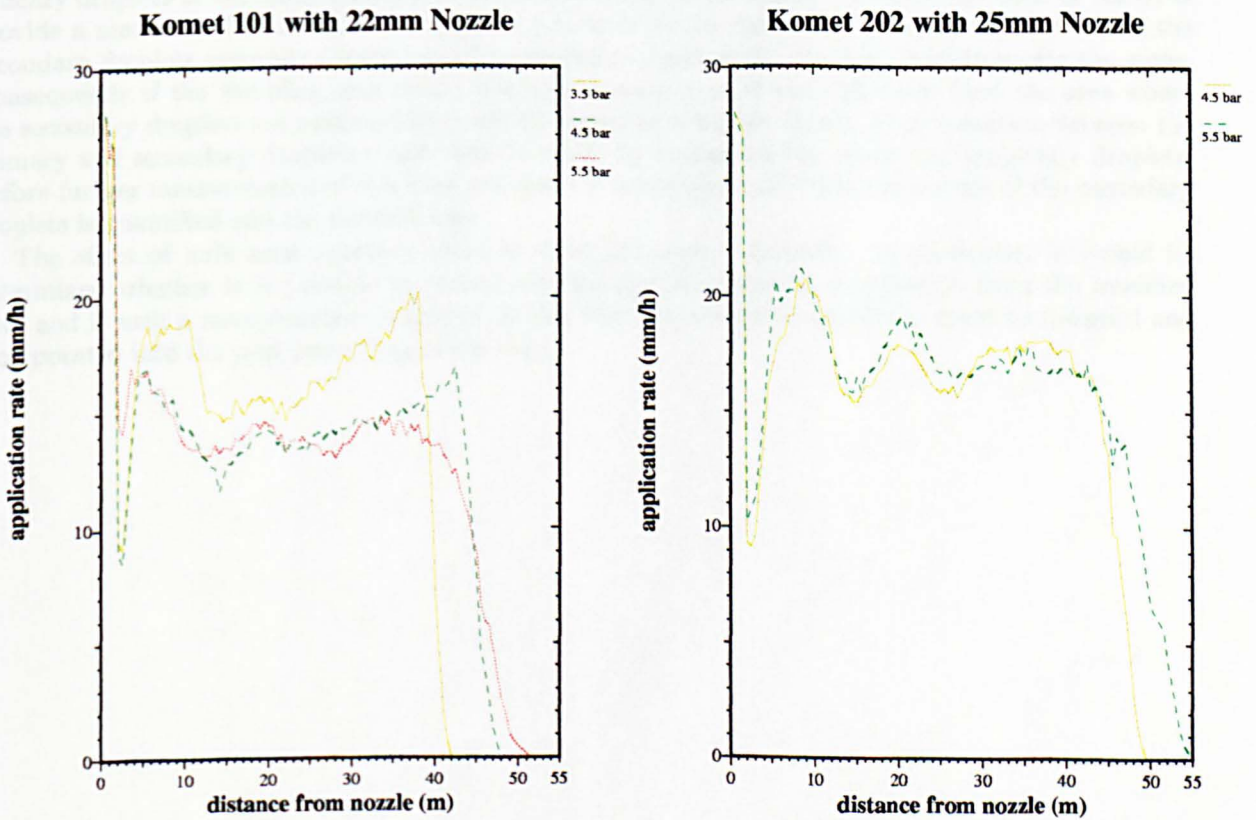
Figure 5.7: Application rates for different sprinkler types and operating pressures.

5.8 Discussion and Conclusions

Although the lognormal distribution provides the best description of the droplet size data when compared to the other distribution types considered, the resulting X^2 value tends to be large. Furthermore, the predicted mode is generally greater than that calculated directly from the data. Unfortunately, it is not possible to use the data to conclusively determine if the droplet size data tend to be lognormal or not, particularly since the data has been perturbed by the mechanisms identified in section 5.5. The statistical description of the data can still be used in the development of a simulation tool based on the model developed in chapter 4. However, given the inclusion of errors in the data the sensitivity of the simulation to perturbations in the number distribution should be assessed.

Comparison of the mean diameters predicted using the continuous distributions to those calculated directly from the data using eqn.(5.20) (see tables to in appendix A.3) indicate that the number mean diameter predicted from the continuous distribution is in good agreement with the data but the other means tend to be less accurate, particularly at the extremities of the sprinklers throw. This is a consequence of using the number data to estimate the parameters of the distribution. The mean diameters calculated from the other distribution types compare less favourably than those produced using the lognormal distribution. In particular, the Rosin-Rammler distribution often results in unrealistic values for the means and for certain samples the estimation method gave $\delta < 3$ preventing the number distribution being used.

Comparison of the number distributions at different distances (figure 5.6) indicate that the mode of the distribution tends not to vary greatly, although the volume of liquid carried by larger diameter droplets increases with distance. This observation is consistent with all of the samples. The number, area, volume and Sauter mean diameter D_{32} are all increasing functions of distance from the sprinkler nozzle.

The manner in which the number of droplets of a given size vary with distance indicate that larger droplets are more common further away from the nozzle than smaller ones. This much is predicted by the simple ballistic theory introduced in chapter 3 however, the distance corresponding to highest number for a particular diameter is still greatly in excess of that as predicted by the theory (5.5). This observation confirms the thesis that an extension to this theory is needed.

Probably the most significant error in the data is the inclusion of secondary droplets produced by the primary droplets in the spray impacting on the instrument in the sample. Neither the OAP or the SPO provide a means of eliminating these spurious counts from the data prior to analysis. The size of the secondary droplets generally appears small compared to most of the primary droplets within the spray. Consequently if the sampling area of the instrument were located some distance from the area where the secondary droplets are produced they will be traveling relatively slowly. Discrimination between the primary and secondary droplets could then be made by examining the speed and trajectory droplets. Before further measurements of this kind are made it is recommended that the nature of the secondary droplets is quantified and the methodology

The effect of bulk area rejection could be analyzed more vigorously. In particular, it should be determined whether it is possible to reconstruct the droplet diameter distribution from the modified data and if such a reconstruction is unique. If this the case a suitable algorithm could be designed and incorporated into the post processing of the data.

Chapter 6

Simulation Output

6.1 Abstract

A means of simulating a static wetting pattern produced by an irrigation sprinkler has been developed. The simulation uses the one dimensional multiphase model developed in chapter 4 and is calibrated using the droplet size distribution data of chapter 5. Once calibrated, the trajectory of the multiphase plume and individual droplets leaving it can be determined. This allows the application rate of an irrigation sprinkler to be predicted for a wide range of operating conditions including the effects of wind. Wetting patterns produced by the simulation have been compared to field measurements. The results of this comparison demonstrate that the predictions made using the simulation are as accurate as those produced by empirical and semi-empirical models. However, the simulation developed here requires significantly less data for calibration than other models. A data base of wetting patterns produced using the simulation has been compiled to enable the water application from moving sprinklers operating under windy conditions to be determined.

Notation			
D	droplet diameter	$d\Lambda(D|\mu,\sigma)$	lognormal distribution
r_d	drive droplet radius	$N(D,x)$	droplet population
η	spray composition	(x,y)	ground coordinate
m_i	i_{th} measured value	s_i	i_{th} simulated value
S_m	set of measured points	S_s	set of simulated points
s	arc length	x	distance from sprinkler
CV	coefficient of variation	RMSE	root mean square error
R^2	coefficient of determination	ϕ	area ration
θ	sprinkler orientation	α	normalisation factor

6.2 Introduction

Unfortunately, the model developed in chapter 4 does not provide a means of predicting the manner in which droplets leave the multiphase plume used to represent the interior of the plume. Consequently, before the model can be used to predict wetting patterns produced by an irrigation sprinkler it is necessary to determine the number and distribution of droplets that leave the multiphase plume at each point along

33

its length. Once this has been established the fate of the droplets can be determined using conventional droplet trajectory (ballistic) methods by solving eqn.(3.5) with initial conditions provided by the dynamics of the multiphase plume (section 4.4). In addition, this information allows the drive droplet radius and the sink/source terms in eqns.(4.15) and (4.16) to be determined. To achieve this the droplet size data analysed in chapter 5 is used.

Once calibrated, the model can be used to simulate the application rate of a sprinkler operating in windy conditions. To do this it is necessary to determine the quantity of water arriving at a point in the wetting pattern from the number and size of droplets arriving there. This is achieved by integrating the volume contained in the droplets using a grid of regular non overlapping elements. Although this method is considerably more efficient than many other techniques it still entails the use of considerable computational resources. To eliminate the need for such resources when simulating the application rate produced by a moving sprinkler a data base of static wetting patterns corresponding to different operating conditions has been compiled.

6.3 Model Calibration

Each droplet size distribution measured at ground level using the SPO has been modelled using the lognormal distribution (appendix A.2) which allows them to be described in terms of the two parameters μ and σ. The droplet distribution at an arbitrary point on the ground can then be determined by interpolating the values of μ and σ between the points at which the distributions were measured. As indicated in chapter 5 the SPO measurements cannot be reliably used to determine the total number of droplets arriving at a point. However, accurate measurements of application rate at 0.5m intervals along the ground under no wind conditions have been made by Augier [4]. An interpolation of this data can be used to normalize the distributions in the manner described in section 5.7 using a version of eqn.(5.21) that is continuous in terms of the distance x from the sprinkler. Thus if $q(x)$ is the measured application rate at x then from the third moments of the lognormal distribution (appendix A)

$$\frac{4\pi\alpha(x)}{3}\int_0^\infty D^3(x)\mathrm{d}\Lambda(D(x)|\sigma(x),\mu(x)) = \frac{4\pi\alpha(x)}{3}\lambda_3(x) = \frac{4\pi\alpha(x)}{3}e^{3\mu(x)+\frac{9}{2}\sigma^2(x)} = q(x). \qquad (6.1)$$

Evaluation of $\alpha(x)$ using eqn.(6.1) allows the number of droplets of size $D(x)$ that arriving at x to be determined using

$$N(D,x) = \frac{\alpha(x)}{D\sigma(x)\sqrt{2\pi}}\exp\left[-\frac{1}{2\sigma^2(x)}(\ln(D)-\mu(x))^2\right]. \qquad (6.2)$$

Eqn.(6.2) fully specifies the composition of the spray produced by the sprinkler at ground level. However, for calibration of the model this information is required within the plume. In order to determine the number of drops of size D leaving from a point in the multiphase plume it is necessary to solve for the trajectory of the droplet in no wind conditions. The calibration method is realised by numerically solving the equations of motion for the plume and at each spatial step liberating droplets covering a range of diameters. Solving for the trajectories of these droplets allows the point x where they strike the ground to be determined. Subsequent evaluation of the appropriate $N(D,x)$ allows the distribution of droplets leaving the plume to be constructed. When doing this it is necessary to account for the rotation of the sprinkler head such that the number of droplets leaving the plume is given by $xN(D,x)$. By evaluating the third moments of the distribution the volume of fluid exiting the plume can be evaluated allowing the the source/sink terms in (4.16) to be determined. For this method to work it is necessary to assume that droplets of size D arriving at a point x on the ground originate from a unique point on the plume trajectory. This assumption is justifiable when the sprinkler has a flat ejection angle and the rate of change of speed of the plume interior with respect to arc length s is not too great.

Since the composition of the spray from which the plume is composed varies along its length it is necessary to modify the droplet radius used to represent the plume interior. Let the distribution of droplet diameters D at a point s along the plume be given by $\eta(D,s)$. Furthermore, assume that the plume is fully formed close to the sprinkler nozzle and that no further breakup takes place along the plumes length. This assumption allows the composition of the plume at the nozzle to be determined since clearly

$$\eta(D,0) = \int_0^R xN(D,x)dx \qquad (6.3)$$

where R is the throw of the sprinkler. Furthermore, since the calibration method enables the distribution of droplets leaving the plume to be determined then $\eta(D,s)$ can be determined at each point along the
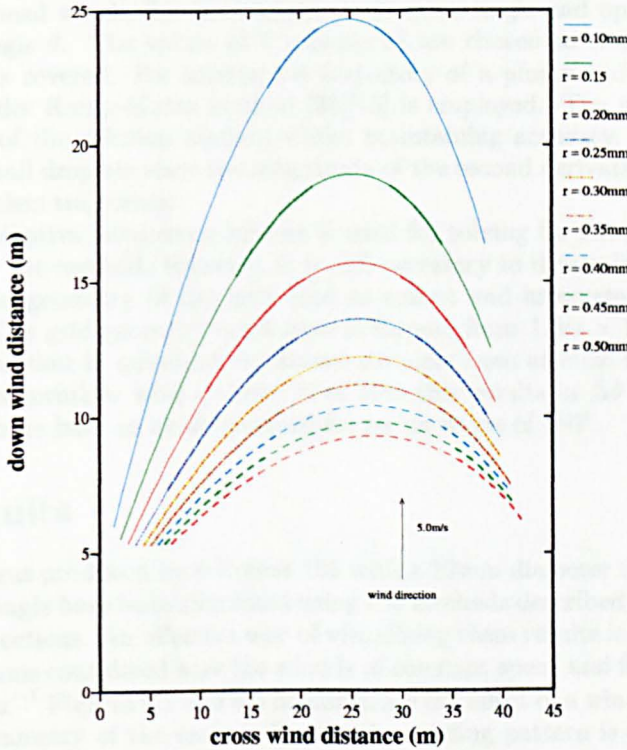
Figure 6.1: Curves representing the position on the ground where droplets of a given radius r arrive having left different points on the plume. Data corresponds to a Komet 101 sprinkler using a 22mm nozzle operating at 4.5 bar.

plume. The drive drop radius $r_d(s)$ is then evaluated using the Sauter mean diameter (sections 4.3.2 and 3.6) as

$$r_d(s) = \sum_i \eta(D_i, s)D^3 / 2 \sum_i \eta(D_i, s)D^2 \tag{6.4}$$

The calibration process has to performed once for a given sprinkler and operating pressure. Once calibrated it is assumed that $\eta(D, s)$ remains the same in the presence of a cross wind.

6.4 Determination of Static Sprinkler Wetting Patterns in Windy Conditions

Once calibrated the dynamics of the plume and droplets leaving can be determined by solving the equations of motion numerically and the point at which droplets arrive on the ground can be recorded.

For a given wind speed and direction, sprinkler orientation and droplet size these points form a curve in the plane of the ground. A family of such curves is shown in figure 6.1. Essentially these curves represent a wind dependent mapping from the s, D plane to the x, y plane. The number of droplets of diameter D arriving at a point (x, y) can be determined by evaluating the appropriate $\eta(D, s)$.

To determine the volume of water arriving on the ground it is necessary to integrate the total volume contained in the droplets. In principle it is possible to numerically approximate the Jacobian of the mapping of the s, D plane to the x, y plane. This would allow the surface representing the volume of water to be modelled and integrated numerically. However, in general this integration is performed by dividing the x, y plane into non-overlapping regions and summing up the volume contained in the droplets which fall into any given region. This method is considerably more efficient than those required for approximating the Jacobian, particularly when evaluating the complete wetting pattern produced by rotating the sprinkler.

In order to represent the rotation of the sprinkler it is necessary to determine the trajectory of a number of plumes. Each plume corresponds to a different initial condition that is provided by the orientation of the sprinkler head which, for fixed height, inclination angle and operating pressure can be represented by a single angle θ. The values of θ considered are chosen so that the full sector angle employed by the sprinkler is covered. For solving the trajectory of a plume and the droplets leaving it an adaptive fourth-fifth order Runge-Kutta method [38][15] is employed. The use of an adaptive method increases the efficiency of the solution method whilst maintaining accuracy. This is particular important when considering small droplets since the magnitude of the second derivative in eqn.(3.5) can vary significantly along the droplets trajectory.

Since an adaptive integration scheme is used for solving for the plume trajectory the step size Δs is determined by the method. However, it is still necessary to determine the magnitude of $\Delta\theta$. This choice depends on the geometry of the grid used to collect and integrate the volume of droplets arriving on the ground. The grid geometry used here is formed from 1.0m × 1.0m square elements. The value of $\Delta\theta$ is chosen so that in quiescent conditions droplets from at least three different plumes arrive in each element. For a sprinkler with a throw R of 50m this results in $\Delta\theta = 0.006$ radians such that over 500 plume trajectories have to be determined for sector angle of 180°.

6.5 Results

Wetting patterns produced by a Komet 101 with a 22mm diameter nozzle operating at 5.5bar employing a 220° sector angle have been simulated using the methods described above for a number of different wind speeds and directions. An effective way of visualizing these results is by employing contour plots. In each of the simulations considered here the wind is of constant speed and fixed direction and the contour values are in mm.hour^{-1} Figures 6.2 and 6.3 demonstrate the effect of a wind directed toward the sprinkler along the axis of symmetry of the sector. Clearly the wetting pattern is moved down wind and the throw of the sprinkler perpendicular to the wind is reduced. Such distortion of the wetting pattern is consistent with experimental observations (chapter 2). Figure 6.4 shows how the wetting pattern is distorted due to winds from different directions.

The validity of the simulation has been assessed by comparing the simulated data with field measurements of application rate obtained by using catch cans The comparisons are made at points corresponding to the locations of the catch cans in the field experiments. From this data several quantities are determined. The root mean square error RMSE defined by

$$\text{RMSE}^2 = \frac{1}{n-1}\sum_i (m_i - s_i)^2 \tag{6.5}$$

where m_i and s_i are respectively the measured and simulated values and n is the number of measured values. The coefficient of variation CV

$$\text{CV} = \frac{\text{RMSE}}{\bar{m}} \tag{6.6}$$

where $\bar{m}$ is the mean measured value. The coefficient of determination

$$R^2 = 1 - \left[\sum_i (e_i - \bar{e})^2 / \sum_i (m_i - \bar{m})^2\right] \tag{6.7}$$

where $e_i = m_i - s_i$ and $\bar{e}$ is the mean of the e_i. Also determined is the area ratio defined as

$$\phi = \frac{S_m \cap S_s}{S_m \cup S_s} \tag{6.8}$$

where the S_m and S_s are respectively the sets of (non zero) measured and simulated values.

Wind Speed ms^{-1}	Wind Direction (°)	RMSE	CV	ϕ	R^2
1.80	118	0.49	0.49	0.79	0.74
3.80	87	0.41	0.35	0.78	0.87
7.15	116	0.56	0.33	0.69	0.89

Table 6.1: Statistical Summary of Simulation Data - Komet 101 with 18mm diameter nozzle operating at 3.5bar

Wind Speed ms^{-1}	Wind Direction (°)	RMSE	CV	ϕ	R^2
2.20	68	0.20	0.36	0.80	0.85
6.09	97	0.37	0.36	0.66	0.87
8.71	104	0.43	0.34	0.59	0.89

Table 6.2: Statistical Summary of Simulation Data - Komet 101 with 18mm diameter nozzle operating at 5.5bar

Wind Speed ms^{-1}	Wind Direction (°)	RMSE	CV	ϕ	R^2
1.80	358	0.26	0.36	0.78	0.85
3.97	96	0.31	0.32	0.75	0.89
6.47	110	0.40	0.29	0.62	0.91

Table 6.3: Statistical Summary of Simulation Data - Komet 101 with 22mm diameter nozzle operating at 3.5bar

Tables 6.1 to 6.4 show the results of comparing simulated and measured data. The comparisons have been made for several nozzle sizes and operating pressures and for a range of wind speeds and directions. Tables 6.1 to 6.4 show the values of the above statistical quantities for each case.

6.6 Discussion and Conclusions

Comparison of the simulated and measured data suggest that the simulation is reasonably consistent in predicting wetting patterns for a range of sprinkler types and operating conditions. It is noticeable that the R^2 value tends to improve with increasing wind speed. This is probably due to the contribution to the wetting pattern of spray produced by the interrupter arm which is not accurately accounted for in the model. This spray is generally very fine and produces a peak in the wetting pattern close to and centred about the sprinkler. In the presence of wind this local peak is distributed over the wetting pattern and has less significance in terms of the R^2 value.

Variation in the area ratio due to increasing wind speed is due to the simulation tending to over predict drift. This may be due to inaccuracies in the droplet data used to calibrate the model. However, it should be noted that the simulation accounts for the drift of droplets which may be too small to measure using the catch can method. Because the area ratio figure penalizes any differences in the shape of the wetting pattern irrespective of the actual value of application rate it is considered to be the strictest measure for this kind of simulation. Further differences between the measured and simulated values are due to the averaging over a period of an hour of the varying wind speed and direction during the catch can measurements.

In general, the values of R^2, RMSE and CV are comparable to existing empirical and semi-empirical methods and are significantly better than those for other deterministic models. However, the area ratio is generally better for empirical and semi-empirical methods such as that due to Richards and Weatherhead. This is primarily due to these models being calibrated directly from wetting pattern measurements. However, the amount of data required for calibrating the deterministic model is significantly less than any other type of model currently available and it is this feature which is considered the single most important feature of the simulation.

The time required to simulate a single wetting pattern using a single 300Mhz Pentium II is approximately two hours. In general this prevents the simulation being integrated directly into other simulation tools. However, it is possible to generate a database of results which enable rapid use of the data. The

Wind Speed ms^{-1}	Wind Direction (°)	RMSE	CV	ϕ	R^2
1.40	110	0.23	0.39	0.83	0.82
3.27	109	0.32	0.47	0.74	0.76
3.90	97	0.31	0.43	0.78	0.80
6.46	90	0.35	0.37	0.67	0.86
7.27	109	0.37	0.32	0.61	0.90

Table 6.4: Statistical Summary of Simulation Data - Komet 101 with 22mm diameter nozzle operating at 4.5bar

data base consists of patterns produced by individual plumes specified by the sprinkler orientation θ. These patterns are produced for values of $-\pi/2 <= \theta <= \pi/2$ and a wind direction of $\pi/2$ for different wind speeds. From these results data for any wind direction, sprinkler orientation and sector angle can be constructed. Such a data base can be formed for any sprinkler type, nozzle diameter, operating pressure and operating height so long using only single leg catch can and droplet distribution data for calibration. Such a data base is used in chapter 7 to simulate total application from a moving sprinkler operating in windy conditions.
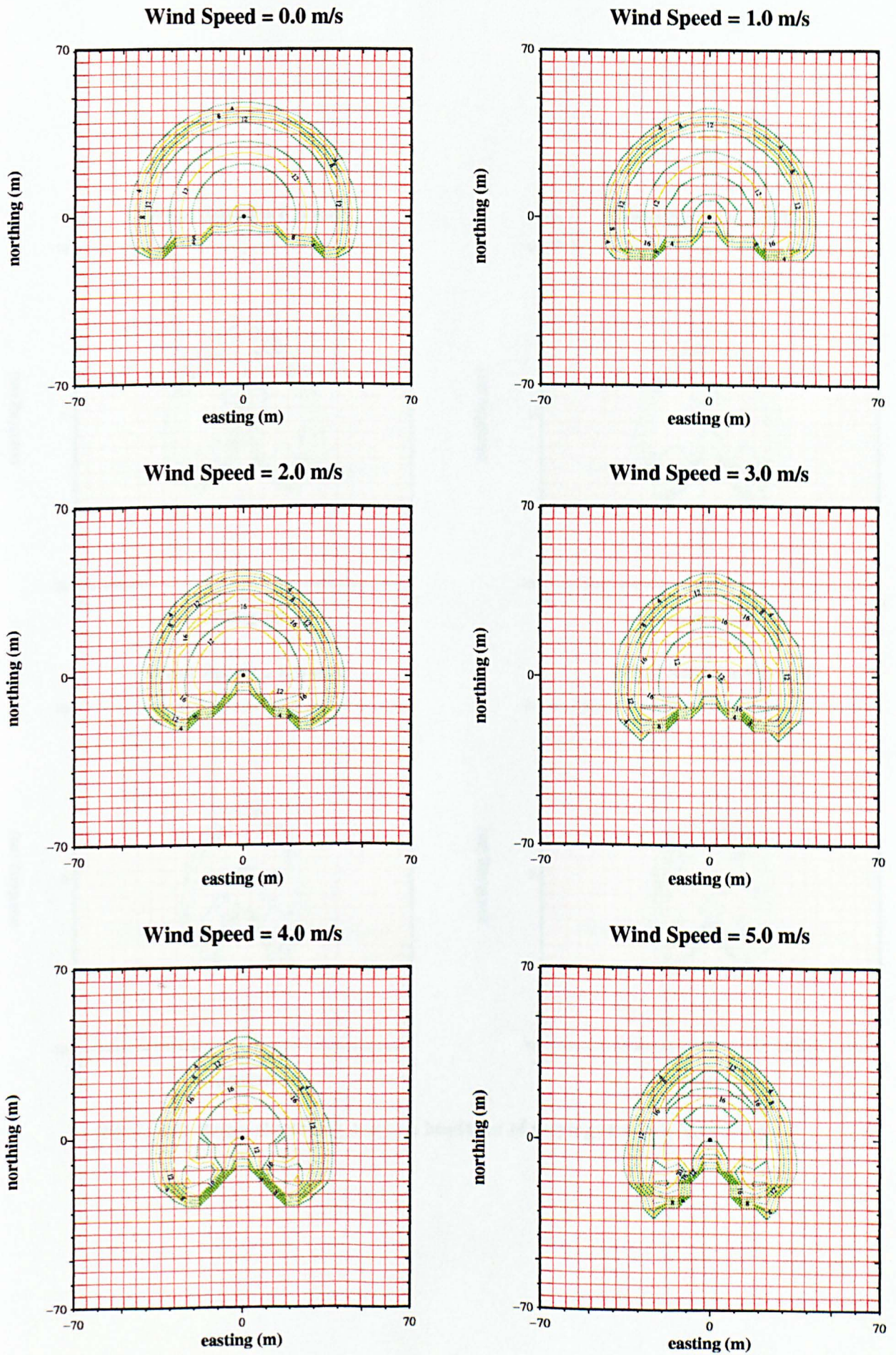
Figure 6.2: Range shortening due to a headwind of varying strength

Wind Speed = 6.0 m/s

Wind Speed = 7.0 m/s

Wind Speed = 8.0 m/s

Wind Speed = 9.0 m/s
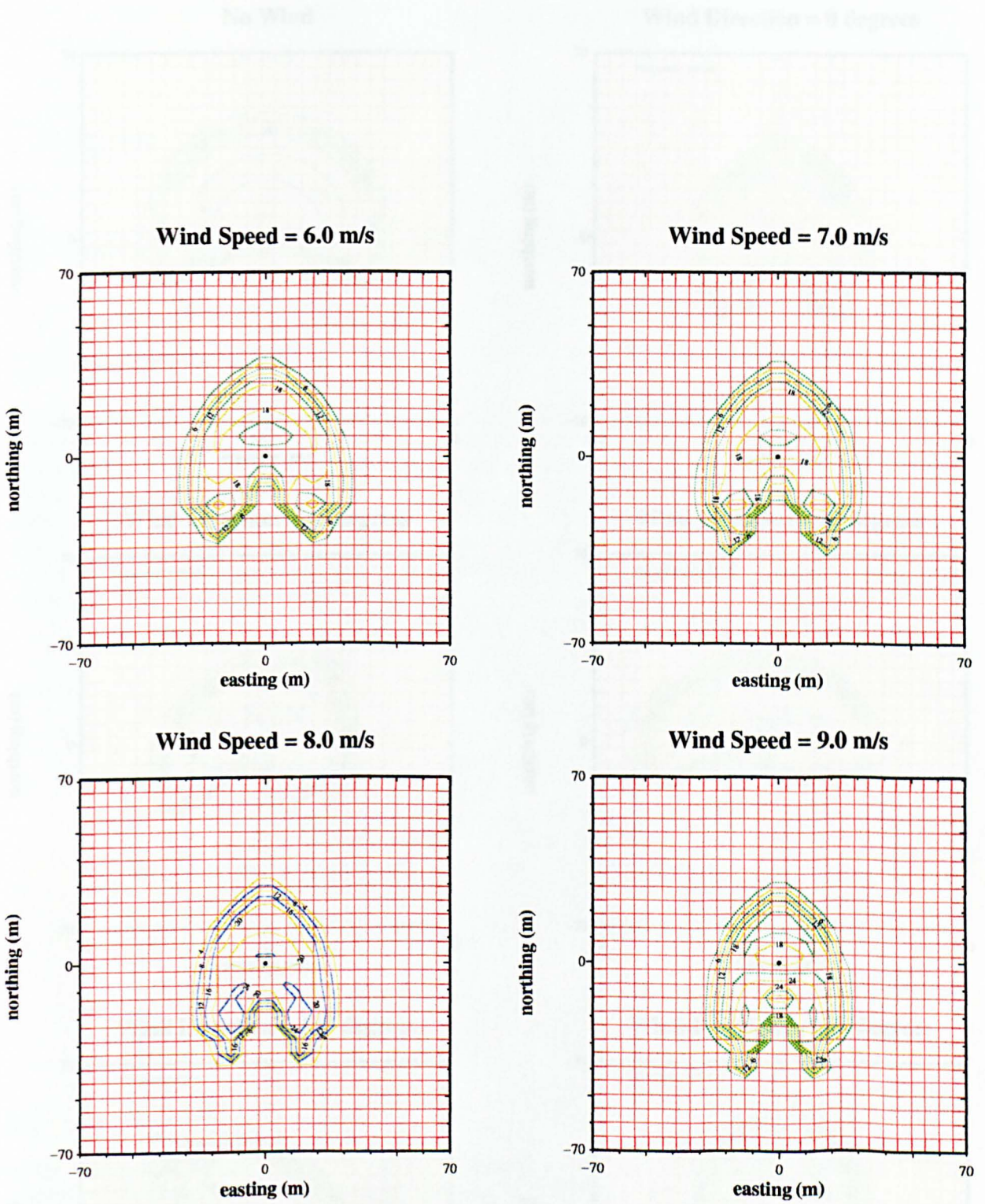
Figure 6.3: Range shortening due to a headwind of varying strength (continued)
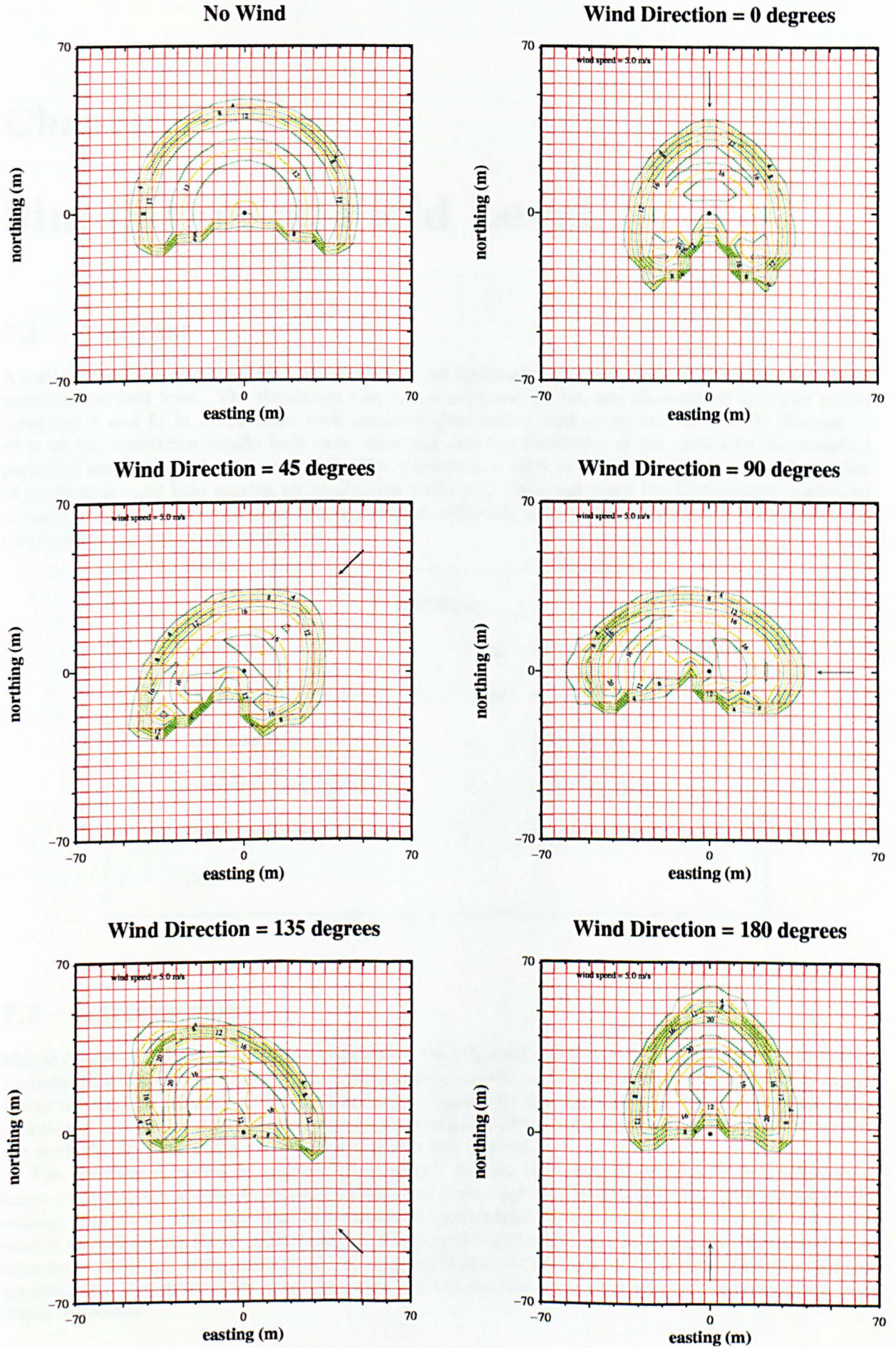
Figure 6.4: Disstortion of wetting pattern due to varying wind direction

Chapter 7

Simulation at Field Level

7.1 Abstract

A method has been developed for simulating the total application of water produced by mobile irrigation sprinklers at field level. The simulation uses dqata produced by the one dimensional sprinkler model (chapters 4 and 6) in conjunction with meteorological data (wind speed and direction). Sources of error in the simulation results have been examined and the sensitivity of the results to the sampling period of meteorological data examined. The simulation is used to assess the effects of wind, number of applications and lane spacing on application uniformity evaluated using the Christiansen coefficient of uniformity (CU). The optimum spacing between adjacent "pulls" of the sprinkler is determined and compared to current recommendations.

Notation			
Q	application	(x,y)	wetting pattern coordinate
(ζ,ξ)	sampling grid coordinate	(λ,μ)	sprinkler coordinate
ψ	field orientation	ω	wind speed
ω_m	maximum wind speed	R	sprinkler throw
υ	application rate	ν	sprinkler speed
t	time		

7.2 Introduction

Mobile irrigation sprinklers are used extensively in the UK, continental Europe and the USA for irrigating a number of different crop types (for example potatoes, onions, lettuce and maize). The sprinkler is drawn across the field on a trolley pulled by a hose reel powered by the water supply. Typically the sprinkler operates at a height of 1.0m - 1.5m using a sector angle of 180° - 240° symmetrical about the direction of travel, the dry zone being between the sprinkler and hose reel.

The sprinkler is pulled in adjacent lanes spaced so that the water application from neighbouring lanes overlap. This is done to ensure that areas of under application do not occur. The extent of the overlap depends on the equipment being used and the meteorological conditions at the site. It is not usually altered during the irrigation season. The scheduling of the irrigation is usually determined from measurements of soil water content and/or crop physiology parameters and generally consists of several applications. The quantity of water delivered at each application is equivalent to between 10mm and 30mm of rainfall.

The uniformity of application is dependent on the meteorological conditions, number of applications, height and inclination of the sprinkler and lane spacing. Too much or too little irrigation can have a significant effect on yield quality and uniformity. The value of a field level simulation is that it can replace time consuming and expensive field trials.

The purpose of this work is not to exhaustively simulate all possible irrigation scenarios but rather to establish the validity of the simulation by comparing the predicted dependence of application uniformity on different operating and environmental conditions to those found through field trials. Hopefully this will provide the confidence in and motivation for the simulation to be used in conjunction with existing crop physiology and ground water dynamics models to predict crop yield.

7.3   Translation of Model Output to Field Level

The post processor described in chapter 6 can be used to generate wetting patterns for a static sprinkler for any wind speed and direction. However, the time required to generate these patterns is such that in general it is not feasible to use the post processor as an integral part of a field level simulation when a wide range of changing meteorological conditions are encountered. A more practical method is to use the post processor to compile a database of static wetting patterns prior to simulating the sprinkler movement. For a given sprinkler values within the database correspond to points (x, y, ω, θ) in four space where x and y represent a ground coordinate relative to the sprinkler, ω and θ being the wind speed and direction respectively. To allow for continuous variations in the values of wind speed and direction within a simulation interpolations between the patterns in the database are made. For the purposes of simulation the database can then be considered as a continuous function $v : \mathcal{R}^4 \to \mathcal{R}$ defined in the region $-67.5 \leq x \leq 67.5$, $-67.5 \leq y \leq 67.5$, $0 \leq \theta < 2\pi$ and $0 \leq \omega \leq \omega_m$ where ω_m is the maximum wind speed used during database generation. The range of x and y corresponds to the dimensions of the grid used by the post processor, (chapter 6). Outside this region $v = 0$. Values for $\omega(t)$ and $\theta(t)$ are usually provided by discrete data collected from automatic weather stations. Typically these data represent a summary of values for the preceding sampling period[1] and consequently no interpolation in time is necessary within the simulation. An implicit assumption in using the static wetting patterns produced by the post processor to simulate water application at field level is that the translational velocity of the sprinkler is very much smaller than its rotational velocity.

The total water application Q at any point in the field (ζ, ξ) can be determined by integrating the application rate with respect to time

$$Q(\zeta, \xi) = \int_\tau v(\zeta - \lambda(t), \xi - \mu(t), \omega(t), \theta(t) - \psi) dt \qquad (7.1)$$

where τ is the period of the simulation and ψ is the field orientation and $(\lambda(t), \mu(t))$ the sprinkler location in the field. The manner in which $(\lambda(t), \mu(t))$ relates to the field coordinates (ζ, ξ) defines the sprinklers motion. For simplicity the simulations considered here the sprinkler always travels in a direction parallel to the ζ axis such that the sprinklers motion is given by

$$\lambda(t) = \begin{cases} \zeta_0^0 & t_s^0 \leq t < t_f^0 \\ \zeta_0^1 & t_s^1 \leq t < t_f^1 \\ \vdots & \vdots \\ \zeta_0^n & t_s^n \leq t \leq t_f^n \\ \text{undefined} & \text{otherwise} \end{cases} \qquad (7.2)$$

and

$$\mu(t) = \begin{cases} \xi_0^0 + \nu^0 t & t_s^0 \leq t < t_f^0 \\ \xi_0^1 + \nu^1 t & t_s^1 \leq t < t_f^1 \\ \vdots & \vdots \\ \xi_0^n + \nu^n & t_s^n \leq t \leq t_f^n \\ \text{undefined} & \text{otherwise} \end{cases} \qquad (7.3)$$

where t_s^i and t_f^i are the start and finish times of the i_{th} "pull" of the sprinkler with speed ν^i having started at (ζ_0^i, ξ_0^i). Figure 7.1 shows details of the field configuration used for simulation purposes.

---

[1] In the case of wind speed the arithmetic mean is used. For wind direction the formulation of a summary is complicated by the discontinuity at 360°. Several methods have been proposed for over coming this difficulty, for example Selkirk [34], however this and other methods are flawed in other respects. The automatic weather station used to provide wind data for simulations in this work calculates the mode to summarize the wind direction in any given sampling period.

(ζ_0^0, ξ_0^0) (ζ_0^1, ξ_0^1) (ζ_0^2, ξ_0^2) (ζ_0^3, ξ_0^3)

Data Base Grid

N

ψ

Calculation Region

$(\lambda(t), \mu(t))$

300m

ξ

ζ

Lane Spacing

Grid

280m
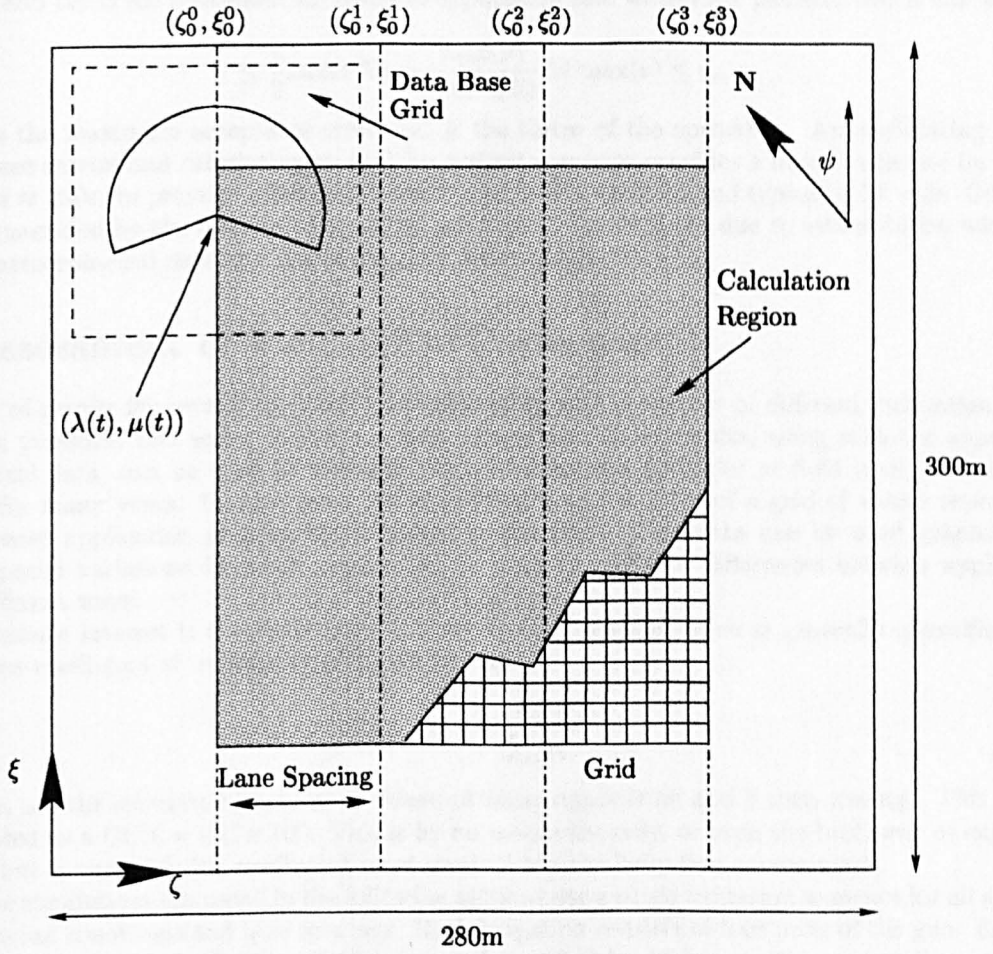
Figure 7.1: Details of field layout used for simulation.

To assess the total field application it is necessary to evaluate eqn.(7.1) at a number of points in the field. Typically these points are spaced in a regular manner at 5m intervals about the field[2] to form a grid (figure 7.1). The integral of eqn.(7.1) is approximated using quadrature as

$$Q(\zeta, \xi) = \int_\tau v(\zeta - \lambda(t), \xi - \mu(t), \omega(t), \theta(t) - \psi) dt$$

$$\simeq \frac{\Delta t}{2} \sum_{i=0}^{n-1} [v(\zeta - \lambda(t_{i+1}), \xi - \mu(t_{i+1}), \omega(t_{i+1}), \theta(t_{i+1}) - \psi) + \cdots$$

$$\cdots + v(\zeta - \lambda(t_i), \xi - \mu(t_i), \omega(t_i), \theta(t_i) - \psi)] \qquad (7.4)$$

where $n\Delta t = \tau$. Since the simulation uses linear interpolation between points in the database, the error ϵ induced through use of eqn.(7.4) is easily quantified. If $\Delta\tau$ is the maximum time taken for a complete wetting pattern to traverse a point on the field, (or the sampling period of the meteorological data if this is greater), and Δv is the maximum variation in application rate within the pattern then it can easily be shown that

$$\epsilon \le \frac{1}{2}\Delta t \Delta \tau \Delta v = \frac{\max(\nu)}{4 \min(R)} \Delta t \max(v) \le \epsilon_m \qquad (7.5)$$

where ϵ_m is the maximum acceptable error and R the throw of the sprinkler . Approximating $\min(R)$ from database entries and calculating $\max(\nu)$ for typical scenarios provides a liberal estimate for a lower bound of $\Delta t \approx 200s$. In practice much smaller values than this are used and typically $\Delta t = 3s$. Of course, the errors generated by the method of eqn.(7.4) are in addition to those due to interpolation within the database, meteorological data and use of the post processor.

7.4 Assessment of Field Level Performance

A database of results for several sprinkler types operating with a number of different inclination angles, nozzle sizes, pressures and sector angles has been generated. These results, along with the appropriate meteorological data, can be used to simulate the operation of a sprinkler at field level for a range of conditions for many years. Output from the simulation is in the form of a grid of values representing the total water application at preselected points in the field. This data can be used graphically to represent spatial variations in water application or used to quantify differences between applications made in different ways.

Of immediate interest is the uniformity of irrigation application which is generally quantified using Christiansens coefficient of uniformity (CU) defined by

$$CU = 1 - \frac{\sum_i |v_i - \bar{v}|}{\sum_i v_i} \qquad (7.6)$$

where the v_i are the simulated (measured) values of water application and $\bar{v}$ their average. This value is usually quoted as a CU% = CU $\times$ 100. This is by no means the only, or even the best, way of expressing uniformity but is currently the coefficient most used within the irrigation community[3].

All of the simulations discussed in the following sections use a single irrigation sequence for all sprinkler types, operating conditions and lane spacings. Each irrigation consists of four pulls of the gun. Each pull starts at the top edge of the field at 06:00 hours and is pulled for 12 hours. The next pull starts at the same time next day on the adjoining lane. The dimensions of the calculation region are chosen such that its sides coincide with the pull of the sprinkler on the first and fourth day and the top and bottom edges receive a complete application pattern, (see figure 7.1). Day one of the irrigation sequence can correspond to any day (the start day) during the period April 1st to September 30th (a typical UK irrigation season) for the years 1992 through 1998[4]. For clarity, the starting dates are enumerated, April 1st corresponding to start day 0. The meteorological data was provided by the Cranfield University automatic weather station located in Silsoe, Bedfordshire.

On the hardware used[5] the typical simulation time for a single irrigation was ~ 25 seconds such that it was feasible to study a large number of irrigation scenarios. This short simulation time along with the

---

[2]The dimensions of the field used for simulation were chosen to meet the requirements of the NIWASAVE research programme.

[3]The Christiansens coefficient was first suggested at a time when mechanical calculators were in common use and it is believed that its form was chosen for ease of calculation compared to other statistical measures containing roots such as the standard deviation.

[4]Excepting 1996, this year is missing from the data archive used.

[5]Linux OS on a single Pentium II 200Mhz.
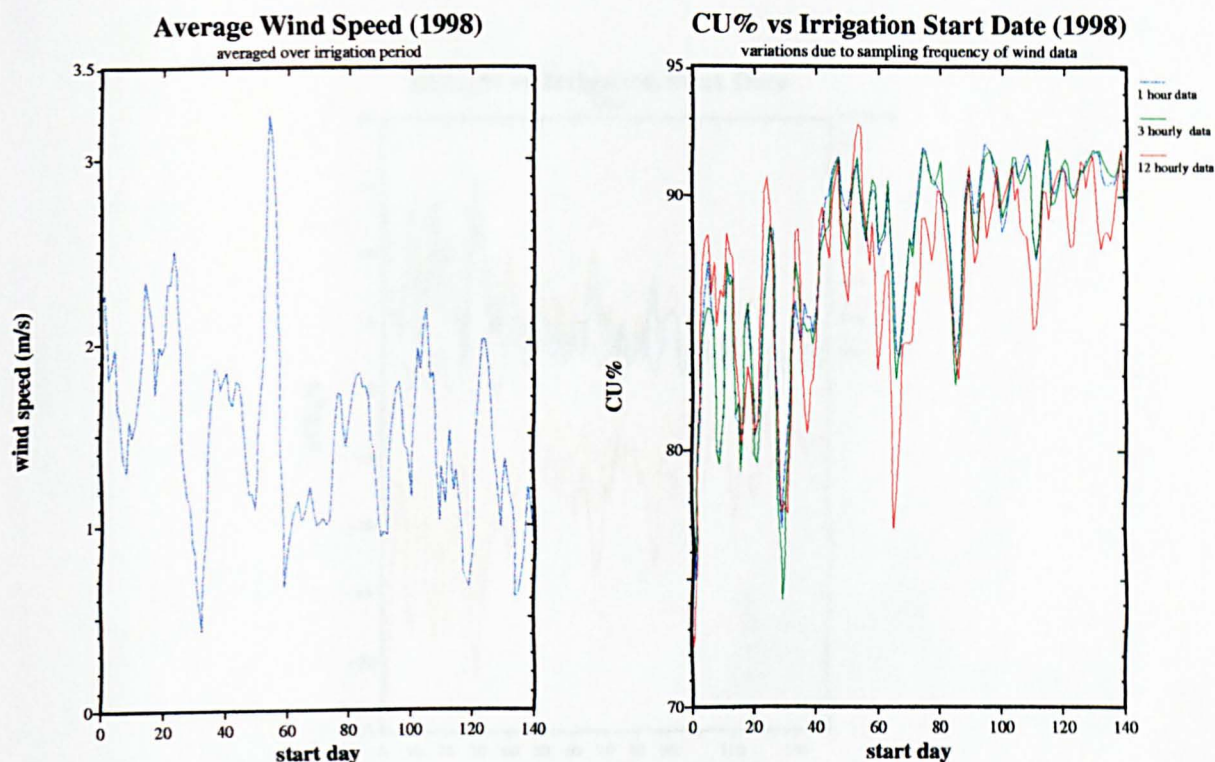
Figure 7.2: Effect of varying wind speed. The wind speed is averaged over the irrigation period of four days (left). Demonstration of sensitivity of simulation to sampling period of the meteorological data (right).

wide range of possible scenarios allow general conclusions regarding sprinkler irrigation practice to be formed, as opposed to most field trials which generally only study a single scenario.

7.4.1 Sampling Frequency of the Meteorological Data

Errors in the simulated data due to the discrete methods associated with the post processor, database interpolation and numerical integration can be quantified by statistical comparison with experimental data (chapter 6). However, further errors are induced within the simulation when using meteorological data sampled at discrete intervals. Since it is is often difficult to acquire meteorological data sampled at short intervals over long periods it is useful to determine a lower limit for the sampling period for use in the simulation. Of course, errors will be incurred for all but continuous data. The issue at hand is when do errors incurred via use of discrete meteorological data become significant relative to other error sources? In this sense the sensitivity of the simulation output to changes in sampling period requires understanding.

An obvious and simple way of qualitatively examining this sensitivity is to run simulations with meteorological data sampled at different intervals and compare the output using eqn.(7.6). This was done on the simulated field (figure 7.1) for a number of different sprinklers using different lane spacings and meteorological data over several years. Meteorological data was immediately available that had been sampled hourly. From this data it is possible to calculate the values for wind speed and direction that would have been obtained if the sampling period were longer than this. Sampling intervals of between 1 hour and 12 hours were used. Figure 7.2 shows a typical time series of CU versus starting day of the irrigation sequence during the irrigation season for 1998. The variation in average wind speed during irrigation for this period is also shown. It is clear from these results that the simulation is sensitive to the sampling frequency since the use of a 12 hour sampling period consistently leads to lower values of CU in comparison to simulations run with wind data sampled every hour or three hours. However, it is also clear that there is little difference in the simulation output when using data sampled at three hourly or hourly intervals. These results are consistent for simulations of different sprinkler types (nozzle size, pressure) and for different spacings between adjacent pulls of the sprinkler. The latter observation
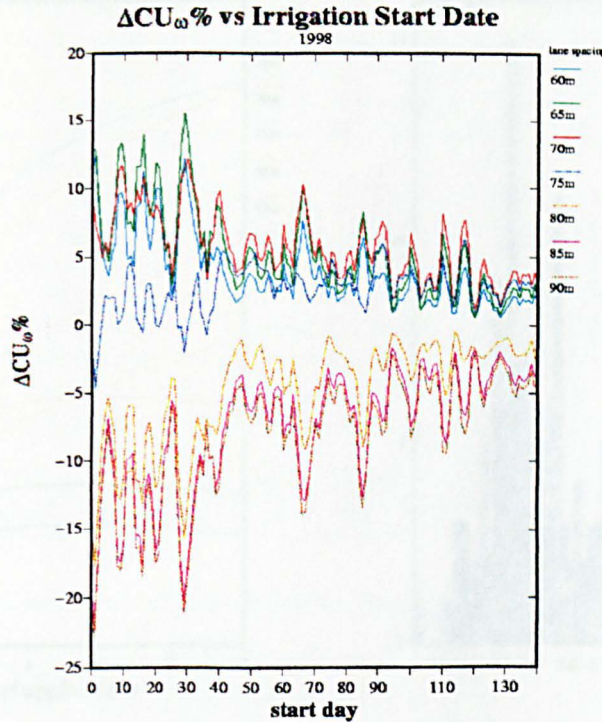
Figure 7.3: ΔCU% from quiescent conditions at different lane spacings. Sprinkler type is a Komet 101 operating at 5.5bar with a 22mm nozzle inclined at 24°.

suggests that reducing the sampling period to less than 1 hour would have little effect on the simulation output, signifying that this data can in general be used for the purposes of simulation. Of course, if data is available which has been sampled at higher frequency this should be used although in practice, this would be subject to processing constraints. All subsequent simulations in this work use meteorological data sampled at one hourly intervals.

7.4.2 The Effect of Wind on Application Uniformity

An immediate question which arises in the context of any type of overhead irrigation is what is the effect of wind on application uniformity? To arrive at a general answer to this question for sprinkler irrigation a number of sprinkler types operating at different pressures and lane spacings were simulated using meteorological data over a period of six years. For each sprinkler and lane spacing combination the CU that would have been obtained if there were no wind (the quiescent CU) was calculated. The difference between the predicted CU and the quiescent CU due to the effects of wind (ΔCU$_w$) indicates whether the presence of wind increases (ΔCU$_w > 0$) or decreases (ΔCU$_w < 0$) application uniformity. Figure 7.3 shows a family of ΔCU$_w$% time series for 1998 corresponding to one sprinkler type and a range of lane spacings.

It is clear from figure 7.3 that wind does affect application uniformity. Of more interest is that for closer lane spacings application is improved in the presence of wind as opposed to wider spacings where the uniformity decreases. This can also be seen in the way local maxima in ΔCU$_w$ for closer spacings correspond to minima at larger spacings. Furthermore, the deviations in ΔCU$_w$ are greater at the beginning of the irrigation season (day 0 = April 1st). Figure 7.2 indicates that wind speed tends to be higher during the earlier part of the irrigation season suggesting that, in general, higher winds have more affect on application uniformity.

7.4.3 The Effect of Multiple Applications on Uniformity

Generally it is uncommon for all of the irrigation requirements to be met by a single application. The number of applications made depends on a large number of factors such as soil characteristics, crop
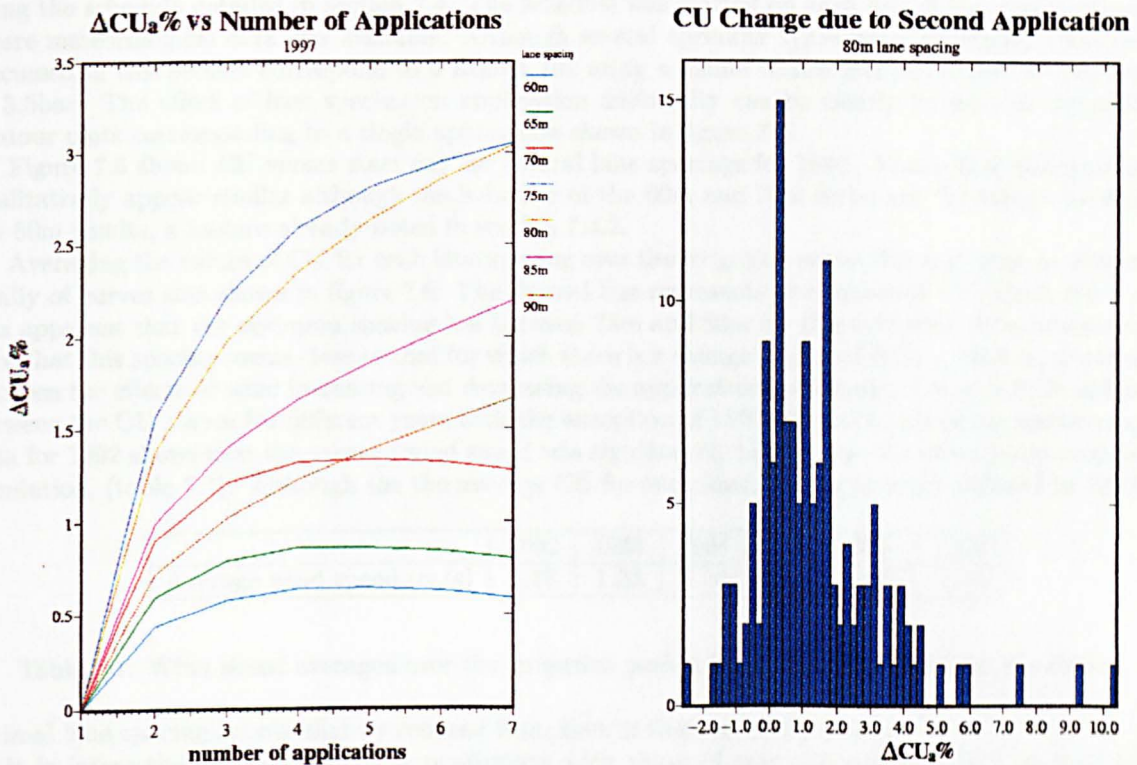
Figure 7.4: Variation in coefficient of uniformity (ΔCU) due to succesive applications for different lane spacings (left). Distribution of changes in application uniformity due to second application for 80m lane spacing (right).

physiology and labour costs for example. To simulate the effect of multiple applications the schedule detailed in section 7.4 was repeated seven times, each application being separated by three days[6] , the CU for the field being calculated for each application. The simulations were started for each day of the irrigation season of 1997 using a range of lane spacings. The change in CU for each application (ΔCU_a) was calculated and averaged over the irrigation season. Figure 7.4 shows the results of the simulation.

Clearly the CU tends to increase due to repeated applications, however for narrower lane spacings the maximum CU is achieved for a smaller number of applications compared to wider spacings. Although the average change in CU over the irrigation season is always positive it is possible for a subsequent application to reduce the uniformity obtained from a single scenario. How changes in CU due to a subsequent applications are distributed is demonstrated by use of a histogram in figure 7.4.

7.4.4 The Effect of Lane Spacing on Application Uniformity

In practice spacings are used such that the water application produced by adjacent pulls of the gun are overlapped. This is necessary to ensure that all of the crop receives the required amount of water irrespective of the effects of wind. However, the wrong choice of overlap can lead to poor uniformity. Furthermore, too much overlap increases the time necessary to complete an application and usually leads to water wastage and can remove nitrogen from the vicinity of the crop. Usually, it is difficult to change the lane spacing to match wind conditions for each pull of the sprinkler. Consequently a decision has to be made regarding the optimum lane spacing based on the specifications of the sprinkler and the meteorological conditions at the site. Since the uniformity of irrigation is dependent upon the random effects of wind it is not immediately obvious how to define an optimum CU. For example, it is natural to assume that the optimum should correspond to the lane spacing for which the mean CU obtained over a long period of irrigation is maximized. However, it may be important to consider how CU's obtained in such a way are distributed allowing for consideration of the likelihood (or risk) of poor irrigation. The former method is chosen as the definition of optimum CU for the purposes of this investigation.

To determine the optimum CU in this way, a large number of different scenarios were simulated

---

[6]This kind of schedule does not reflect normal practice for the UK, but might represent a schedule in a more arid climate.

using the schedule detailed in section 7.4. The schedule was started on each day of the irrigation season where meteorological data was available. Although several sprinkler types were investigated the results discussed in this section correspond to a Komet 101 using a 22mm nozzle inclined at 24° and operating at 5.5bar. The effect of lane spacing on application uniformity can be clearly be seen in the series of contour plots corresponding to a single application shown in figure 7.5.

Figure 7.6 shows CU versus start day for several lane spacings for 1995. Notice how the time series qualitatively appear similar although the behavior of the 60m and 70m series are "inverted" versions of the 80m results, a feature already noted in section 7.4.2.

Averaging the values of CU for each lane spacing over the irrigation season for each year produces the family of curves also shown in figure 7.6. The dashed line represents the quiescent CU. From the results it is apparent that the optimum spacing lies between 75m and 80m for this sprinkler. It is interesting to note that this spacing seems close to that for which there is a change in sign of ΔCU_w, that is, a transition between the effects of wind increasing and decreasing the application uniformity. There is little difference between the CU curves for different years with the exception of 1992. Examination of the meteorological data for 1992 shows that the average wind speed was significantly higher than for other years used in the simulation, (table 7.1). Although the the average CU for each lane spacing is much reduced in 1992 the

Year	1992	1993	1994	1995	1997	1998
Average wind speed (m/s)	2.18	1.33	1.50	1.07	1.21	1.44

Table 7.1: Wind speed averaged over the irrigation period for the years used in the simulation.

optimal lane spacing is only slightly reduced from that in the less windy years.

It is interesting to compare these predictions with those of previous studies based on field trials. The first undertaking in this area was undertaken by Shull and Dyla [13] who developed the empirical relationship

$$s = 52.42 - 6.48u + 0.0453p^{\frac{1}{2}} + 8.0|\sin\theta| \tag{7.7}$$

where s is the optimum lane spacing, u the wind speed, p the nozzle pressure and θ the angle the wind makes with the guns direction of travel[7]. Calculations of the optimum lane spacing according to eqn.(7.7) were made using the same meteorological data that was used by the simulation for the irrigation season of 1997. The wind speed and direction used for the calculations are those as measured between 05:00 and 06:00 hrs. This corresponds to the typical manner in which eqn.(7.7) would be used in practice. Values of s were calculated in this way for each day of the season and the results averaged. The mean value of s obtained was $\bar{s} = 79.42$m which is consistent with the simulation results. It is not known what sprinkler height and inclination were used to obtain the results from which eqn.(7.7) was derived.

Recommendations for the optimum lane spacings have been provided in tabular form by the Food and Agriculture Organization of the United Nations (FAO) [30] though it is unclear how these results were arrived at. Similar results are provided by Keller and Bliesner [6] which are probably based on the work of Shull and Dyla [13] and Collier and Rochester [29].

7.5 Conclusions

The simulation provides a rapid means of assessing the uniformity of water application at field subject to the effects of wind. By undertaking a large number of simulations for a variety of sprinklers and operating conditions it is possible to form conclusions about irrigation practices. In particular

- wind has an effect on application uniformity

- multiple applications tend to result in better uniformity than single applications

- the optimal lane spacing predicted by the simulation is consistent with those currently recommended for irrigation practice

- the effect of wind is to increase application uniformity for lane spacings narrower than optimal, the converse being true when the lane spacing is wider than optimal.

---

[7]Eqn.(7.7) appears in [13] as $s = 52.42 - 6.48u + 0.0453p^{\frac{1}{2}} + 8.0\sin\theta$. However, it seems clear to the author that with the definition of wind direction used the system is symmetrical about 180°, hence the modification.
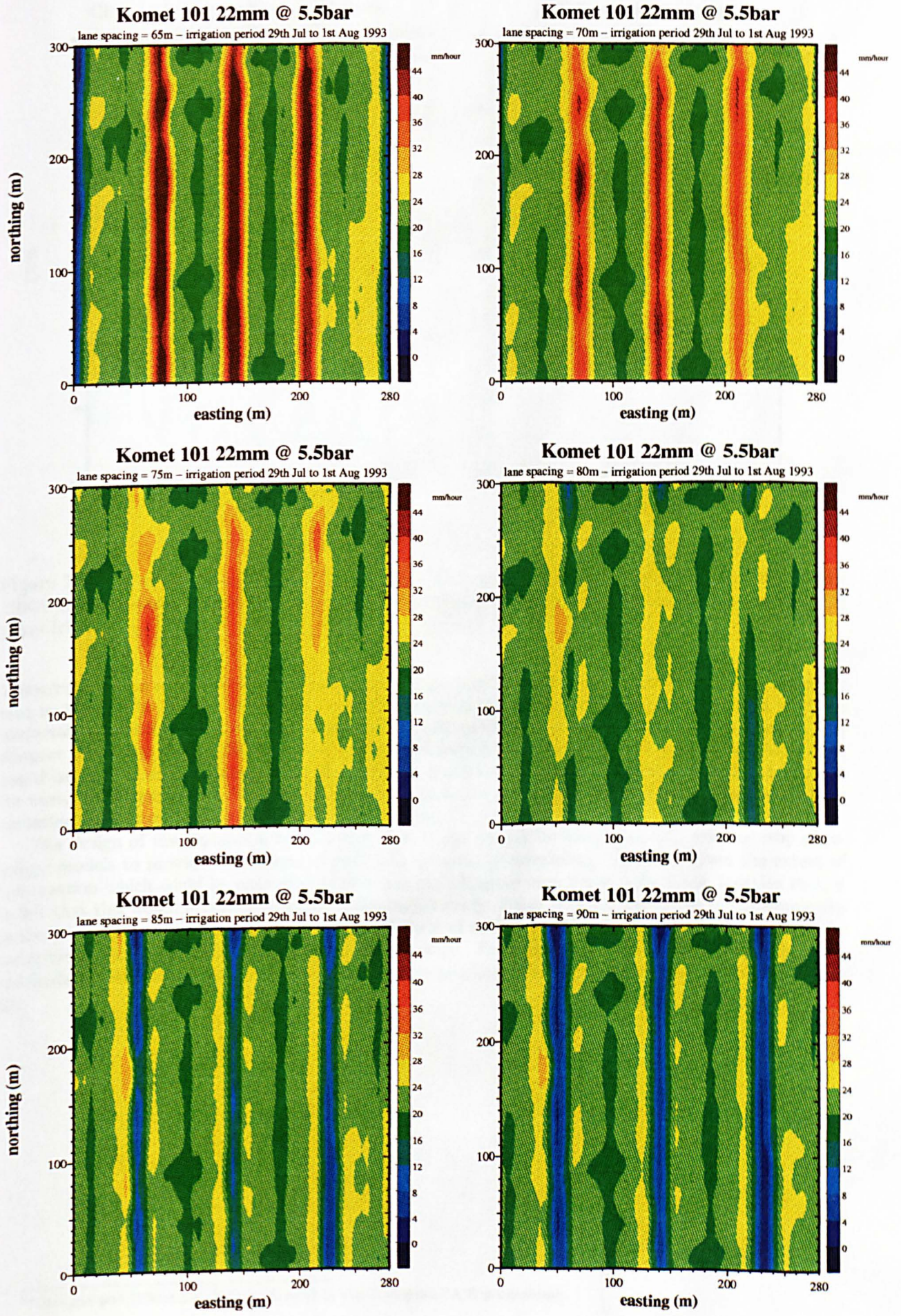
Figure 7.5: The effect of variation in lane spacing on application uniformity.
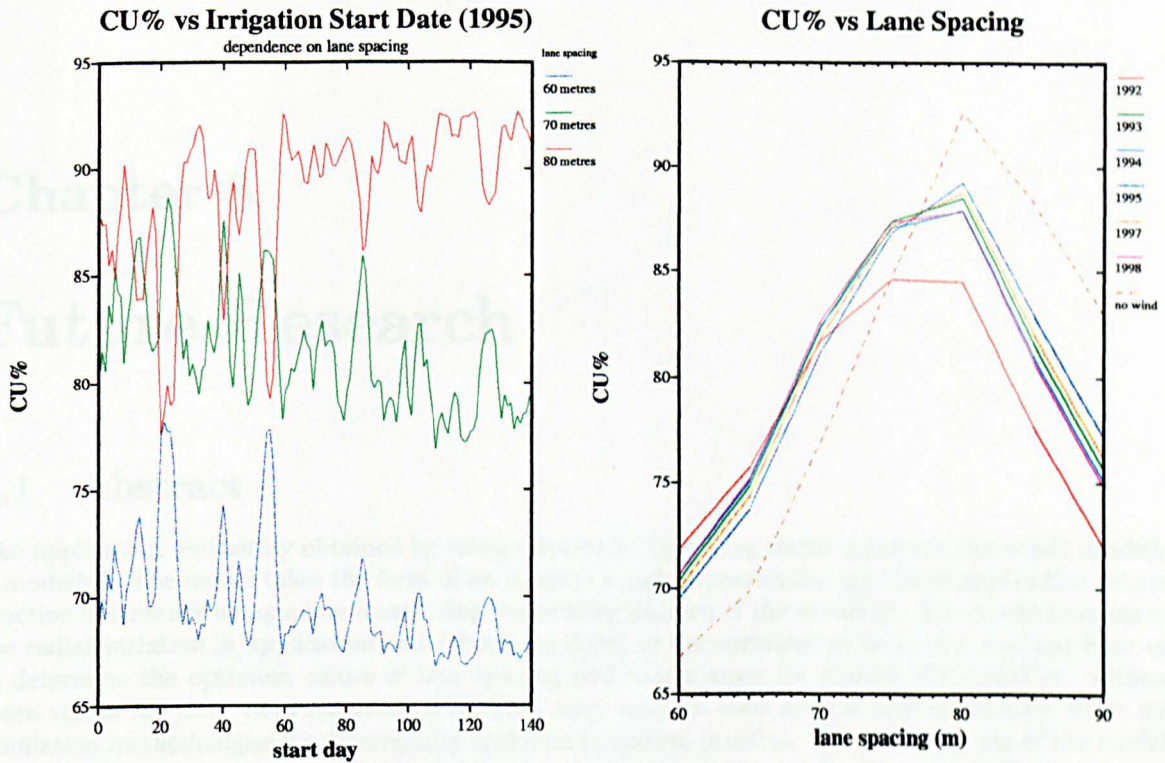
Figure 7.6: Christiansens coefficient of uniformity (CU) at different lane spacings for each day of the 1995 irrigation season (left). Average CU over the irrigation season at different lane spacings for different years (right).

These conclusions are consistent with previous findings based on field trials. This provides the confidence and motivation to use the simulation to comprehensively study the irrigation process at field level, an undertaking which is not practical using experimental techniques alone. The results discussed in this chapter are based on simulation results which form only a small subset of the possible scenarios that could be studied and correspond to a single site in south east England. Possible scenarios can account for variation in sprinkler inclination, height, nozzle pressure, nozzle diameter and sector angle along with variation in meteorological conditions due to location.

The design of the simulation is such such that it can readily be integrated into existing crop physiology models to provide predictions of yield and to optimize scheduling. However, given the extent of information which could be generated in this fashion, (different crop types, soils types, location etc), it is felt that this would necessitate further independent study. Other possibilities for use of the simulation is the prediction of nitrate leaching and quantification of runoff. For these purposes the model has been incorporated into the NIWASAVE[8] simulation package. Furthermore, the simulation could also allow methods for controlling the sprinkler operation to be developed and their performance assessed, (chapter 8).

---

[8]NItrogen and WAter SAV(E)ing - funded by the European FAIR programme.

Chapter 8

Future Research

8.1 Abstract

The application uniformity obtained by using a sprinkler operating under quiescent (no wind) conditions is modelled. The model takes the form of an integral which expresses the sprinklers application rate as a function of distance along a line transecting the wetting pattern of the sprinkler. The model requires only the radial variation in application rate (single leg data) of the sprinkler to be known and has been used to determine the optimum values of lane spacing and sector angle for Komet 101 sprinkler. Although these values are only valid quiescent conditions they may be used as first approximations when using simulation methodologies for determining optimum irrigation practice. The potential use of the model in the design and control of irrigation sprinklers is examined and manner in which simulation methods for determining spatial variability in sprinkler application may be used for future research is discussed.

Notation			
Q	application	x	distance along transect
r	radial distance	D	lane spacing
γ	overlap	R	sprinkler throw
ϕ	sector angle	ϵ	deviation from perfect irrigation
ω	weight function		

8.2 Introduction

One of the reasons for developing a simulation of water application from a sprinkler is to provide a means for determining optimal values for various parameters within the irrigation process. These include sprinkler height, inclination, nozzle diameter, operating pressure, sector angle and lane spacing. However, prior to the use of a simulation methodology for determining the parameters of a system which maximise (or minimise) a specific quantity it is useful to have an approximation as to what values these parameters may take. This is certainly the case for sophisticated simulations which may take hours or even days to produce predicted values of the quantities of interest. In this work a simple model for predicting the application uniformity from a sprinkler of fixed height, nozzle diameter, inclination and pressure operating in no wind conditions is developed. The model is then used to determine optimal values of lane spacing and sector angle for such a system.

Although not the primary purpose of the model there is some scope for its use in defining a performance criteria for irrigation sprinklers. This is discussed in section 8.3.3. Suggestions for future use of the simulation are made and the manner in which it may be used to provide enhanced input for other simulation tools associated with crop production is discussed.
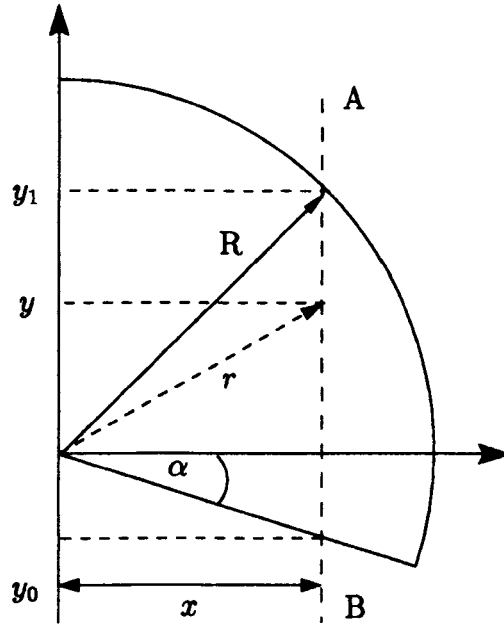
Figure 8.1: Quantities used for deriving transect application rate $Q(x)$ in terms of r and x.

8.3 Quiescent Sprinkler Application

Consider the case of a sprinkler with fixed height, operating pressure and inclination angle with a sector angle of 180° and let the motion of the sprinkler and the angular velocity of the nozzle be such that each point within the sector may be thought of as being irrigated simultaneously. The total application $Q(x)$ at a point distance x from the line of travel of the sprinkler can then be determined by considering figure 8.1.

If R is the throw of the sprinkler and $g(y)$ is the application rate at a position y along the line AB then clearly

$$Q(x) = \int_{y_0}^{y_1} g(y)dy. \tag{8.1}$$

However, it is usual to quote the application rate of a sprinkler radially i.e. using single leg data. If $f(r)$ is the radial variation of application rate then, having noted that

$$dy = r(r^2 - x^2)^{-\frac{1}{2}}dr \tag{8.2}$$

$Q(x)$ can then be written as

$$Q(x; R, \alpha) = \int_{x\sec(\alpha)}^{R} rf(r)(r^2 - x^2)^{-\frac{1}{2}}dr \tag{8.3}$$

where R is the throw of the sprinkler. However, eqn.(8.3) does not account for overlap in the wetting patterns produced by adjacent pulls of the sprinkler. This deficiency can be overcome by expressing the integral of eqn.(8.3) in terms the angular displacement of the sprinkler head. From figure 8.2

$$r = x\sec(\theta) \tag{8.4}$$

$$r(r^2 - x^2)^{-\frac{1}{2}} = \operatorname{cosec}(\theta) \tag{8.5}$$

and

$$dr = x\sec(\theta)\tan(\theta)d\theta. \tag{8.6}$$

The application $Q_0(x; R, \alpha)$ at x from the first pull of the sprinkler is then

$$Q_0(x; R, \alpha) = x \int_{\alpha}^{\cos^{-1}(x/R)} f(x\sec(\theta))\sec^2(\theta)d\theta \tag{8.7}$$
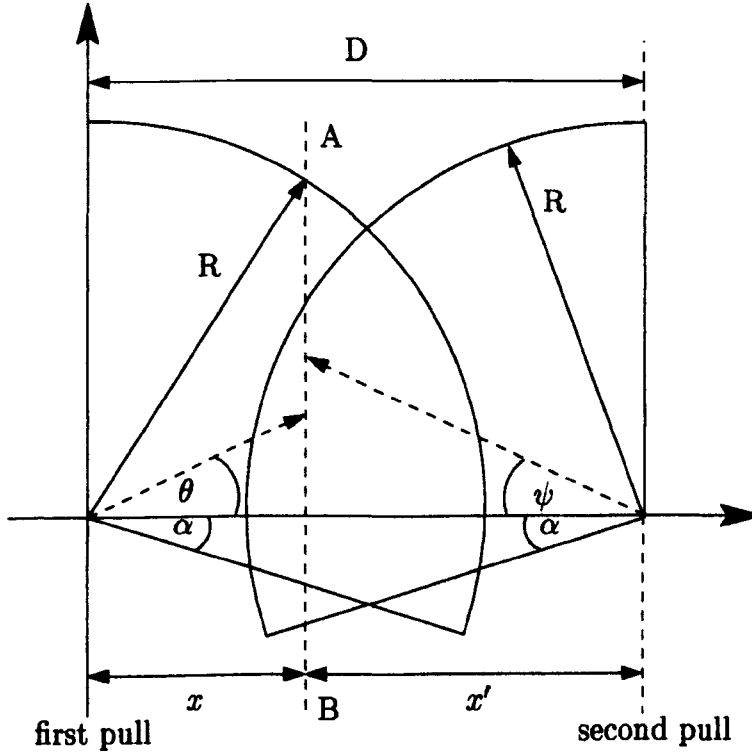
Figure 8.2: Quantities used for deriving transect application rate $Q(x)$ in terms of θ and x.

and in a similar manner the contribution from the second pull is

$$Q_1(x; R, \alpha) = x' \int_\alpha^{\cos^{-1}(x'/R)} f(x' \sec(\psi)) \sec^2(\psi) \mathrm{d}\psi. \tag{8.8}$$

Without loss of generality the above integrals can be simplified by ensuring that $f(r) = 0$ for $r > R$. Having done so we can evaluate the integrals for $x[0, \infty[$ such that the upper limit of integration becomes $\pi/2$. Furthermore, the range of integration in eqn.(8.7) and eqn.(8.8) is now the same allowing $Q_0(x)$ and $Q_1(x)$ to be combined into the single integral

$$Q(x; R, D, \alpha) = \int_\alpha^{\frac{\pi}{2}} [xf(x\sec(\theta)) + (D - x)f((D - x)\sec(\theta))] \sec^2(\theta) \mathrm{d}\theta \qquad -\pi/2 < \theta < \pi/2 \tag{8.9}$$

where D is the lane spacing between adjacent pulls of the sprinkler.

The radial variation in sprinkler application rate $f(r)$ can be determined from catch can measurements [4] and the resulting data used for evaluating eqn.(8.9). Use of discrete data to represent $f(r)$ necessitates forming an approximation to the integral and for the purposes of this work a three point Newton-Cotes formula (Simpsons rule) has been employed. The integral of eqn.(8.9) represents a mathematical formulation of work undertaken at CEMAGREF[1] which forms the basis of international standard ISO 8224.

8.3.1 Dependence of CU on Sector Angle

Evaluation of eqn.(8.9) allows the effect of varying the sector angle ψ on application uniformity evaluated using the Christiansens coefficient of uniformity (section 7.4) to be determined. Catch can data for a Komet 101 using a 22mm nozzle operating at 5.5bar has been used for this purpose and the case of no overlap $(D = 2R)$ has been considered. Figure 8.3 shows how the (normalized) application rate along the transect varies for a number of different sector angles. Also shown is the variation of the resulting CU for α in the range $0 \leq \alpha \leq -\pi/2$ (i.e sector angles of 180° to 360°). Clearly an optimal sector angle is exhibited which corresponds to a sector angle of 236° ($\alpha = -0.49$) and results in uniformity coefficient of CU = 75.6%.

---

[1]Centre National du Machinisme Agricole, du Génie Rural, des Eaux et des Forêts.
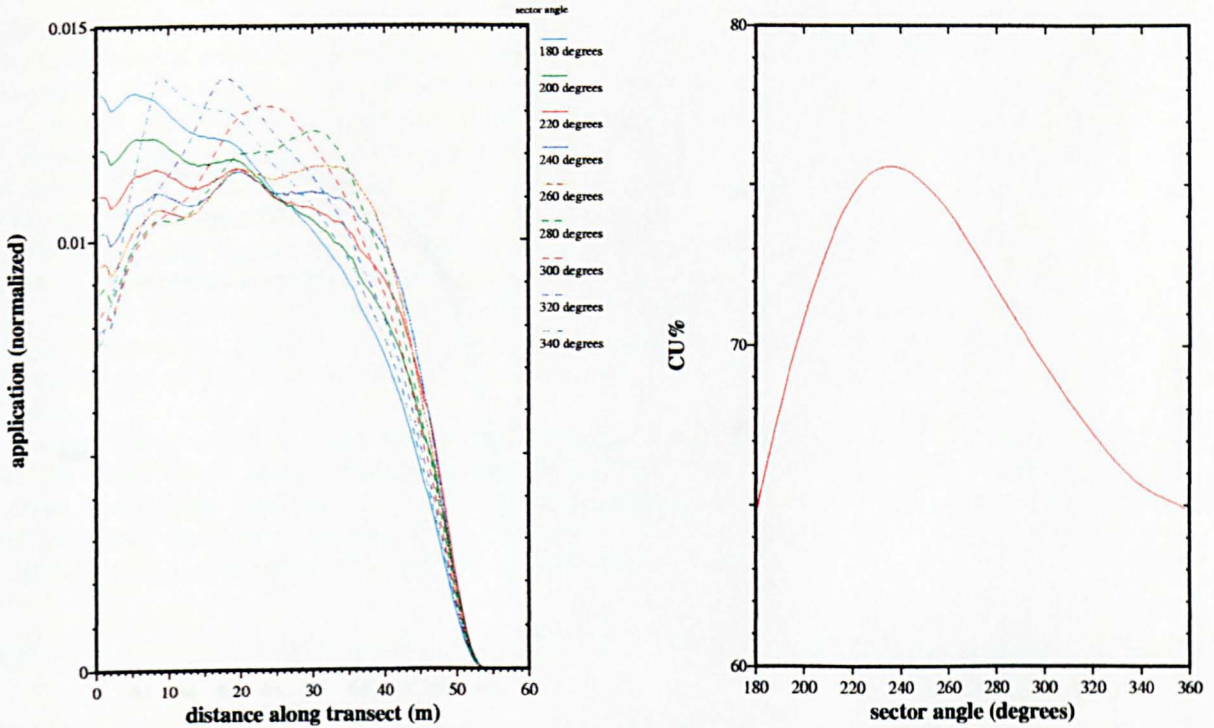
Figure 8.3: Transect application rates for different sector angles (left). Dependence of CU% on sector angle (right).

8.3.2 Dependence of CU on Lane Spacing

In a similar manner, eqn.(8.9) can be used to determine the effect that lane spacing D has on CU. The same catch can data as used in section 8.3.1 was employed. The throw of the sprinkler is $R = 50$m and values of D in the range $45\text{m} \leq D \leq 95\text{m}$ have been considered. The analysis was undertaken for the optimal sector angle of $236°$. Several examples of the resulting application rate along a transect are shown in figure 8.3 along with the variation in CU with overlap. Here, the overlap γ is given from D by

$$\gamma = 2R - D. \tag{8.10}$$

The optimum lane spacing predicted by this method is $D = 81$m which results in a CU of 96.2%. This prediction of optimal lane spacing is in good correspondence with that obtained using the field level simulation for quiescent conditions (section 7.4.4) however, the corresponding value of simulated CU is smaller due to the different sector angle employed for obtaining the simulated results. Use of the simulation demonstrates that the presence of wind results in only small changes in optimal overlap. This suggests that the optimal overlap for a sprinkler can be determined by considering only quiescent conditions using eqn.(8.9). However, it would be necessary to consider simulation results produced using meteorological data from many different locations before general conclusions could be drawn.

8.3.3 Sprinkler Design

During the design process of a sprinkler it is normal for the engineer to measure the radial variation in application of the sprinkler i.e. $f(r)$ is determined experimentally. From this data an assessment of the sprinkler performance is made. Although it is often the aim of the engineer to maximise the sprinklers throw R, application uniformity is still of considerable concern. Normally, field level uniformity is determined from field measurements involving an array of a large number of catch cans. The integral of eqn.(8.9) provides a means of assessing field level application uniformity using just single leg application data.

A further application of eqn.(8.9) is to provide a simple means for defining sprinkler performance. If we assume that "perfect" irrigation corresponds to a coefficient of uniformity of unity everywhere then the
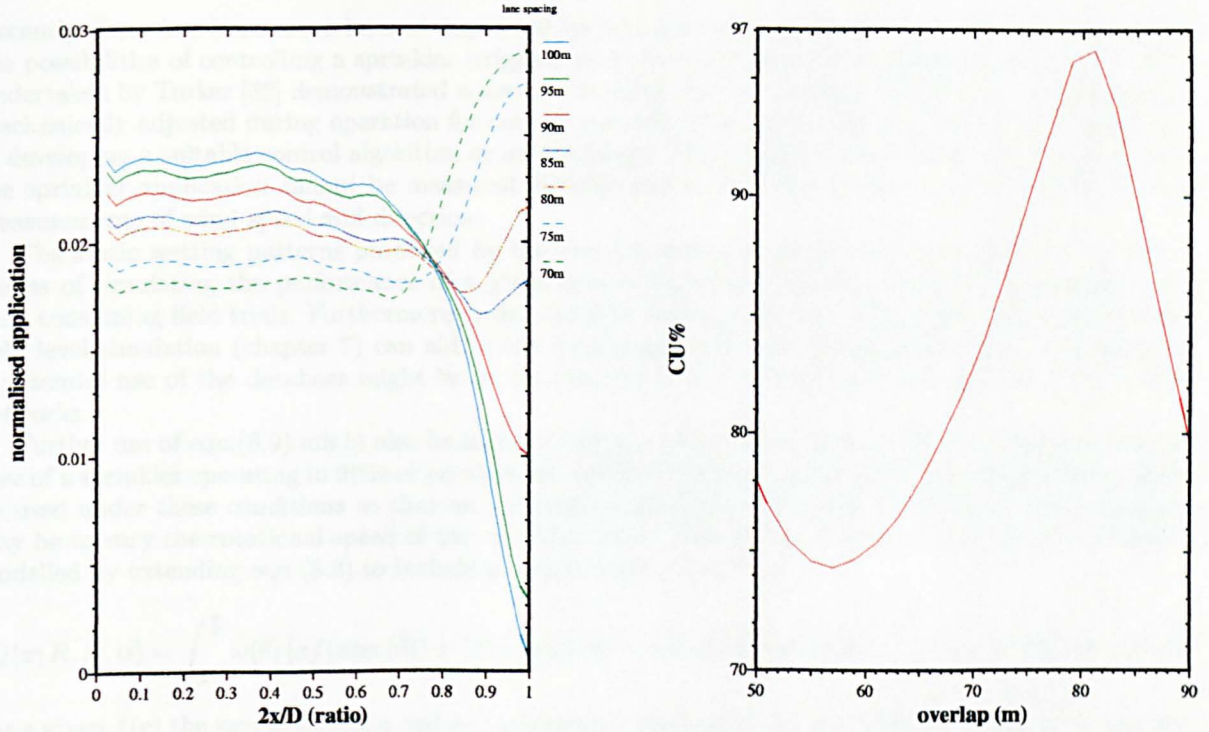
Figure 8.4: Transect application rates for different lane spacings D. Dependence of CU% on lane spacing (right).

closeness to perfect irrigation for a given sector angle, sprinkler throw and lane spacing may be defined as

$$\epsilon(R, D, \alpha) = \int_0^R (1 - \hat{Q}(x; R, D, \alpha))^2 \mathrm{d}x \qquad (8.11)$$

where $\hat{Q}(x; R, D, \alpha)$ is the normalized application along a transect given by

$$Q(x; R, D, \alpha) = \hat{Q}(x; R, D, \alpha) \int_0^R Q(x; R, D, \alpha)\mathrm{d}x. \qquad (8.12)$$

Note that Eqn.(8.11) is essentially independent of the coefficient of uniformity[2]. Eqn.(8.11) was derived using the $\mathcal{L}^2$ (least squares) norm, though of course this is by no means a necessary requirement and it may well be more suitable to adopt an alternative norm under different circumstances. For example, if large but localised deviations from unity are to be avoided then it may be more suitable to adopt the alternative definition for ϵ of

$$\epsilon(R, D, \alpha) = \max|1 - \hat{Q}(x; R, D, \alpha)|. \qquad (8.13)$$

A natural question to ask is for what $f(r)$ is $\epsilon(R, D, \alpha)$ minimized. Eqn.(8.11) provides a means of answering this question although there are no analytical methods of determining $f(r)$ from the integral. Consequently only a finite number of discrete points in $r[0, R]$ can be considered and an appropriate optimization scheme adopted for determining $f(r)$ at these points. An additional complication is that it is unclear if there is an $f(r)$ such that $\epsilon(R, D, \alpha) = 0$ and furthermore, if not, how many local optima for $f(r)$ exist. In the event of the latter case particular care must be taken when determining an approximation to $f(r)$. Further study and analysis of the integral of eqn.(8.9) is currently being undertaken.

---

[2]However, it is assumed that perfect uniformity corresponds to the value of the coefficient of uniformity being unity. If this is not the case eqn.(8.11) can be appropriately modified.

8.4   Control of Sprinkler Irrigators

Recently there has been some interest expressed by sprinkler manufacturers and researchers regarding the possibilities of controlling a sprinkler irrigator with view to improving application uniformity. Work undertaken by Turker [39] demonstrated a manner in which the orientation of the sprinkler head may be mechanically adjusted during operation for control purposes. However, little has been achieved in terms of developing a suitable control algorithm or methodology. The primary reason for this deficiency is that the sprinkler application cannot be measured directly during operation and can only be inferred from measurements of wind speed and direction.

The static wetting patterns produced by the one dimensional multiphase model (chapter 4) offer a means of simulating the performance of a given control algorithm without resorting to expensive and time consuming field trials. Furthermore, a data base of wetting patterns such as that generated for the field level simulation (chapter 7) can aid in the development of such control algorithms. For example, a potential use of the database might be as the training data for controllers based on artificial neural networks.

Further use of eqn.(8.9) might also be made in the area of sprinkler control. For example consider the case of a sprinkler operating in little or no wind. It is instructive to consider what control algorithms could be used under these conditions so that an optimum application uniformity is achieved. One approach may be to vary the rotational speed of the sprinkler head. The effects of such a control action are easily modelled by extending eqn.(8.9) to include a weight function $\omega(\theta)$ to

$$Q(x; R, D, \alpha) = \int_{\alpha}^{\frac{\pi}{2}} \omega(\theta) \left[x f(x\sec(\theta)) + (D - x) f((D - x)\sec(\theta)) \right] \sec^2(\theta) d\theta \quad -\pi/2 < \theta < \pi/2 \quad (8.14)$$

For a given $f(r)$ the weight function, subject to certain constraints, may be determined in similar manner as that used for determining the sprinklers optimum radial variation in application rate.

8.5   Integration with other Simulation Tools

The one dimensional multiphase model developed in chapter 4 can be used to generate an extensive database of static wetting patterns covering a wide range of sprinkler operating conditions and many different wind speeds and directions. This data when combined with the simulation methodology developed in chapter 7 provides a means of determining the application uniformity at field level. This can be used to help optimize the manner in which sprinkler irrigators are used. However, application uniformity is not the only factor involved in crop production. For example, soil type/uniformity and the availability of nitrates also play an important part in crop quality and uniformity of yield.

There are a number of simulation tools that have been developed for predicting crop yield based on inputs such as rainfall, nitrate levels, soil moisture content, sunlight etc. Indeed, some of these simulations have been combined with economic models with view to optimizing the complete process of crop production - no small task given the dimensionality of the underlying parameter space and the random nature of some of the simulation inputs. Most of these models require information regarding the quantity of water applied through irrigation, however only a few accurately account for spatial variability in the water application. There is much scope therefore for incorporating such simulations with that developed in chapter 7 for determining any correlations between spatial variability in irrigation and economic return. Such an integration has been undertaken as part of the NIWASAVE[3] research programme.

Chapter 9

Conclusions

Due to the extensive use of large mobile sprinkler irrigation and its economic and environmental impact there is much interest in obtaining a better understanding of the process and hence the need for some form of model. Because of the costs associated with the acquisition of accurate field measurements of water application from large sprinklers the model should have as little dependence on data for calibration as possible. Preferably, the model should be based on well established physical principles and be deterministic in nature.

Previous deterministic models have been developed which use the dynamics of individual droplets to describe the distribution of water produced by a sprinkler. However, it is clear that results produced in such a way do not predict the water application accurately. Primarily this is because such an approach fails to account for the momentum balance between the droplets and the surrounding air. A model has been developed based on the principles of multiphase continuum mechanics which describes the trajectory of the core of the spray (plume) produced by the sprinkler. The model allows the momentum of the droplet air mixture, surrounding boundary layer and cross-flow to be balanced. The plume trajectory provides the initial conditions necessary to determine the fate of droplets leaving it which in turn allows the water application from the sprinkler to be evaluated. An immediate advantage of this method is that it allows droplets of many different sizes to arrive at a single point on the ground, an observed feature of sprinkler application which is not accounted for by other deterministic models.

To develop the model into a simulation tool it is necessary to determine the number and distribution of droplets leaving the plume. Unfortunately, the mechanism whereby droplets leave the plume is not currently understood. Consequently, measurements of the size distributions of droplets within the spray at ground level have been made to allow the model to be calibrated. The measurements were undertaken using the Spectro Optique Pluviometre (SPO) developed at the L'Institut de Mécanique de Grenoble. Analysis of the distribution of droplet diameters suggest that they are best described using the lognormal distribution. The results show that while the mode of the distribution does not vary significantly the volume carried by larger droplets increases with distance from the sprinkler.

A simulation developed using the multiphase model has been used to predict static wetting patterns produced by sprinklers operating in windy conditions. Analysis of the predictions show that they compare favourably with field measurements made of water application and appear as accurate as those produced by non deterministic models. The advantage of the deterministic model over other types of model is that significantly less data is required for calibration. A disadvantage is that the numerical solutions to the equations of motion for the multiphase plume and droplets leaving it takes considerable processor time. This disadvantage is partially overcome by compiling the simulation results into a database for future use. Such an approach allows other simulation methodologies which require knowledge of sprinkler application to have rapid access to the data.

A data base of static wetting patterns corresponding to several different sprinkler types and operating conditions has been compiled. The data has been used to simulate the water application produced by a travelling sprinkler operating in windy conditions. Simulations have been undertaken for meteorological data (wind speed and direction) spanning a period of several years and the uniformity of application evaluated. These results have been used to determine the optimum lane spacing between successive pulls of the sprinkler and demonstrate the effect of multiple applications on uniformity. The results obtained indicate that the simulation provides a powerful tool for determining optimum irrigation practice. A data base produced by the simulation is being used as part of an integrated model (NIWASAVE)[1] used to simulate the overall process of crop production.

---

[1] NItrogen and WAter SAV(E)ing - funded by the European Union FAIR 4 programme.

To aid in using the simulation for optimizing irrigation practice a model has been developed to predict water application from a travelling sprinkler operating in still air ("quiescent model"). Predictions for optimum lane spacing, sector angle, operating pressure, sprinkler height and inclination can easily be determined using the model with minimal computational effort. These results can be used as a first approximation to optimal operating conditions when using the full simulation to determine these values in windy conditions. It is interesting to note that using quiescent model results in a prediction for optimum lane spacing which is in close agreement with the values found using the simulation. This may suggest that the effects of wind are such that during the irrigation process their effects on uniformity are averaged away. This prompts for the use of model for predicting other operating parameters. So far it has been used for predicting the optimum sector angle. The predicted value is greater than the angle of ~ 220° commonly adopted by farmers. The quiescent model can also be used to aid in the design and control of sprinkler irrigation. It is intended that the model will be used in this manner in future work.

The use of multiphase models for predicting spray dynamics is not restricted to sprinkler irrigators. By solving the equations of motion in three dimensions using methods such as finite volume or finite element analysis the manner in which sprays in general interact with cross flows could be studied. An immediate agricultural application of such an approach would be predicting the fate of spray used for delivering pesticides and other chemicals. Of course, before such a study is undertaken, the underlying equations should be studied so as to assess their suitability for numerical analysis.

The models and simulations that have been developed here provide a means of accurately describing many features of sprinkler irrigation. Simulation results have been obtained to demonstrate how they may be used to predict the application of water from static and moving irrigation sprinklers. It is this, rather than exhaustive simulation of the irrigation process, which was the intention of this work.

Appendix A

Statistical Summary of Droplet Size Spectra

A.1 Summary of Distribution Functions

Tables A.1 and A.1 provide a summary of the properties of the probability functions considered for modelling the droplet diameter data of the sprinklers.

Name	Probability Function	Moments λ_m
Lognormal	$dn = \frac{1}{D\sigma\sqrt{2\pi}}\exp\left[-\frac{1}{2}(\ln(D)-\mu)^2\right]dD$	$e^{m\mu+\frac{1}{2}m^2\sigma^2}$
Nukiyama-Tanasawa	$dn = \frac{\delta b^{\frac{3}{\delta}}}{\Gamma(3/\delta)}D^2 e^{-bD^\delta}dD$	$\frac{b^{-\frac{m}{\delta}}\Gamma((m+3)/\delta)}{\Gamma(3/\delta)}$
Rosin-Rammler	$dn = \frac{\delta\alpha^{3-\delta}}{\Gamma(1-3/\delta)}D^{\delta-4}e^{-(D/\alpha)^\delta}dD$	$\alpha^{m-3}\Gamma(1-(m-3)/\delta)$
Upper Limit Lognormal	$dn = \frac{D_u}{D(D_u-D)\sigma\sqrt{2\pi}}e^{-\frac{1}{2\sigma^2}\left[\ln\frac{D}{D_u-D}-\mu\right]^2}dD$	$\frac{D_u^m}{\sigma\sqrt{2\pi}}\int_{-\infty}^{\infty}\frac{e^{mz}}{(1+e^z)^m}e^{-\frac{1}{2\sigma^2}(z-\mu)^2}dz$

Table A.1: Definition and Moments of Probability Functions Considered for Modelling the Sprinkler Data

Name	$\bar{D}_{10}$	$\bar{D}_{20}^2$	$\bar{D}_{30}^3$	$\bar{D}_{32}$	$\bar{D}_{pq}^{p+q}$
Lognormal	$e^{\mu+\frac{1}{2}\sigma^2}$	$e^{2\mu+2\sigma^2}$	$e^{3\mu+\frac{9}{2}\sigma^2}$	$e^{\mu+\frac{1}{2}\sigma^2}$	$e^{(p-q)\mu+\frac{1}{2}(p-q)^2\sigma^2}$
Nukiyama-Tanasawa	$\frac{b^{1/\delta}\Gamma(4/\delta)}{\Gamma((3)/\delta)}$	$\frac{b^{2/\delta}\Gamma(5/\delta)}{\Gamma(3/\delta)}$	$\frac{b^{3/\delta}\Gamma(6/\delta)}{\Gamma(3/\delta)}$	$\frac{b^{1/\delta}\Gamma(6/\delta)}{\Gamma(5/\delta)}$	$\frac{b^{(q-p)/\delta}\Gamma((p+3)/\delta)}{\Gamma((q+3)/\delta)}$
Rosin Rammler	$\frac{\alpha\Gamma(1-2/\delta)}{\Gamma(1-3/\delta)}$	$\frac{\alpha^2\Gamma(1-1/\delta)}{\Gamma(1-3/\delta)}$	$\frac{\alpha^3}{\Gamma(1-3/\delta)}$	$\frac{\alpha}{\Gamma(1-1/\delta)}$	$\frac{\alpha^{p-q}\Gamma(1+(p-3)/\delta)}{\Gamma(1+(q-3)/\delta)}$

Table A.2: Mean Diameters of the Probability Functions Considered for Modelling the Sprinkler Data

Notes

Entries for the means of the upper limit lognormal distribution have been omitted since the integral associated with the m_{th} moment (see table A.1) does not have a closed form solution. The Gamma function $\Gamma(z)$ is defined by

$$\Gamma(z) = \int_0^\infty t^{z-1} e^{-t} dt \quad z > 0. \tag{A.1}$$

Series expansions for the Gamma function are of limited use. Tables of values for the Gamma function can be found in Abramowitz and Segun [33]. Mugele and Evans [16] provide a good overview of the distributions considered and Aitchison and Brown [9] is the definitive source for the properties of the lognormal distribution.

A.2 Distribution Parameters

The droplet size spectra acquired by the SPO $\{D_i\}$ are modelled using the two parameter lognormal distribution $\Lambda(D|\mu, \sigma^2)$ having probability density function

$$d\Lambda(D|\mu, \sigma^2) = \frac{1}{D\sigma\sqrt{2\pi}} \exp\left[\frac{1}{2\sigma^2}(\ln(D) - \mu)^2\right] dD. \qquad (A.2)$$

For each data set the parameters μ and σ were estimated using the method of maximum likelihood [9] [15]. Tables A.3 to A.11 give the the values of μ and σ for each sprinkler nozzle pressure combination examined at each measurement point[1]. The X^2 value associated with the goodness of fit for each $\Lambda(D|\mu, \sigma^2)$ is given along with the population size and number of degrees of freedom (DOF) for each data set.

Distance	μ	σ	Number	DOF	X^2
5m	6.398	0.255	3875	23	294.660
10m	6.507	0.367	2830	43	600.720
15m	6.557	0.417	3510	73	1533.237
20m	6.597	0.486	3142	124	4936.087
25m	6.632	0.532	2783	111	1777.825
30m	6.732	0.606	2742	140	1952.950
35m	6.623	0.780	1272	144	2572.753
40m	-	-	-	-	-
45m	-	-	-	-	-
50m	-	-	-	-	-

Table A.3: Komet 101 18mm nozzle 3.5bar

Distance	μ	σ	Number	DOF	X^2
5m	6.400	0.254	7980	37	20491.811
10m	6.481	0.306	5251	36	666.978
15m	6.556	0.354	6503	73	20950.253
20m	6.618	0.387	8815	72	2246.792
25m	6.632	0.434	8198	68	2444.083
30m	6.674	0.468	8511	113	4277.735
35m	6.724	0.513	10173	146	5024.616
40m	6.811	0.646	3852	119	3888.619
45m	-	-	-	-	-
50m	-	-	-	-	-

Table A.4: Komet 101 18mm nozzle 5.5bar

---

[1]"-" indicates that no data was available for the corresponding distance.

Distance	μ	σ	Number	DOF	X^2
5m	6.441	0.277	8487	34	959.383
10m	6.640	0.403	6854	59	2480506869.295
15m	6.614	0.400	7610	75	2451.826
20m	6.680	0.468	8782	119	4348.132
25m	6.698	0.525	11579	139	43558.463
30m	6.783	0.587	16168	152	12699.638
35m	6.858	0.669	12990	161	9814.388
40m	-	-	-	-	-
45m	-	-	-	-	-
50m	-	-	-	-	-

Table A.5: Komet 101 22mm nozzle 3.5bar

Distance	μ	σ	Number	DOF	X^2
5m	6.383	0.260	8022	87	1002.436
10m	6.566	0.344	6898	42	1054.617
15m	6.559	0.354	5558	54	1216.390
20m	6.610	0.416	5911	108	30830.958
25m	6.639	0.443	8060	119	10624.542
30m	6.669	0.479	7357	111	4016.615
35m	6.735	0.532	7318	144	4128.725
40m	6.806	0.624	5304	161	3599.326
45m	-	-	-	-	-
50m	-	-	-	-	-

Table A.6: Komet 101 22.mm nozzle 4.5bar

Distance	μ	σ	Number	DOF	X^2
5m	6.415	0.269	7298	26	591.017
10m	6.513	0.328	5303	33	763.794
15m	6.561	0.370	4504	70	4528.902
20m	6.600	0.405	5216	86	5072.459
25m	6.615	0.426	7308	112	20411.686
30m	6.668	0.472	4128	105	2155.307
35m	6.657	0.508	5832	124	3380.876
40m	6.705	0.560	4414	132	2774.611
45m	-	-	-	-	-
50m	-	-	-	-	-

Table A.7: Komet 101 22mm nozzle 5.5bar

Distance	μ	σ	Number	DOF	X^2
5m	6.419	0.296	3718	31	436.867
10m	6.612	0.382	3571	39	672.122
15m	6.642	0.392	3934	47	1256.132
20m	6.767	0.472	3633	76	1198.339
25m	6.828	0.497	4664	80	1543.411
30m	6.871	0.527	3749	96	1520.890
35m	6.832	0.550	4838	150	94500.109
40m	6.768	0.576	5856	119	3384.927
45m	6.947	0.668	1838	124	1205.415
50m	-	-	-	-	-

Table A.8: Komet 202 25mm nozzle 4.5bar

Distance	μ	σ	Number	DOF	X^2
5m	-	-	-	-	-
10m	-	-	-	-	-
15m	-	-	-	-	-
20m	-	-	-	-	-
25m	6.637	0.374	4544	76	4146.964
30m	6.626	0.391	7803	109	136645.836
35m	6.673	0.442	7404	110	4594.031
40m	6.667	0.464	12069	145	17288.189
45m	6.697	0.500	10332	134	7444.800
50m	6.764	0.543	9364	126	4728.460

Table A.9: Komet 202 25mm nozzle 5.5bar

Distance	μ	σ	Number	DOF	X^2
5m	6.518	0.341	3587	38	565.212
10m	6.687	0.412	5062	50	1178.663
15m	6.649	0.426	3633	48	924.906
20m	6.646	0.437	5328	106	5015.803
25m	6.745	0.494	3999	101	1627.900
30m	6.834	0.558	2967	128	1602.243
35m	7.116	0.598	744	121	356.397
40m	6.865	0.675	8644	144	6801.096
45m	-	-	-	-	-
50m	-	-	-	-	-

Table A.10: Komet 202 27.5mm nozzle 4.5bar

Distance	μ	σ	Number	DOF	X^2
5m	6.412	0.273	6618	33	862.687
10m	6.550	0.318	10432	31	1204.798
15m	6.559	0.361	7345	44	1267.232
20m	6.572	0.395	7333	93	19438.666
25m	6.716	0.468	6244	115	2616.544
30m	6.890	0.492	3986	93	1218.326
35m	7.119	0.552	3052	137	1146.728
40m	7.217	0.584	2268	146	974.664
45m	7.221	0.614	3468	152	1653.543
50m	6.993	0.705	1989	161	1515.253

Table A.11: Komet 202 27.5mm nozzle 5.5bar

A.3 Mean Diameters

For each observed droplet size sample $\{D_i\}$ the commonly encountered mean diameters have been calculated using

$$D_{pq}^{p-q} = \sum_i D_i^p / \sum_j D_j^q \qquad (A.3)$$

The corresponding predicted mean diameters were evaluated from the lognormal distributions used to model the data using the definition for the jth moment

$$
\begin{aligned}
\lambda_j &= \int_0^\infty D^j d\Lambda(D|\mu,\sigma^2) \\
&= \int_{-\infty}^\infty e^{jy} dN(y|\mu,\sigma^2) \qquad (A.4) \\
&= e^{j\mu+\frac{1}{2}j^2\sigma^2}
\end{aligned}
$$

such that

$$D_{pq}^{p-q} = \lambda_p / \lambda_q. \qquad (A.5)$$

Tables A.12 to A.20 contain the observed and predicted values for the number (D_{10}), area (D_{20}), volume (D_{30}) and Sauter (D_{32}) mean diameters for each sprinkler nozzle pressure combination examined.

Distance	Number		Area		Volume		Sauter	
	Observed	Predicted	Observed	Predicted	Observed	Predicted	Observed	Predicted
5m	0.621	0.620	0.642	0.641	0.665	0.662	0.713	0.707
10m	0.719	0.716	0.777	0.766	0.844	0.820	0.998	0.937
15m	0.774	0.768	0.865	0.838	0.988	0.914	1.288	1.087
20m	0.842	0.825	1.023	0.928	1.319	1.044	2.191	1.322
25m	0.897	0.874	1.123	1.007	1.468	1.160	2.510	1.540
30m	1.042	1.009	1.376	1.212	1.855	1.457	3.374	2.105
35m	1.107	1.020	1.723	1.382	2.448	1.873	4.938	3.440
40m	-	-	-	-	-	-	-	-
45m	-	-	-	-	-	-	-	-
50m	-	-	-	-	-	-	-	-

Table A.12: Komet 101 18mm nozzle @ 3.5bar

Distance	Number		Area		Volume		Sauter	
	Observed	Predicted	Observed	Predicted	Observed	Predicted	Observed	Predicted
5m	0.622	0.622	0.644	0.642	0.670	0.663	0.724	0.707
10m	0.685	0.684	0.720	0.717	0.759	0.751	0.844	0.825
15m	0.750	0.748	0.806	0.797	0.875	0.848	1.031	0.961
20m	0.810	0.807	0.886	0.869	0.979	0.937	1.198	1.088
25m	0.840	0.834	0.948	0.916	1.087	1.007	1.430	1.215
30m	0.896	0.884	1.050	0.986	1.281	1.100	1.905	1.370
35m	0.967	0.950	1.171	1.083	1.464	1.236	2.287	1.608
40m	2.153	1.118	1.522	1.378	1.981	1.698	3.359	2.578
45m	-	-	-	-	-	-	-	-
50m	-	-	-	-	-	-	-	-

Table A.13: Komet 101 18mm nozzle 5.5bar

Distance	Number		Area		Volume		Sauter	
	Observed	Predicted	Observed	Predicted	Observed	Predicted	Observed	Predicted
5m	0.652	0.652	0.680	0.678	0.710	0.704	0.774	0.760
10m	0.832	0.829	0.909	0.899	0.996	0.975	1.194	1.147
15m	0.813	0.807	0.901	0.875	1.017	0.948	1.295	1.113
20m	0.901	0.889	1.053	0.992	1.281	1.107	1.895	1.378
25m	0.949	0.930	1.163	1.068	1.475	1.225	2.371	1.614
30m	1.080	1.048	1.396	1.246	1.843	1.480	3.211	2.088
35m	1.232	1.190	1.671	1.488	2.231	1.861	3.978	2.911
40m	-	-	-	-	-	-	-	-
45m	-	-	-	-	-	-	-	-
50m	-	-	-	-	-	-	-	-

Table A.14: Komet 101 22mm nozzle 3.5bar

Distance	Number		Area		Volume		Sauter	
	Observed	Predicted	Observed	Predicted	Observed	Predicted	Observed	Predicted
5m	0.613	0.612	0.638	0.633	0.683	0.655	0.784	0.700
10m	0.755	0.754	0.803	0.800	0.855	0.849	0.968	0.955
15m	0.753	0.751	0.810	0.800	0.879	0.851	1.033	0.964
20m	0.817	0.810	0.923	0.883	1.089	0.963	1.516	1.145
25m	0.853	0.843	0.984	0.929	1.187	1.025	1.728	1.247
30m	0.898	0.884	1.066	0.991	1.327	1.111	2.057	1.398
35m	0.989	0.969	1.218	1.116	1.561	1.286	2.567	1.706
40m	1.132	1.098	1.496	1.333	1.991	1.619	3.527	2.388
45m	-	-	-	-	-	-	-	-
50m	-	-	-	-	-	-	-	-

Table A.15: Komet 101 22mm nozzle 4.5bar

Distance	Number		Area		Volume		Sauter	
	Observed	Predicted	Observed	Predicted	Observed	Predicted	Observed	Predicted
5m	0.634	0.634	0.658	0.657	0.683	0.681	0.737	0.732
10m	0.711	0.711	0.752	0.750	0.796	0.791	0.891	0.881
15m	0.758	0.757	0.818	0.810	0.892	0.868	1.061	0.995
20m	0.803	0.798	0.894	0.866	1.026	0.940	1.354	1.107
25m	0.825	0.817	0.942	0.894	1.134	0.979	1.644	1.173
30m	0.892	0.879	1.047	0.983	1.279	1.098	1.907	1.371
35m	0.903	0.885	1.104	1.007	1.421	1.146	2.355	1.483
40m	0.978	0.955	1.233	1.117	1.607	1.307	2.730	1.789
45m	-	-	-	-	-	-	-	-
50m	-	-	-	-	-	-	-	-

Table A.16: Komet 101 22mm nozzle 5.5bar

Distance	Number		Area		Volume		Sauter	
	Observed	Predicted	Observed	Predicted	Observed	Predicted	Observed	Predicted
5m	0.641	0.641	0.672	0.670	0.705	0.700	0.776	0.764
10m	0.801	0.800	0.865	0.860	0.935	0.925	1.091	1.071
15m	0.830	0.827	0.906	0.893	0.994	0.965	1.195	1.125
20m	0.978	0.971	1.117	1.086	1.290	1.214	1.722	1.516
25m	1.052	1.044	1.213	1.181	1.404	1.337	1.883	1.711
30m	1.119	1.108	1.324	1.273	1.577	1.462	2.240	1.930
35m	1.099	1.079	1.357	1.255	1.730	1.460	2.813	1.976
40m	1.052	1.026	1.325	1.211	1.684	1.430	2.717	1.992
45m	1.328	1.299	1.734	1.624	2.223	2.029	3.655	3.168
50m	-	-	-	-	-	-	-	-

Table A.17: Komet 202 25mm nozzle 4.5bar

Distance	Number		Area		Volume		Sauter	
	Observed	Predicted	Observed	Predicted	Observed	Predicted	Observed	Predicted
5m	-	-	-	-	-	-	-	-
10m	-	-	-	-	-	-	-	-
15m	-	-	-	-	-	-	-	-
20m	-	-	-	-	-	-	-	-
25m	0.821	0.818	0.894	0.877	0.989	0.940	1.210	1.081
30m	0.819	0.814	0.906	0.879	1.037	0.948	1.360	1.105
35m	0.880	0.872	1.006	0.961	1.192	1.060	1.672	1.289
40m	0.889	0.875	1.049	0.975	1.310	1.086	2.045	1.347
45m	0.937	0.918	1.148	1.040	1.491	1.179	2.519	1.515
50m	1.026	1.003	1.269	1.163	1.601	1.348	2.548	1.810

Table A.18: Komet 202 25mm nozzle 5.5bar

Distance	Number		Area		Volume		Sauter	
	Observed	Predicted	Observed	Predicted	Observed	Predicted	Observed	Predicted
5m	0.719	0.718	0.766	0.761	0.817	0.807	0.931	0.906
10m	0.875	0.873	0.957	0.951	1.045	1.035	1.248	1.227
15m	0.850	0.845	0.945	0.926	1.058	1.014	1.326	1.215
20m	0.854	0.846	0.968	0.931	1.131	1.024	1.542	1.239
25m	0.972	0.960	1.142	1.085	1.370	1.226	1.971	1.565
30m	1.107	1.086	1.372	1.269	1.744	1.483	2.817	2.025
35m	1.485	1.473	1.818	1.762	2.232	2.107	3.366	3.013
40m	1.245	1.203	1.681	1.510	2.225	1.896	3.893	2.990
45m	-	-	-	-	-	-	-	-
50m	-	-	-	-	-	-	-	-

Table A.19: Komet 202 27.5mm nozzle 4.5bar

Distance	Number		Area		Volume		Sauter	
	Observed	Predicted	Observed	Predicted	Observed	Predicted	Observed	Predicted
5m	0.633	0.632	0.659	0.656	0.689	0.681	0.752	0.734
10m	0.736	0.736	0.775	0.774	0.817	0.814	0.909	0.900
15m	0.755	0.753	0.812	0.804	0.878	0.858	1.027	0.977
20m	0.778	0.773	0.858	0.836	0.968	0.904	1.232	1.057
25m	0.931	0.921	1.076	1.028	1.284	1.147	1.828	1.427
30m	1.113	1.109	1.270	1.252	1.455	1.413	1.911	1.800
35m	1.446	1.438	1.719	1.675	2.076	1.951	3.029	2.648
40m	1.630	1.616	1.984	1.917	2.427	2.274	3.631	3.200
45m	1.668	1.652	2.066	1.994	2.548	2.408	3.875	3.511
50m	1.435	1.396	1.975	1.790	2.652	2.295	4.786	3.772

Table A.20: Komet 202 27.5mm nozzle 5.5bar

Bibliography

[1] Y. A. Al-Rumikhani. *Modelling and Measuring the Performance of Medium and Large Irrigation Sprinklers.* PhD dissertation, Cranfield University, 1994.

[2] S.A. Morsi A.J. Alexander. An investigation of particle trajectories in two phase flows. *Journal of Fluid Mechanics,* 55(2):193–208, 1972.

[3] H. Arastoopour. *Pneumatic Transport of Solids,* volume 3 of *Encyclopedia of Fluid Mechanics.* Gulf Pub. Co., Book Division, Houston, 1986.

[4] P. Augier. *Contribution à l'Étude et à la Modélisation Mecaniste-Statistique de la Distribution Spatiale des Apports d'eau sous un Canon d'Irrigation : Application à la Caractérisation des Effets du Vent sur l'Uniformité d'Arrosage.* PhD dissertation, École Nationale du Génie Rural, des Eaux et des Fôrets, Montpellier, FR., 1996.

[5] S. M. Arshad Ali A. D. Barefoot. Sprinkler distribution patterns as affected by pressure and wind. *Agricultural Mechanisation in Asia, Africa and Latin America,* 15(2):49–52, 1984.

[6] J. Keller R.D. Bliesner. *Sprinkle and Trickle Irrigation.* Van Nostrand Reinhold, New York, first edition, 1990.

[7] S. Sucec W.W. Bowley. Prediction of the trajectory of a turbulent jet injected into a cross-flowing stream. *Journal of Fluids Engineering, Transactions of the American Society of Mecahnical Engineers,* pages 667–773, December 1976.

[8] R. D. Reitz F. V. Bracco. *Mechanisms of Breakup of Round Liquid Jets,* volume 3 of *Encyclopedia of Fluid Mechanics.* Gulf Pub. Co., Book Division, Houston, 1986.

[9] J. Aitchison J.A.C. Brown. *The Lognormal Distribution - with Special References to its uses in Economics,* volume 5 of *University of Cambridge Department of Applied Economics Monographs.* Cambridge University Press, Reading, Massachusetts, first edition, 1969.

[10] P. Weinacht J. M. Buchlin. *A Numerical Model of Gas Droplet Flow. Application to Liquid Spray and Cooling Towers.* Technical Note 144. von Karman Institute for Fluid Dynamics, Rhode Saint Genèse, Belgium, 1982.

[11] P. Weinacht C. Benocci J-M. Buchlin. *A Prediction Method for the AIR-Droplets Flow in the Inlet Section of a Natural Draught Cooling Tower.* Technical Memorandum #40. von Karman Institute for Fluid Dynamics, Rhode Saint Genèse, Belgium, 1986.

[12] S. Davland. *Effect of Pressure on Hose Reel Raingun Performance at Different Windspeeds.* MSc dissertation, Cranfield University (Silose College), 1986.

[13] H. Shull A.S Dyla. Travelling gun application uniformity in high winds. *Transactions of the American Society of Agricultural Engineers,* 19(2):254–258, 1976.

[14] H. Shull A. S. Dylla. Wind effects on water application patterns from large, single nozzle sprinklers. *Transactions of the American Society of Agricultural Engineers,* 19(3):501–504, 1976.

[15] C. E. Pearson (editor). *Handbook of Applied Mathematics.* Van Nostrand Reinold, New York, second edition, 1974.

[16] R.A. Mugele H.D Evans. Droplet size distributions in sprays. *Industrial and Engineering Chemistry.,* 27:1317–1324, 1951.

[17] J.S. Hadamard. Mouvement permanent lent d'une sphère liquide et visqueuse dans um liquide visquex. *Comptes Rendus de l'Académie des Sciences*, 152:1735–1738, 1911.

[18] K. R. Hipperson. *Development of Instrumentation for Hose-Reel Raingun Irrigators*. MPhil dissertation, Cranfield University (Silose College), 1985.

[19] P. Carrion . M. Tarjuelo J. Montero F. T. Honrubia. *SIRIAS: A Simulation Model of Water Distribution for Sprinkler Irrigation*. Final report of EC project FAIR CT 950088. Universidad de Castilla-la Mancha, Spain, 1999.

[20] N.W. Hudson. *The Flour-Pellet Method for Measuring the Size of Raindrops*. Report bulletin 4, Harare, Zimbabwe, Department of Conservation, 1964.

[21] S. Gosh J.C.R. Hunt. Induced air velocity within droplet driven sprays. *Proceedings of the Royal Society of London A*, 444:105–127, 1994.

[22] D. Gidaspow J. Ding U. K. Jayaswal. Multiphase navier-stokes equation solver. In I. Celik, editor, *Numerical Methods for Multiphase Flow*, pages 47–56, New York, June 1990. American Society of Mechanical Engineers.

[23] M. E. Kay. *Sprinkler Irrigation Equipment and Practice*. B. T. Batsford Ltd, London, first edition, 1983.

[24] S. N. Musa. *A Computer Simulation Methodology for Predicting Water Distribution, Crop Yield, and Economic Return for Mobile Raingun Irrigators (Travellers)*. PhD dissertation, Cranfield University (Silose College), 1988.

[25] C. S. Parkin. Methods for measuring spray droplet sizes. In G. A. Matthews E. C. Hislop, editor, *Application Technology for Crop Protection*, pages 57–84. CAB International, 1993.

[26] S. L. Passman. Stress in dilute suspensions. In R. Decker, editor, *Constitutive Relationships and Models in Continuum Theories of Multiphase Flows*, NASA Conference Publication 3047, pages 57–64, Boston, April 1989. NASA.

[27] E. E. Michaelides Z. J. Plazaola. Singularities in two-phase flow equations - critical flow in nozzles. In I. Celik, editor, *Numerical Methods for Multiphase Flow*, pages 83–89, New York, June 1990. American Society of Mechanical Engineers.

[28] Lord Rayleigh. On the instability of jets. *Proceedings of the Royal Society of London*, 4:10, 1878.

[29] R.L. Collier E.W Rochester. Water application uniformity of hose towed traveler irrigations. *Transactions of the American Society of Agricultural Engineers*, 23(5):1135–1138, 1980.

[30] L. Rolland. *Mechanized Sprinkler Irrigation*. FAO Report #35. Food and Agricultural Organization of the United Nations, Rome, 1982.

[31] W. Rybczynski. Uber die fortschreitende bewegung einer flussigen kugel in einam zahen medoiu. *Bulletin of the International Academy of Science, Cracovie*, (A):40–46, 1911.

[32] H. Schlichting. *Boundary Layer Theory*. McGraw-Hill, New York, second edition, 1960.

[33] M. Abramowitz I. A. Segun. *Handbook of Mathematical Functions*. Dover Publications, New York, fifth edition, 1968.

[34] K.E. Selkirk. *Statistics on a Circle*, volume 4 of *Teaching Statistics*. 1982.

[35] S. L. Soo. *Multiphase Fluid Dynamics*. Science Press, Beijing, first edition, 1990.

[36] C. T. Crowe M. P. Sharma D. E. Stock. The particle-source-in cell (psi-cell) model for gas droplet flows. *Journal of Fluids Engineering*, pages 325–332, June 1977.

[37] T. J. O'Brien M. Syamial. NIMPF: A nonisothermal multiparticle fluidized-bed hydrodynamic model. In I. Celik, editor, *Numerical Methods for Multiphase Flow*, pages 65–72, New York, June 1990. American Society of Mechanical Engineers.

[38] W. H. Press S. A. Teukolsky. *Numerical Recipes in C - The Art of Scientific Computing*. Cambridge University Press, second edition, 1992.

[39] U. Turker. *Precision Irrigation using a Self Travelling Gun.* PhD dissertation, Cranfield University, 1998.

[40] B.R. Morton G.I. Taylor J.S. Turner. Turbulent gravitational convection from maintained and instantaneous sources. *Proceedings of the Royal Society of London A*, 234:1-23, 1956.

[41] I. Seginer D. Nir R. D. von Bernuth. Simulation of wind-distorted sprinkler patterns. *Journal of Irrigation and Drainage Engineering*, 117(2):283-305, 1981.

[42] J.R. Grace T. Wairegi. *Gas-Liquid Flows*, volume 3 of *Encyclopedia of Fluid Mechanics*. Gulf Pub. Co., Book Division, Houston, 1986.

[43] D. J. Grose C. S. Parkin E. K. Weatherhead. Modelling a multi-phase plume in a crossflow - an agricultural application. In A. J. Yule, editor, *Proc. Fourteenth Annual ILASS Conference*, pages 487-492, Manchester, July 1998. ILASS.

[44] P. J. Richards E. K. Weatherhead. Prediction of raingun application patterns in windy conditions. *Journal of Agriculture Engineering Research*, 54:281-291, 1992.

[45] K. Brodowicz T. Dyakowski D. Wierzbicki. Two-phase gas-particle flow through venturi. In X. Chen, editor, *Multiphase Flow and Heat Transfer - Second International Symposium*, pages 1159-1166. Hemisphere Publishing Co., 1989.